



UNIVERSITY OF
TORONTO



**PMT Analysis and Neutrino Oscillation Simulations for the
Research and Development of Hyper-K and T2KK**

by

Shaghayegh Atashi

August 31, 2016

Under Supervision of:
Professor Sampa Bhadra
Dr. Arturo Fiorentini

This report is a description of the work I've done as a research assistant with the Tokai to Kamioka (T2K) experiment group at York University during the summer of 2016.

Shaghayegh Atashi

Undergraduate student at the University of Toronto
S.Atashi@mail.utoronto.ca

Contents:

1. Introduction
2. Setup

Part 1: PMT analysis

3. Voltage vs gain measurements
4. Dark count vs gain measurements
5. Dark count vs time measurements
6. Timing resolution measurements

Part 2: Simulations with Neutrino Oscillation Formulae

7. Simulations with electron neutrino appearance probability as a function of length and energy
8. Simulations of muon neutrino survival probability vs electron muon neutrino appearance probability
9. Neutrino Oscillation Applet

Chapter 1

Introduction

Tokai to Kamioka (T2K) is a long-baseline neutrino experiment that is studying neutrino oscillations. The Japan Proton Accelerator Research Complex (J-PARC) in Tokai produces a proton beam that collides with a graphite target to produce pions, which quickly decay into muons and muon neutrinos. The pions and muons are stopped by a second layer of graphite, but the muon neutrino beam travels a distance of 295 km to the Super Kamiokande (Super-K) detector in Kamioka. The neutrinos enter a large tank of ultapure water in Super-K, where some can interact with water. The interaction with water produces light, which can be detected by the photomultiplier tubes that line the walls of Super-K (illustration 1).

The Hyper-Kamiokande (Hyper-K) detector, the successor of Super-K, is a proposed long base-line water cherenkov detector whose main purpose is to study CP asymmetry in the lepton sector using neutrino and anti-neutrino beams. Part 1 of this report outlines the PMT analysis I've done toward the research and development of the Hyper-K detector. Part 2 of this report outlines the analysis I've done with neutrino oscillation formulae to investigate the benefits of the proposed long-baseline detector in Korea (T2KK) (illustration 2).

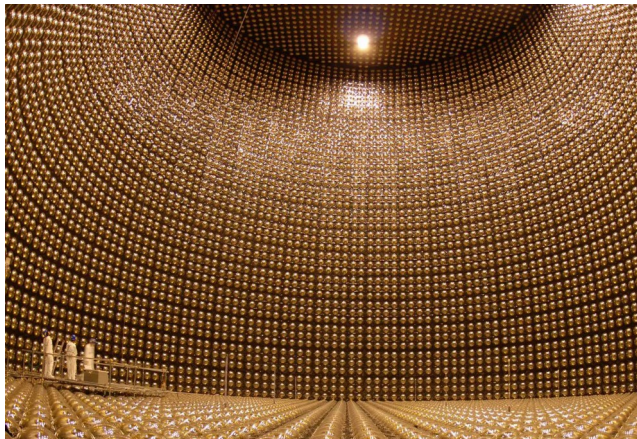
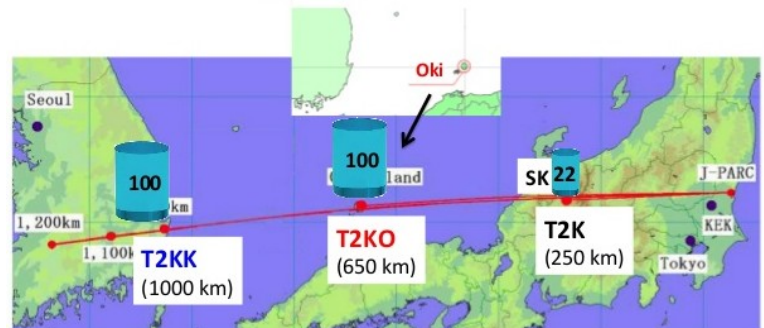


Illustration 1: Sensitive photomultiplier tubes line the walls of Super-K.

(source on page 68)

T2KK and T2KO proposals



T2KK: 100 kton in **Korea** [hep-ph/0410229, 0504026, 0901.1517, 1001.5165]

T2KO: 100 kton in **Oki Island** [0804.2111, 1209.2763]

* **SK** (22.5kton) will be used as a near detector

Illustration 2

Photomultiplier Tubes

Photomultiplier tubes (PMT's) are devices that detect very weak sources of light. When a photon hits the photocathode of the PMT (figure 2), an electron is emitted inside the PMT by the photoelectric effect. The electron passes through several dynodes, which multiply the electron through the process of secondary emission. The large number of electrons leave through the anode, generating a current that is large enough to detect.



Figure 1: A photomultiplier tube (PMT)

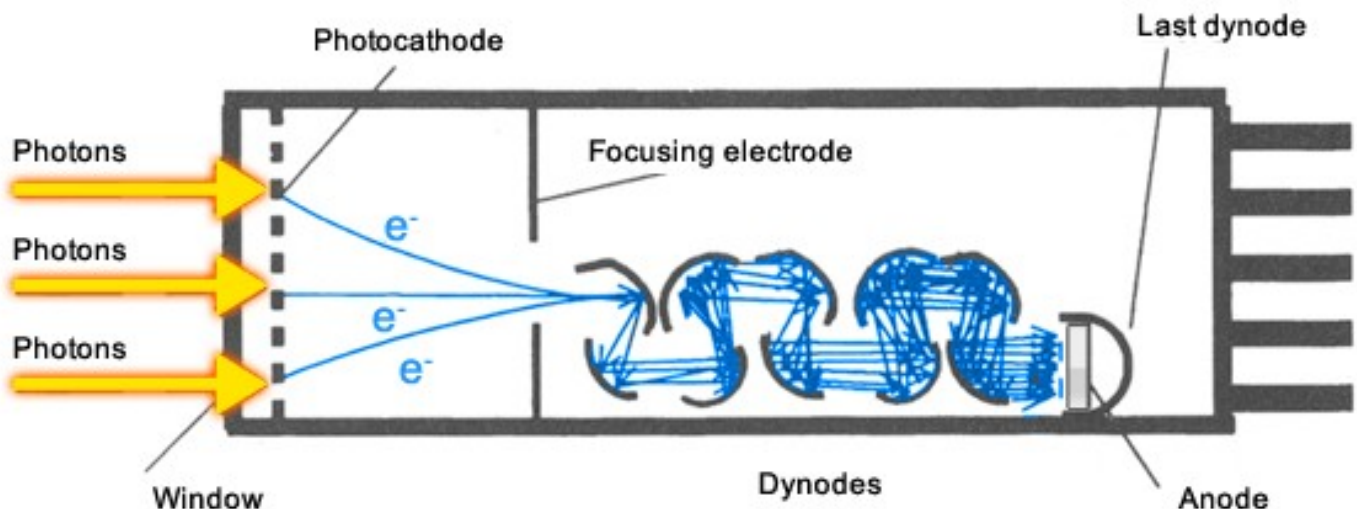


Figure 2: Schematic diagram of a PMT (source on page 68)

Chapter 2

Setup

Most of our measurements require two different PMT's: one monitor PMT, and one test PMT. The monitor PMT is always the Hamamatsu H10721P-110 (figure 3), while the test PMT is any one of the 3-inch Hamamatsu R12199 (figure 4), HZC XP5312 (figure 5), ETEL 9320KB (figure 6), or the HZC 72B20 (figure 7).



**Figure 3: Monitor PMT:
Hamamatsu H10721P-110**



**Figure 4: Test PMT :
Hamamatsu 3-inch R12199**



**Figure 5: Test PMT: 3-inch
HZC XP5312**

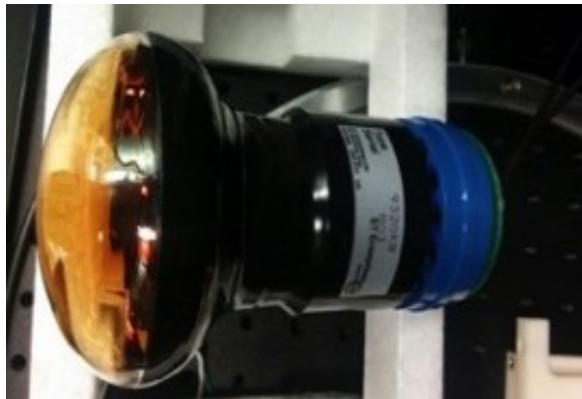


**Figure 6: Test PMT: 3-inch ETEL
9320KB**



Figure 7: Test Pmt: 3-inch HZC

We place the monitor and test PMT's inside the dark box. In order to avoid light leakage when doing dark count measurements, we place each test PMT inside a mini box (made of cardboard), cover the mini box with dark cloth, and put the mini box in the larger dark box (figure 8).

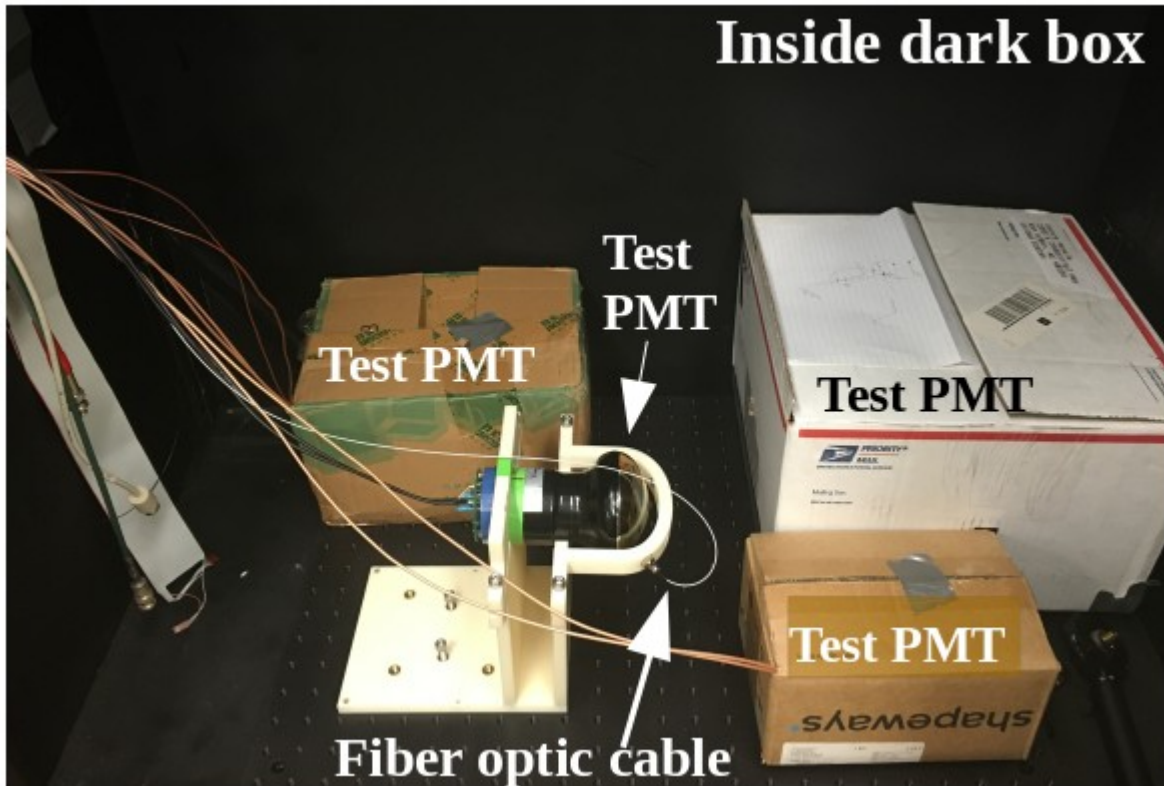


Figure 8: Inside the dark box: the fiber optic cable connects to the stand where the test PMT is taking data with laser light. We cover the cardboard boxes with dark cloth when taking dark count data with the PMT's inside.

Our pulsed light source (Tamadenshi Picosecond Optical Pulse Generator LDB-200) sends light of 405 nm wavelength and 70 ps width through a fiber optic cable. The fiber optic cable enters the dark box, where 90% of the light reaches the monitor PMT and 10% reaches the test PMT (figure 9).

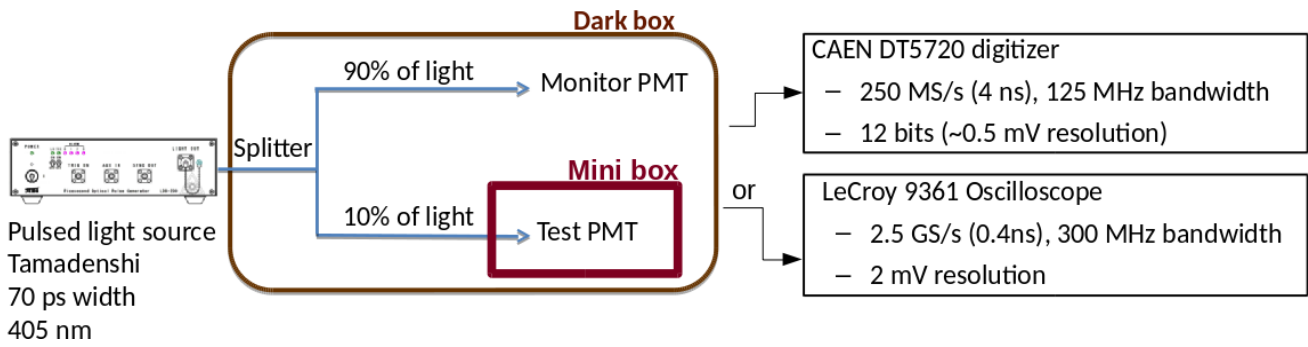


Figure 9: Setup of the equipment

Two signal wires come out of the black box and carry the information to either the digitizer or the oscilloscope. The digitizer is a CAEN DT5720, which has a sampling rate of 250 Mega Samples/second (4 ns), 12 bits (~ 0.5 mV resolution), and a bandwidth of 125 MHz. The oscilloscope is a LeCroy 9361, which has a sampling rate of 2.5 Giga Samples second (0.4 ns), 300 MHz bandwidth, and 2mV resolution. We run the code

`/home/t2k/work/daq/hyperk-fadc/convertToRoot.sh` on the raw digitizer data to produce a .root file, which contains many waveforms like the one in figure 10.

Notice the y -axis is in ADC counts for the digitizer data, which can be converted to voltage using a conversion factor that depends on the digitizer (1 V/2048 ADC counts for the CAEN dt5720 digitizer).

We run the code `/home/t2k/work/daq/oscilloscope/serial_daq.py` to obtain the oscilloscope data, and `/home/t2k/work/daq/oscilloscope/read_data.C` to convert the data into a root file. We then run

`/home/t2k/work/daq/analysis/charge_distribution.C` on the .root file to produce histograms of the integrated charge, heights, peak times, and pedestals of the pulses in the waveforms.

ETEL 3-inch 9320KB sample waveform

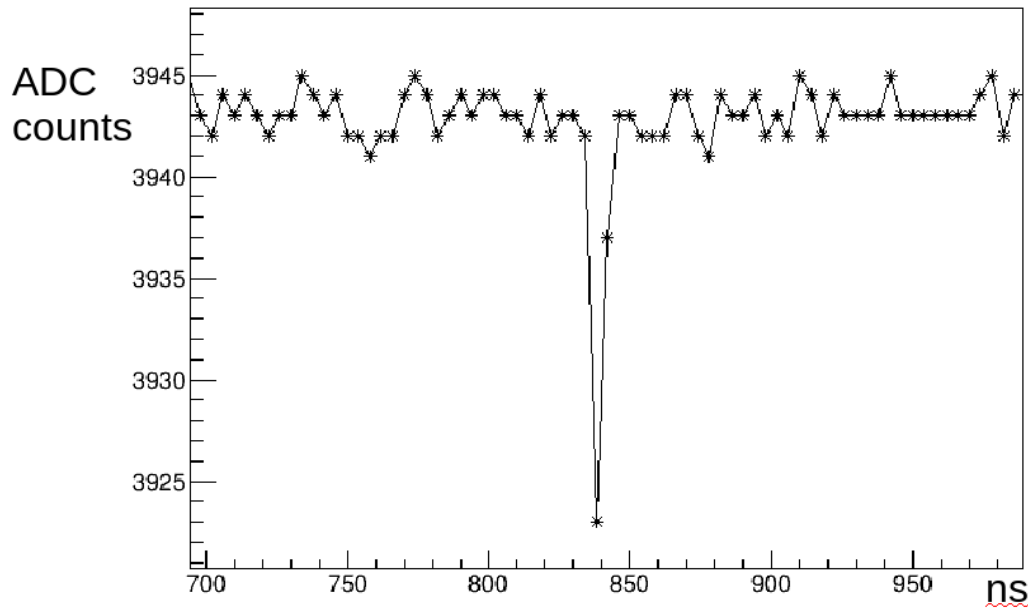


Figure 10: After running a code on the data, we get a large number of waveforms like this. The peak in the waveform indicated a current at the anode of the photocathode. ADC counts can be converted to volts using a factor that depends on the digitizer we use.

Occupancy

In most cases, when laser light is shined at the PMT, a photon hits the photocathode and eventually results in a produced current at the anode, which is the pulse we see in that waveform. However, if there is not enough current produced at the anode (e.g. a photoelectron is not emitted or the photon doesn't actually hit the photocathode), the waveform will not have a pulse. Occupancy is defined by the number of waveforms that have a pulse divided by the total number of waveforms. We can change the light intensity of our pulser, which determines how many photons are sent to the PMT during a time frame (the PMT's timing resolution). If the light intensity is high, many photons are sent to the PMT, so a greater fraction of the waveforms will have a pulse in them. This gives us a high occupancy. On the other hand, if the light intensity is low, fewer photons are sent to the photocathode in the time frame. This gives us a lower occupancy. The one photoelectron level (1 p.e. level) is when the light intensity is so low that only one photoelectron is emitted within the timing window of the

digitizer/oscilloscope. A light intensity of 78 mA in our pulsed light source corresponds to a lower occupancy compared to the higher occupancy light intensities of 83 or 85 mA.

Chapter 3

Measuring Gain of the PMT's

We can calculate the gain of a PMT at a certain voltage, which essentially tells us how much the PMT amplified the signal. We calculate the charge of the electrons produced at the anode in the PMT, and divide by the charge of a single electron to find the factor by which the initial photoelectron is multiplied. For example, if one photoelectron is created at the photocathode of the PMT, and 10^7 electrons are created at the anode, the gain is

$$10^7 \text{ final electrons} \div 1 \text{ initial photoelectron} = 10^7 \text{ gain}$$

Increasing the operating voltage of the PMT can increase the potential between the dynodes, which can increase the number of electrons created at the anode and subsequently increase the gain.

Calculating gain:

The code “/home/pmt_pc_2/software/code/read_chargedistribution.C” calculates the gain of the PMT at several operating voltages. We first calculate the pedestal of each waveform by taking the average of the points that lie outside the pulse region, which is where the pulse usually occurs (800-900ns) (figure 11). Then, we subtract the pedestal from the pulse and multiply the y-axis by

$$\frac{1 \text{ Volt}}{2048 \text{ ADC counts}} \frac{1}{50 \text{ ohms}} \quad \text{to convert ADC counts to current (since } I = \frac{V}{R} \text{ and we}$$

have an input impedance of 50 ohms) (figure 12). We then integrate the area

under the pulse in the current vs time graph according to $\text{Total Charge} = \int_{\text{all time}} I dt$ to get the integrated charge.

ETEL 3-inch 9320KB sample waveform

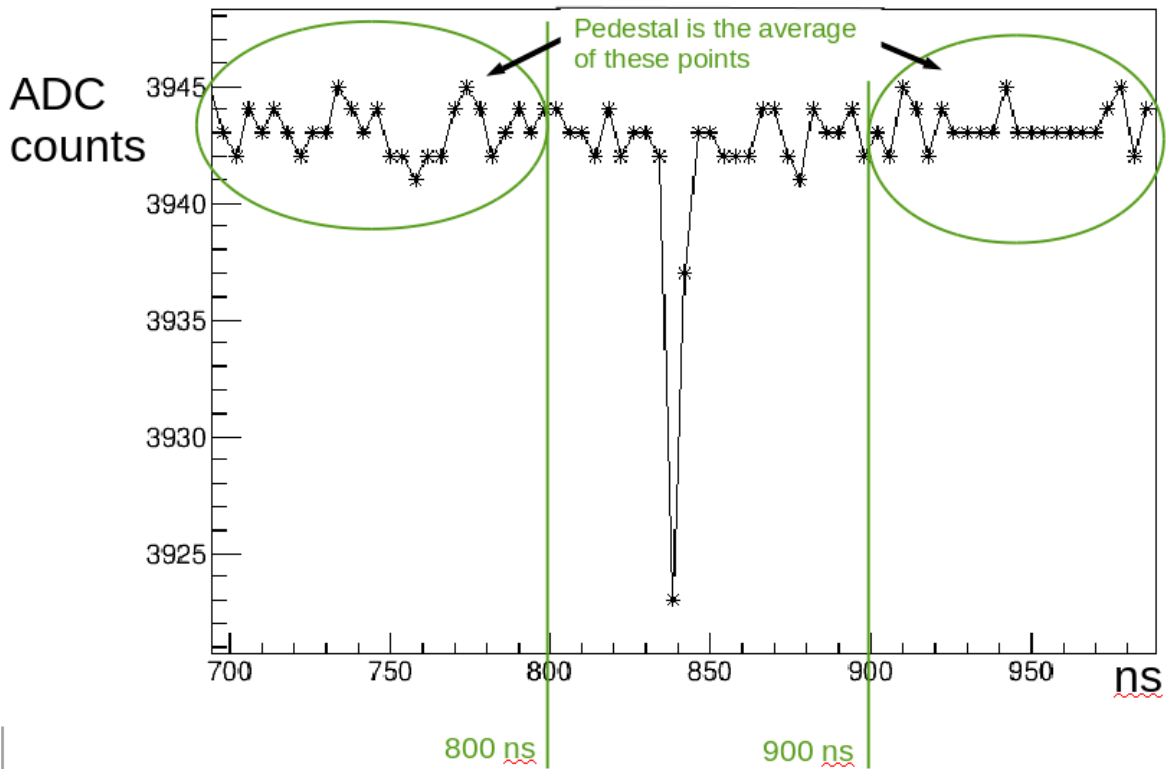


Figure 11: We calculate the pedestal of each waveform by taking the average of the points outside the pulse region (800-900 ns).

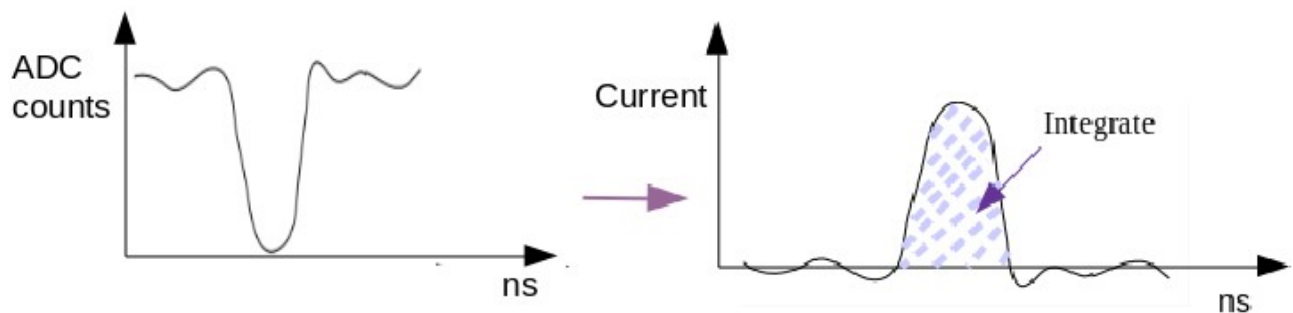


Figure 12: We subtract the pedestal from the pulse, convert ADC counts to current, and integrate the area under the pulse to get charge.

The following are the integrated charge histograms made for the Hamamatsu PMT at a pulser light intensity of 83mA and varying voltages (made by `read_chargedistribution.C`).

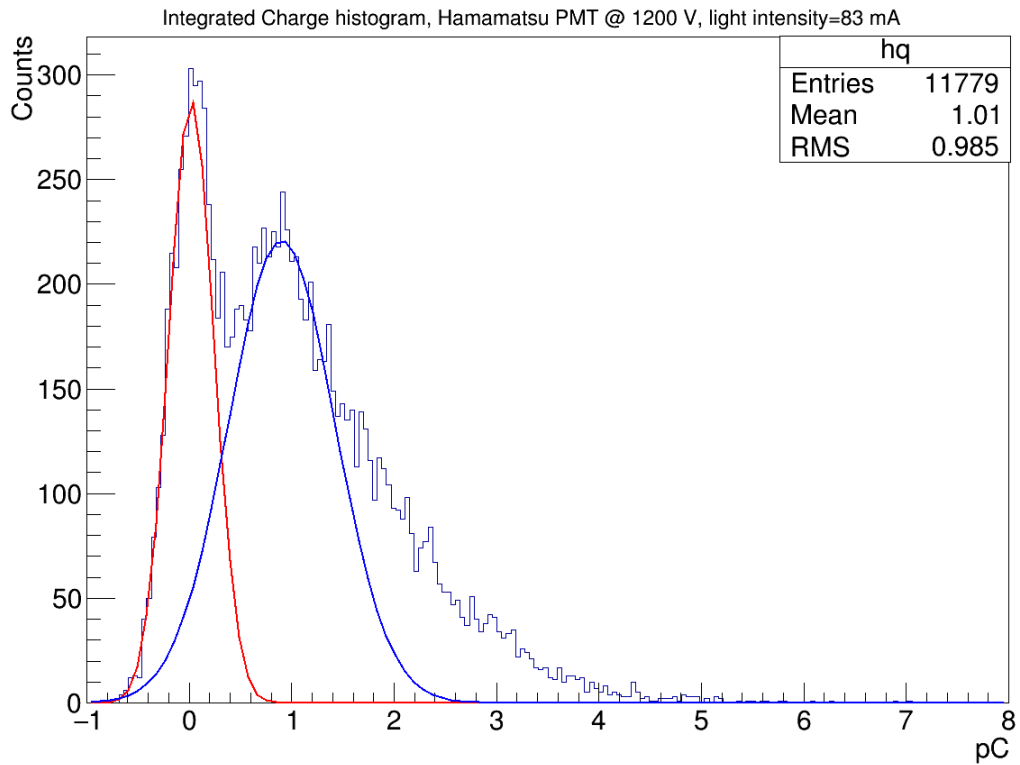


Figure 13

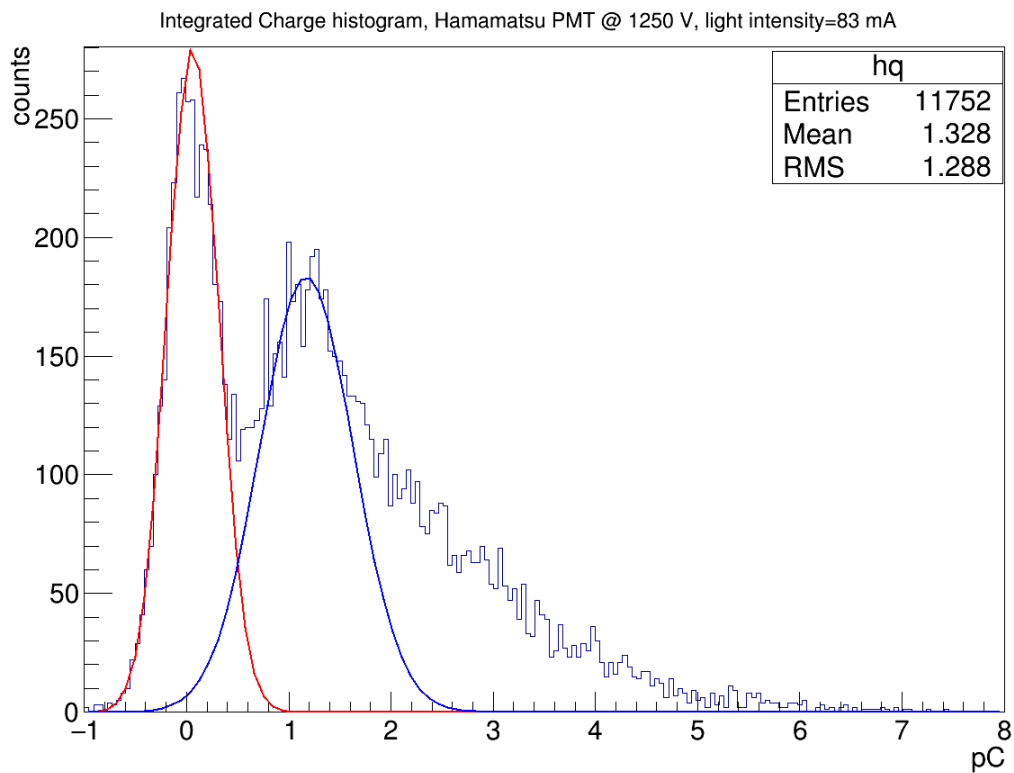


Figure 14

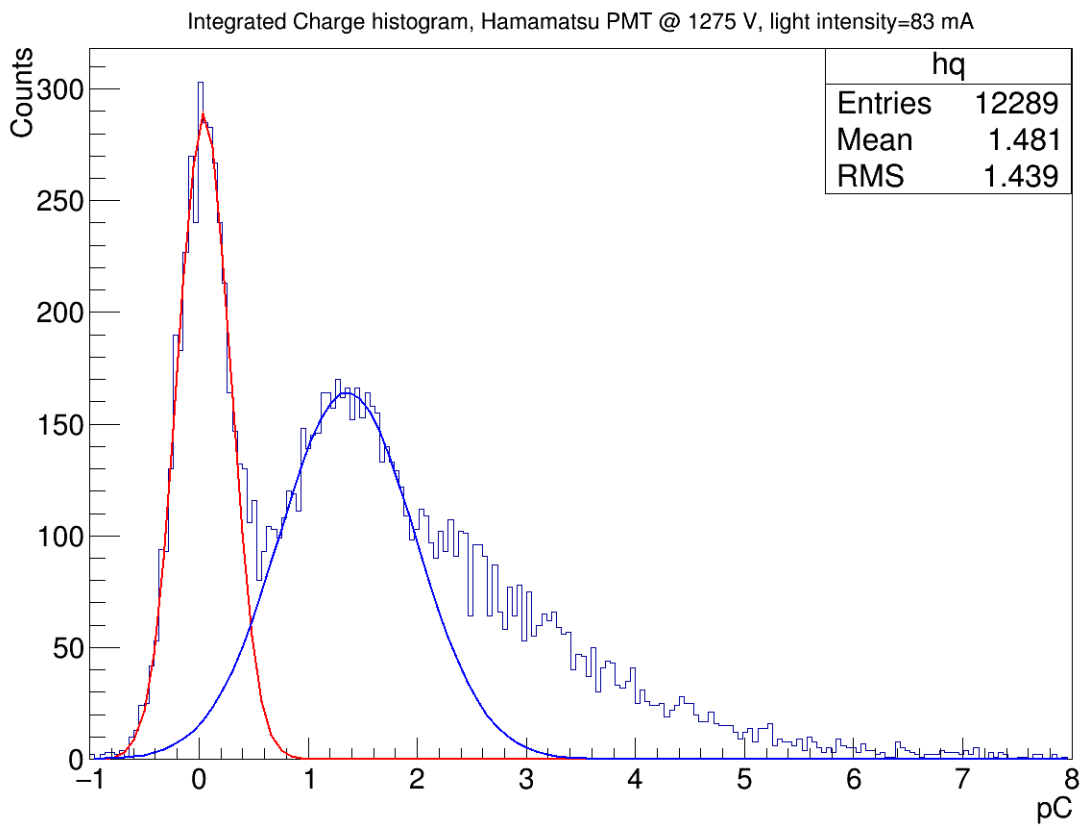


Figure 15

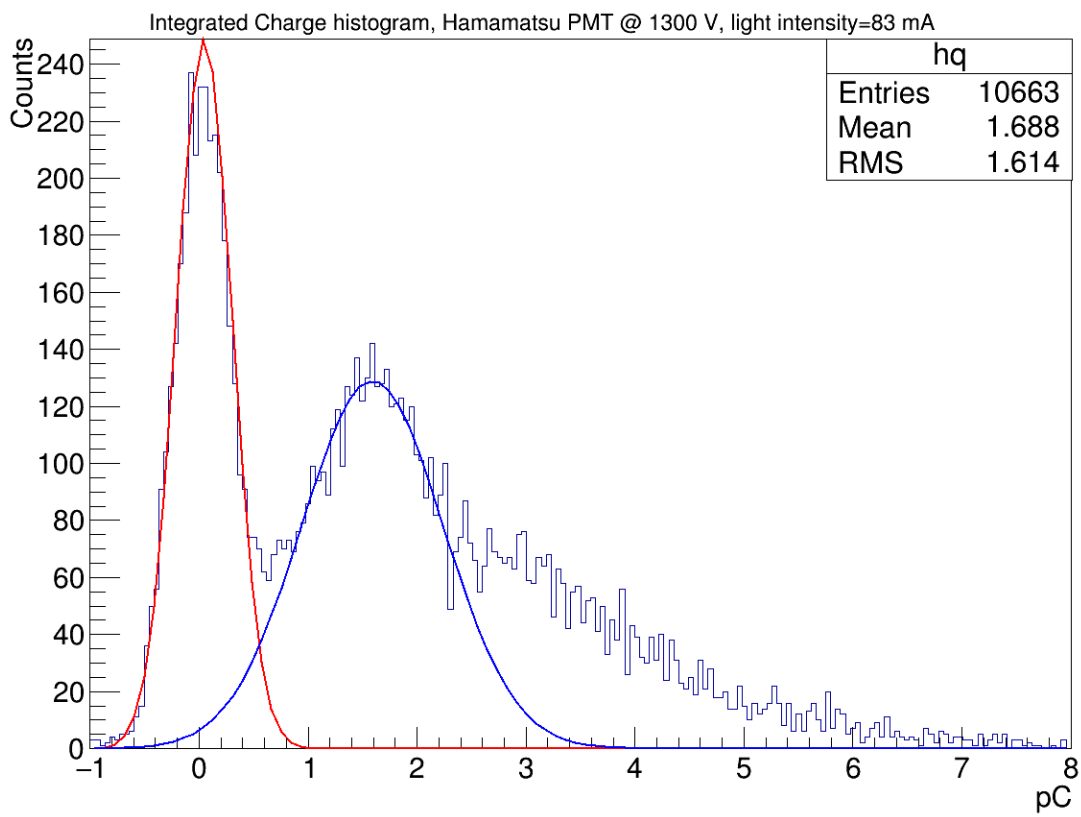


Figure 16

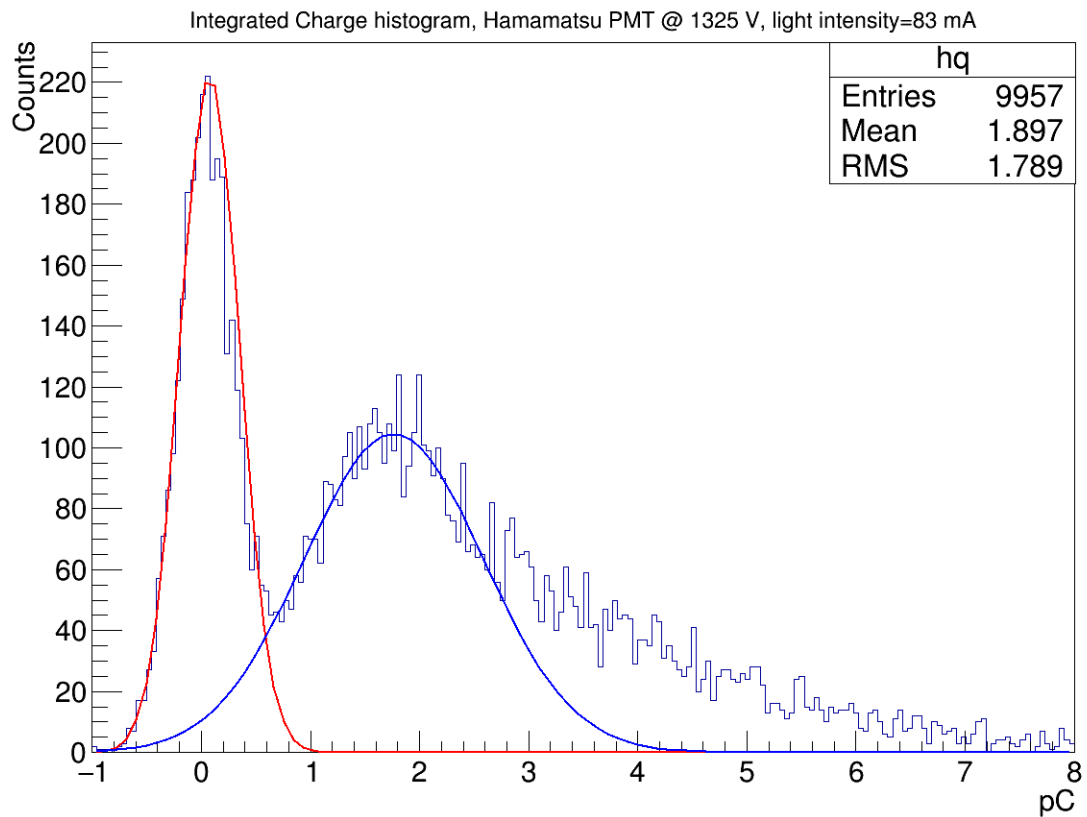


Figure 17

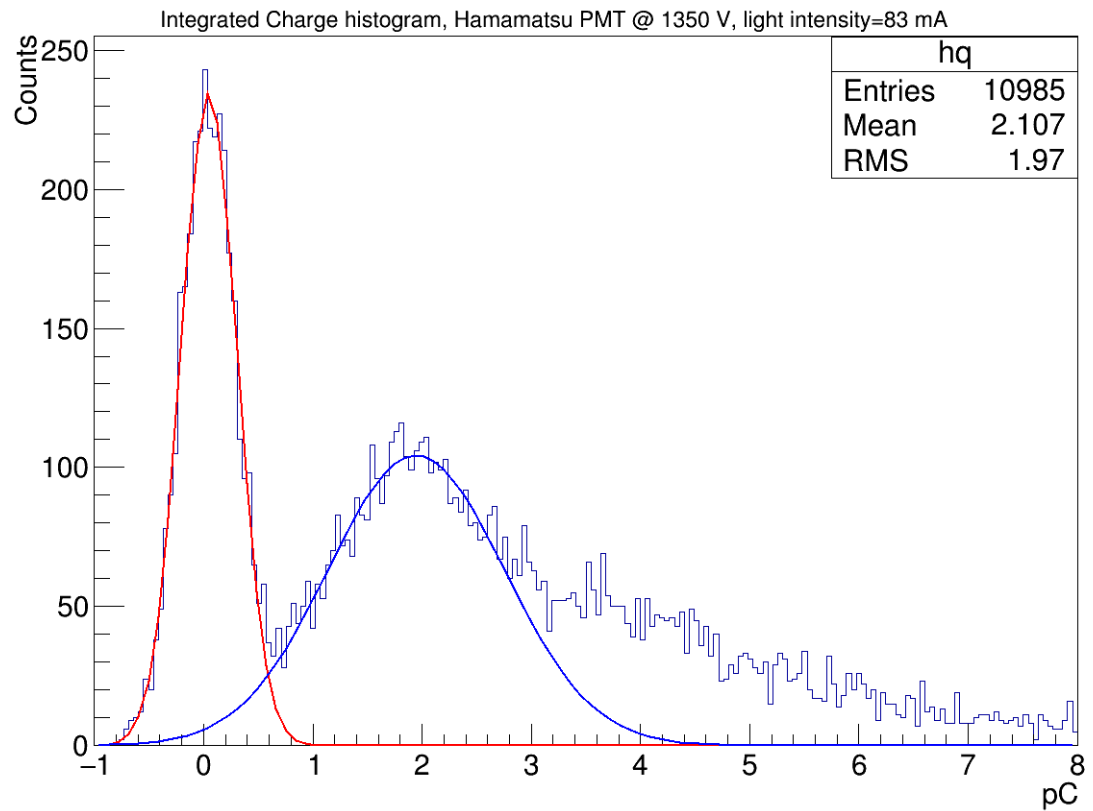


Figure 18

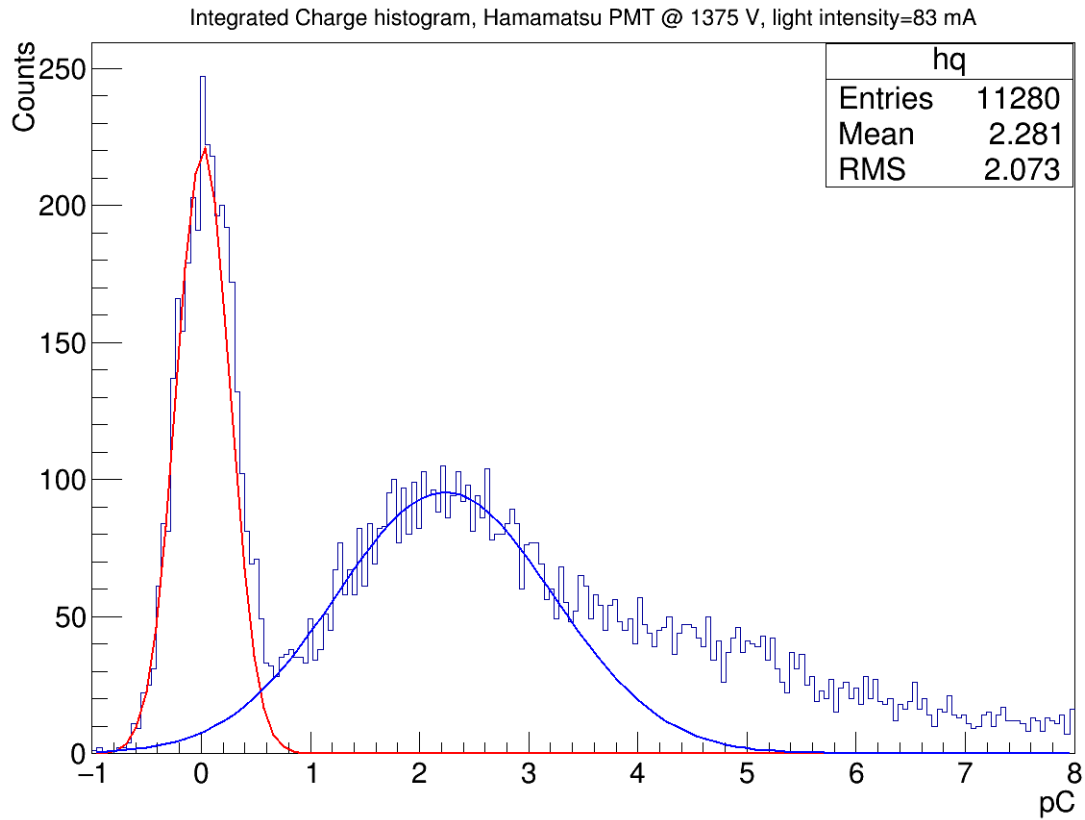


Figure 19

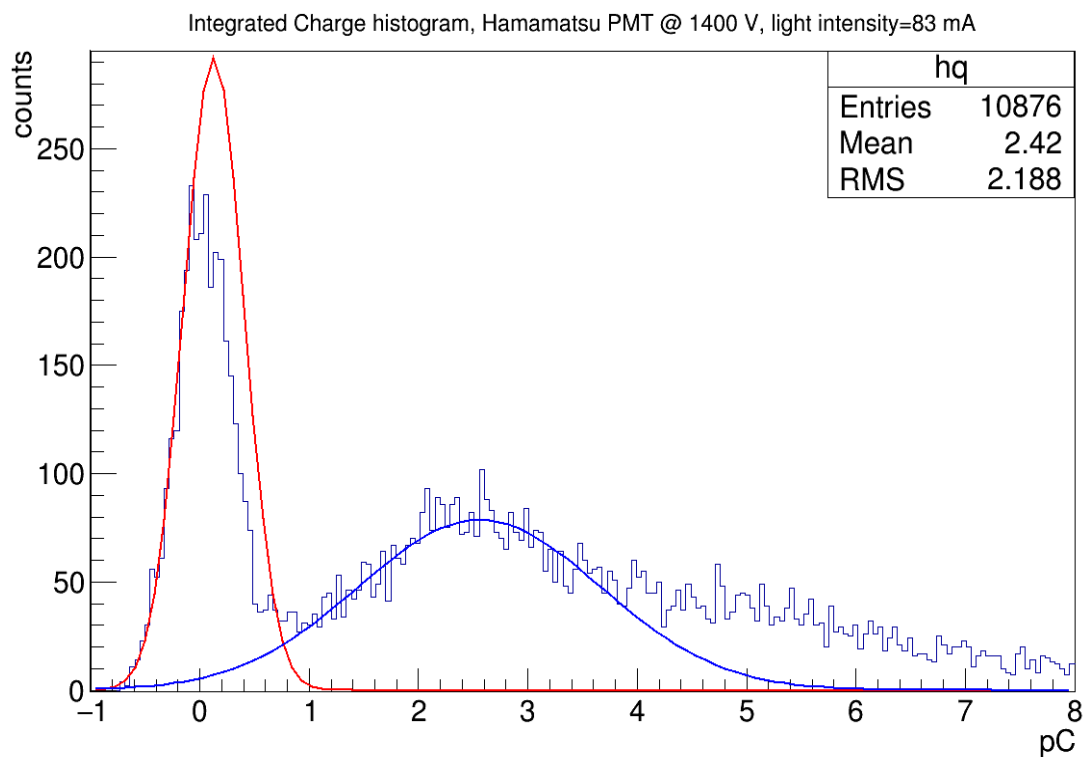


Figure 20

Notice that there is a substantial tail to the right of the graphs in figures 13-20. This tail is created because at 83 mA light intensity, there are many higher p.e. pulses, which are bigger than 1 p.e. pulses and have greater charge. The tail in the right artificially pulls the 1 p.e. peak to the right, which can give us a higher gain than what we actually have. In order to get less higher p.e. pulses in our data and minimize their effect in calculating gain, we took data with lower intensity light (80 mA). The results are shown in figures 21 to 33. The error of the gain reported here is error of the mean from the fit divided by the charge of the electron.

Peak to valley ratio:

The peak to valley ratio is a way of measuring the separation between the 0 p.e. peak and the 1 p.e. peak. Here, this number is the maximum of the fit to the 1 p.e. peak (blue line) divided by the minimum of the sum of the fits to the 0 p.e. and 1 p.e. peaks (sum of blue and red lines).

The following are integrated charge histograms for the Hamamatsu PMT with 80 mA light intensity and varying voltages (made by `read_chargedistribution.C`):

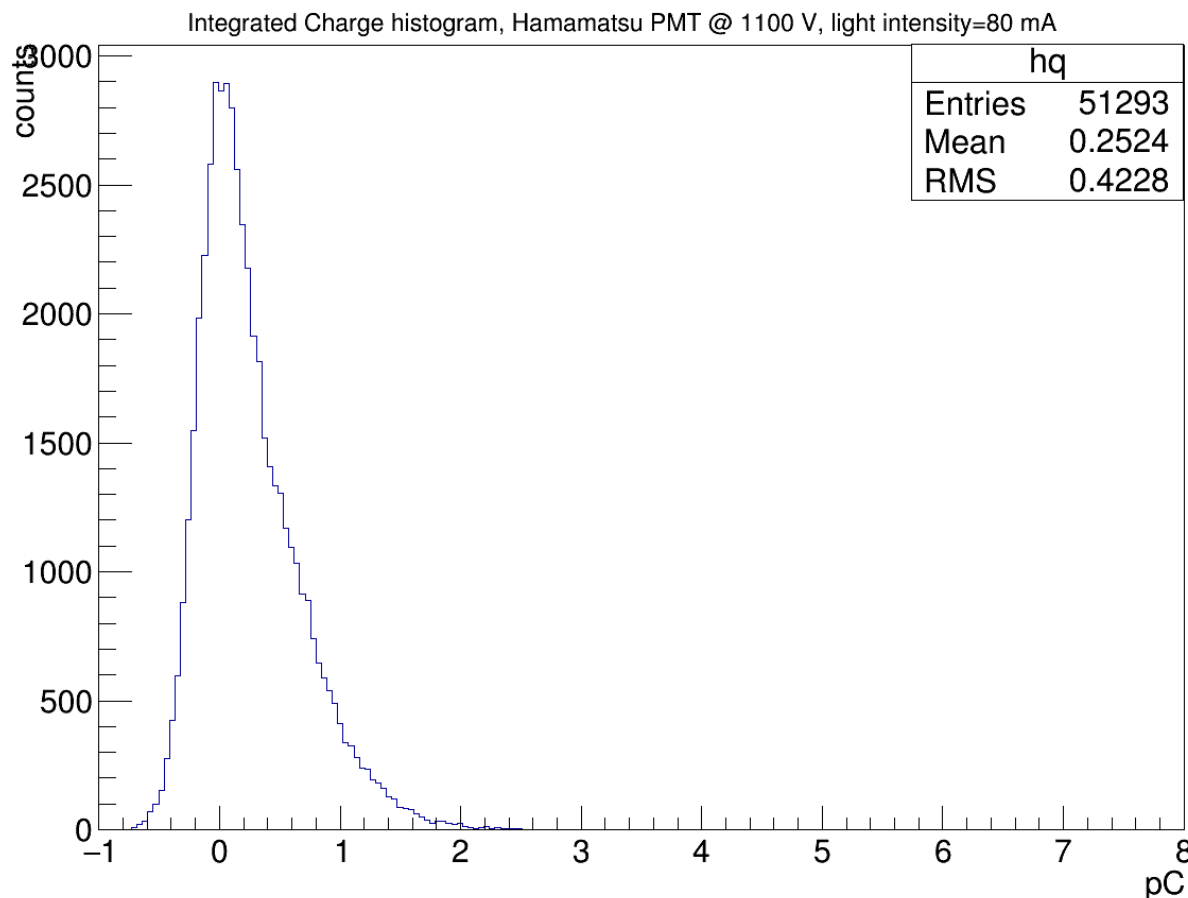


Figure 21: 1100 V is too low for the photoelectrons emitted to multiply substantially and create a distinct 1 p.e. peak.

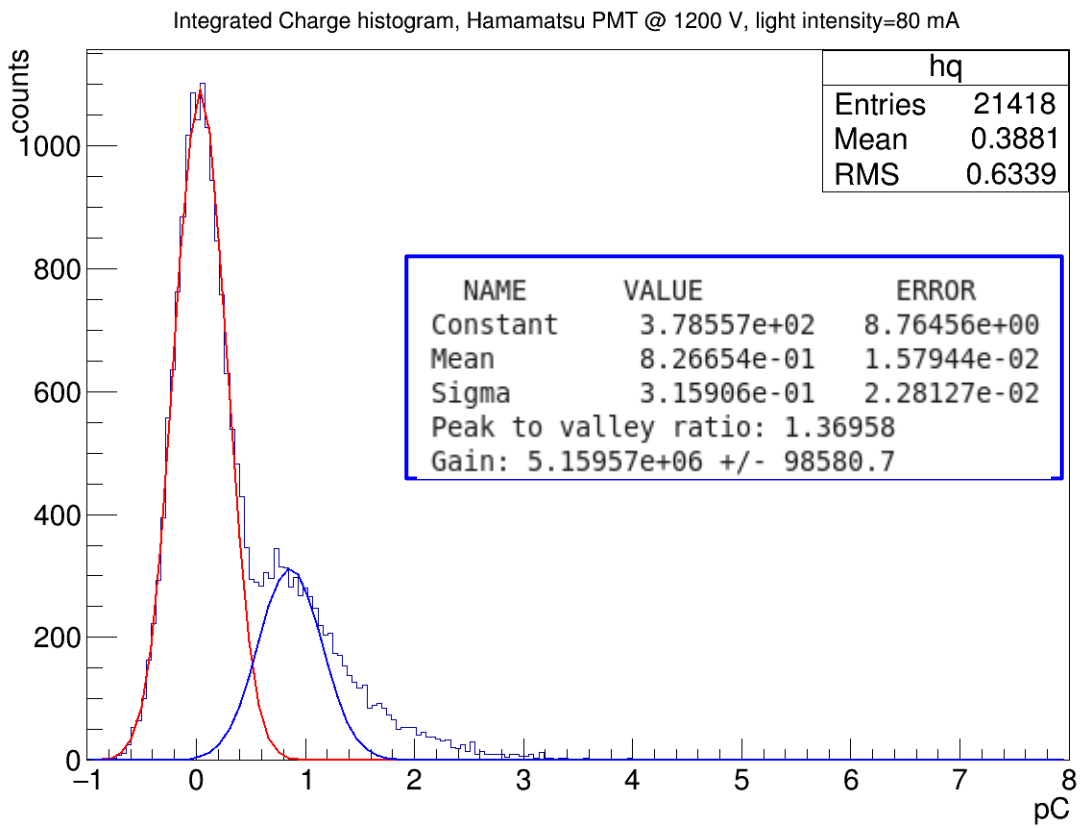


Figure 22: peak to valley ratio: 1.37, Gain: $5.16 \pm 0.10 \times 10^6$

The fit parameters in the blue box belong to the fit of the 1 p.e. peak.

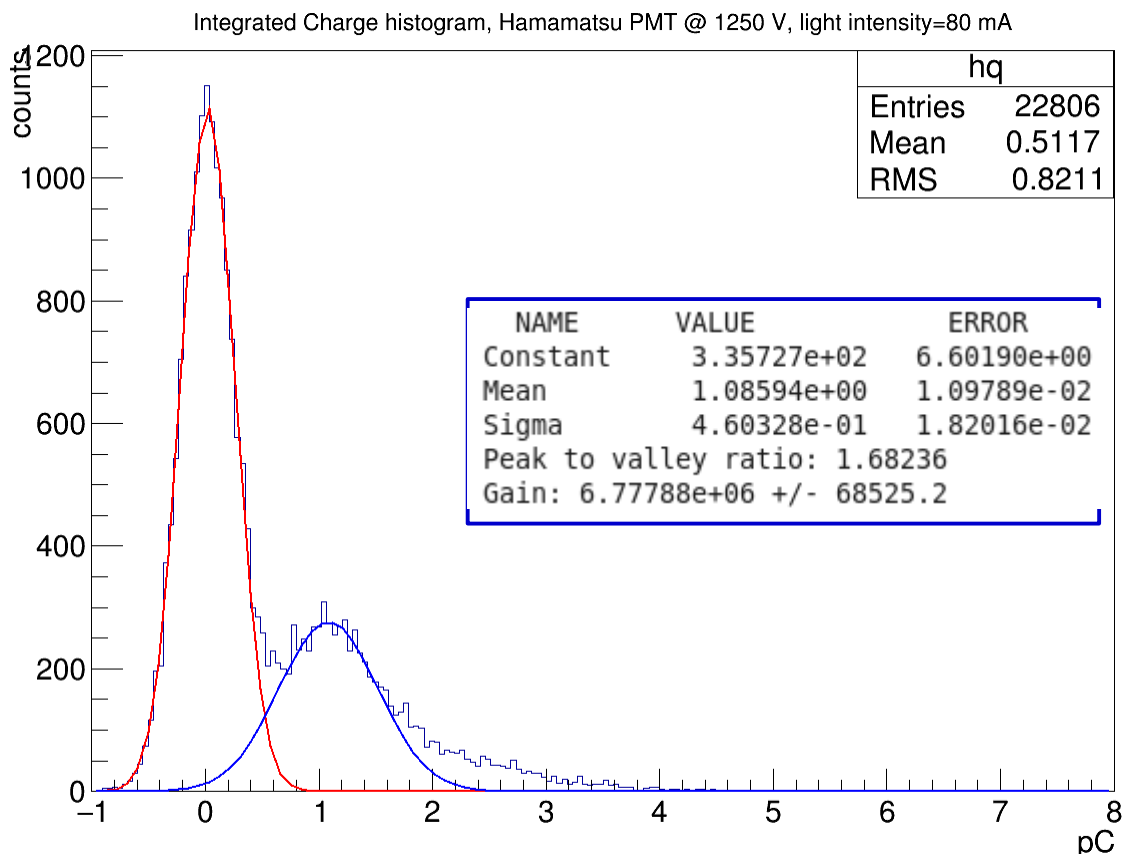


Figure 23

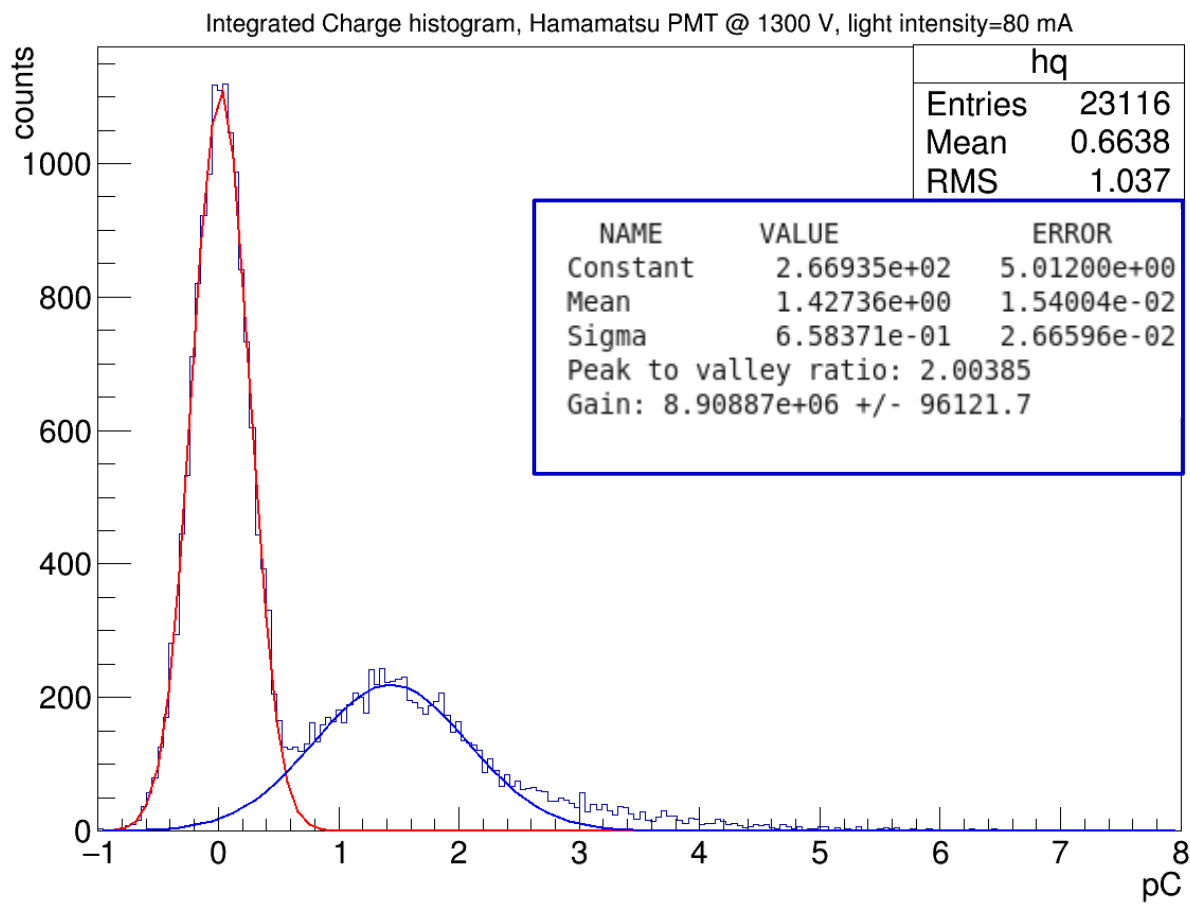


Figure 24

Integrated Charge histogram, Hamamatsu PMT @ 1330 V, light intensity=80 mA

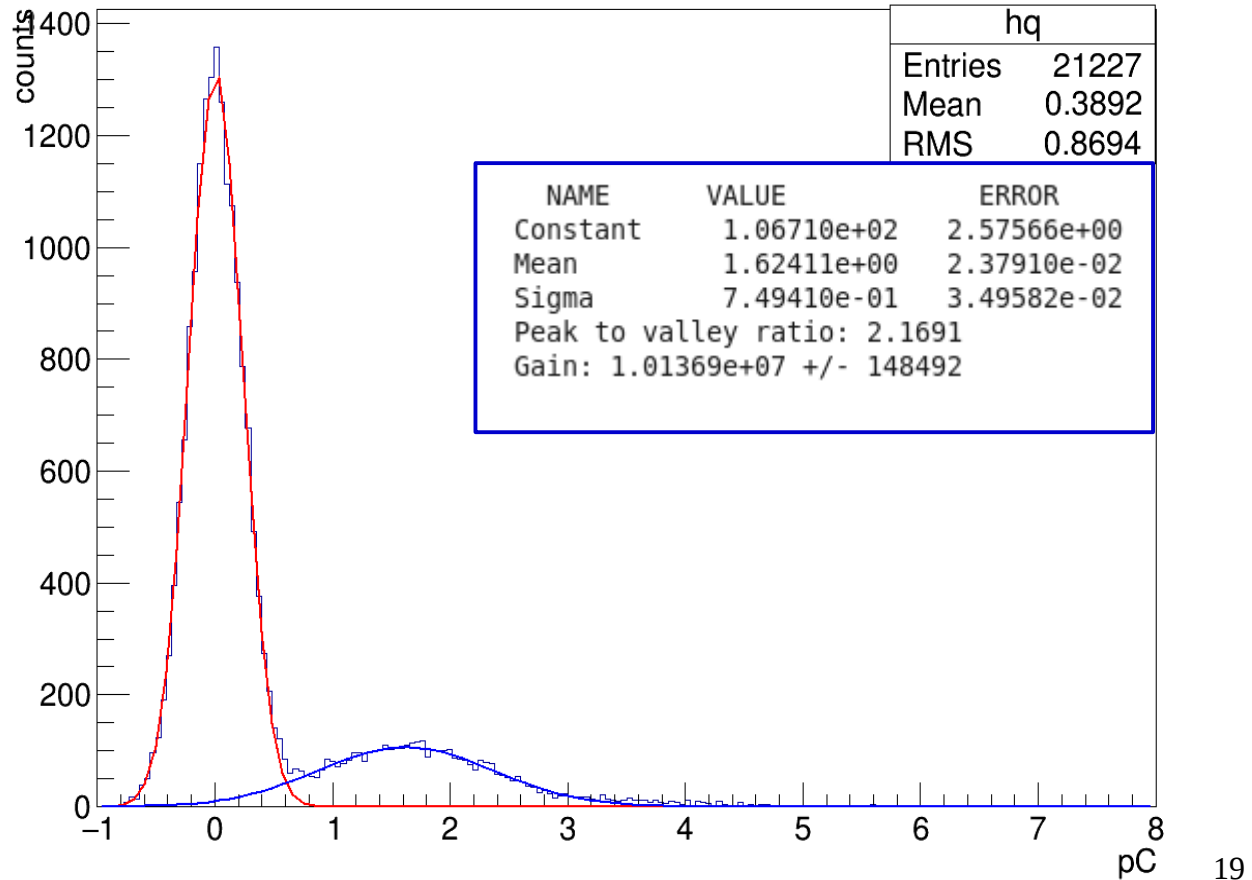


Figure 25:

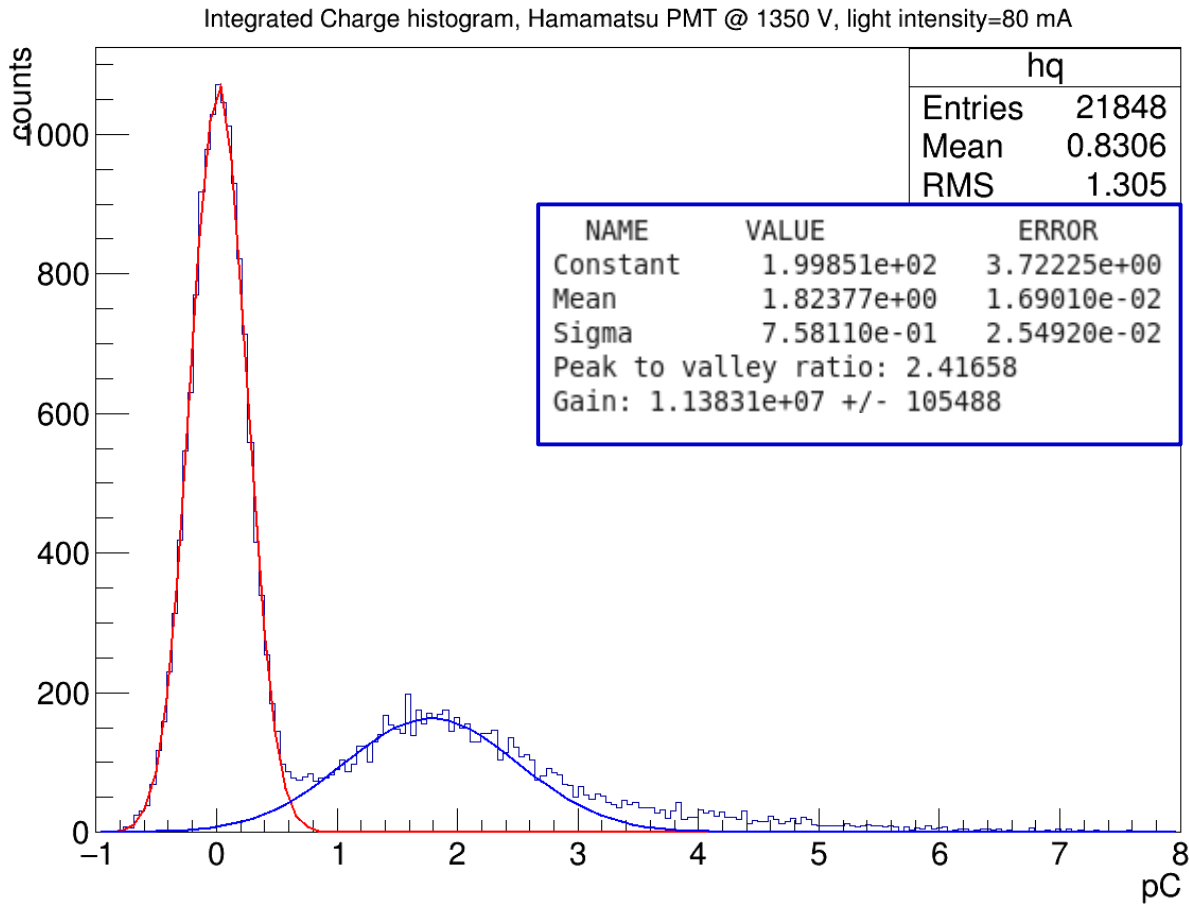


Figure 26

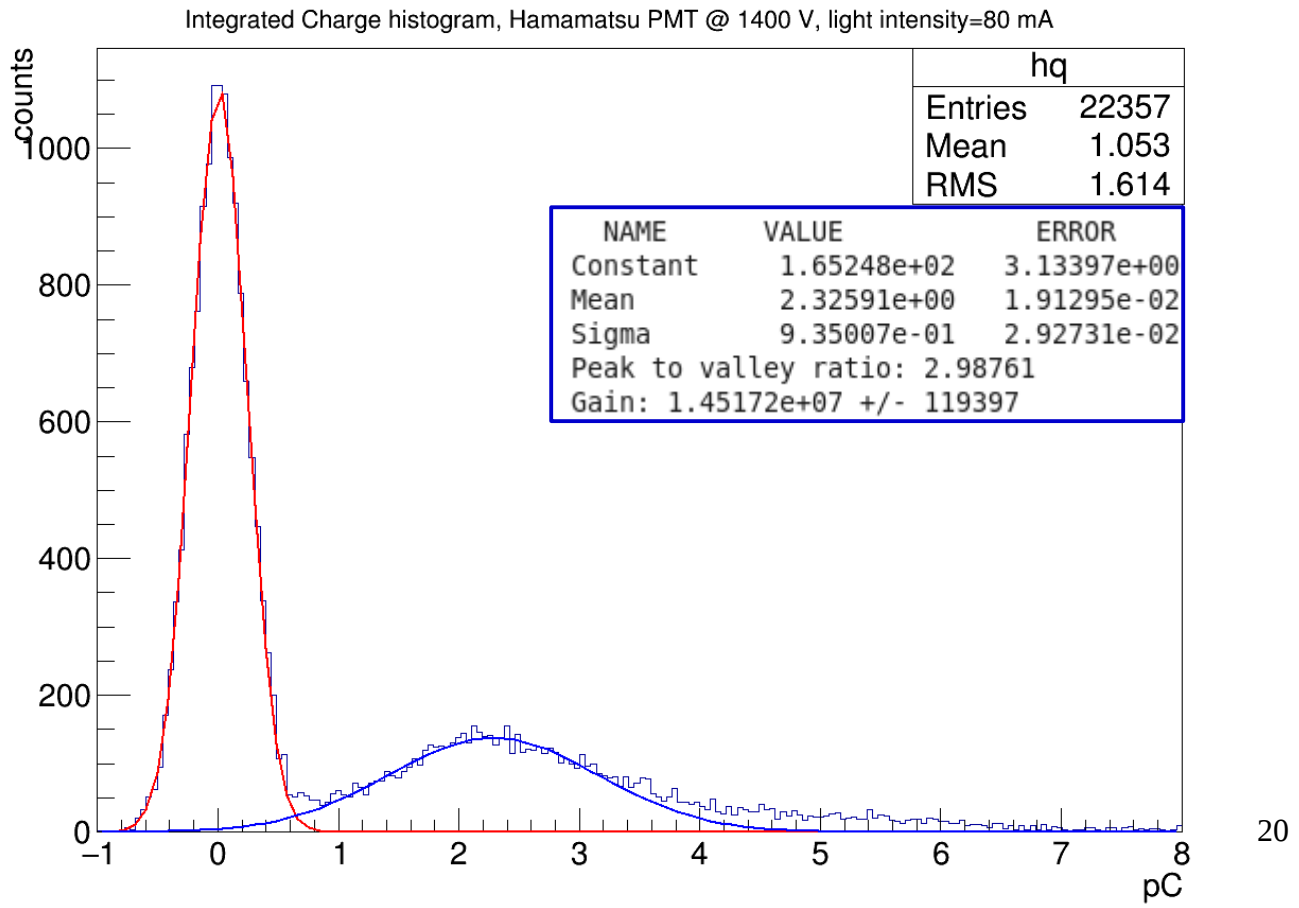


Figure 27

Notice that the tail to the right of the histograms are much smaller, which allows us to better determine the maximum of the 1 p.e. peak. Also notice that the integrated charge histogram for the Hamamatsu PMT at 1100 V (figure 21) does not have two distinct peaks. Instead, it has one main peak centered around 0 pC for the case where no current was produced at the anode. This is because 1100 V is too low for the photoelectrons emitted to multiply and produce substantial charge at the anode. So the 1 p.e. peak is very small and cannot be separated from the 0 p.e. peak. The plot of natural logarithm of gains vs high voltage is shown below (made using `read_chargedistribution.C`):

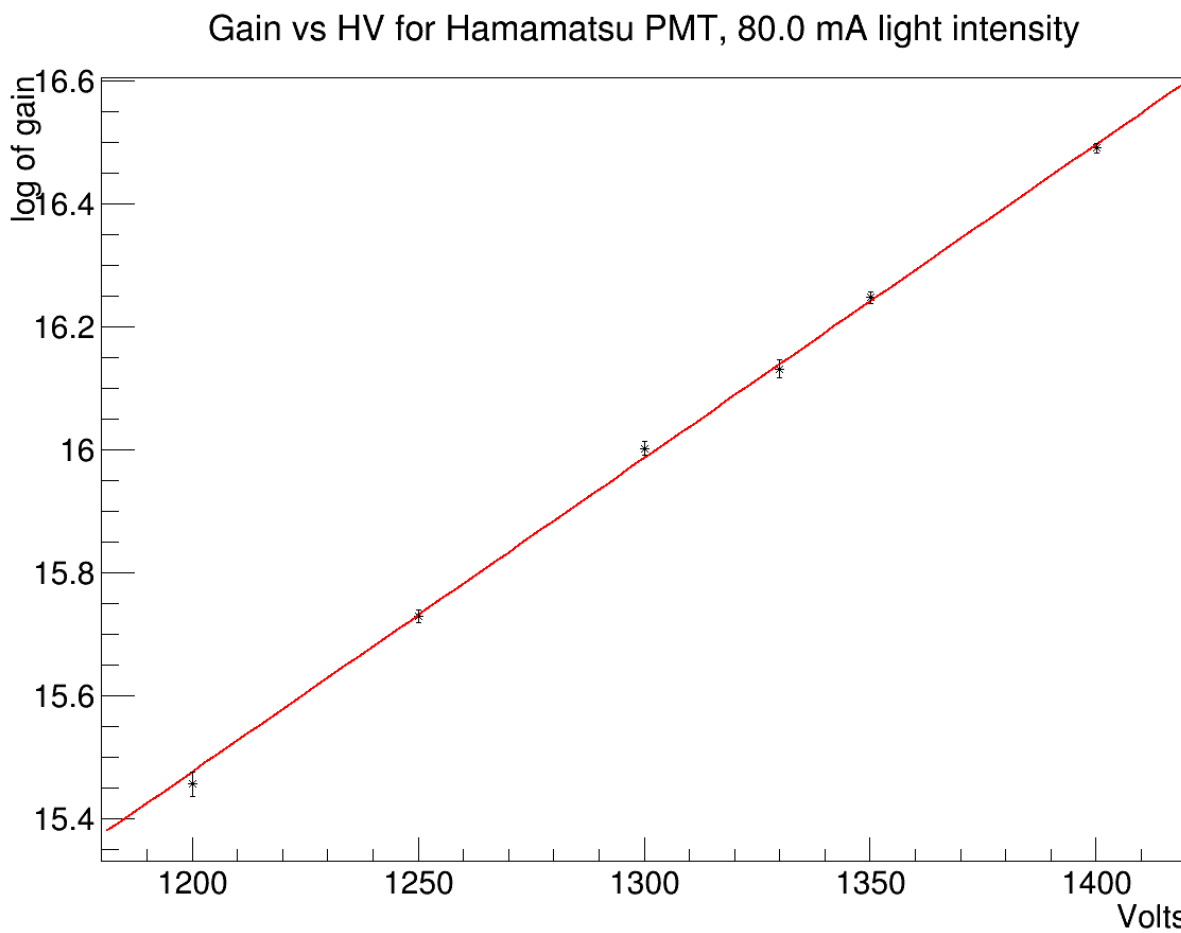


Figure 28: natural logarithm of gain (from integrated charge plots in figures 22-27) vs High Voltage.

The following are integrated charge plots for the ETEL PMT at a light intensity of 80 mA and varying voltages:

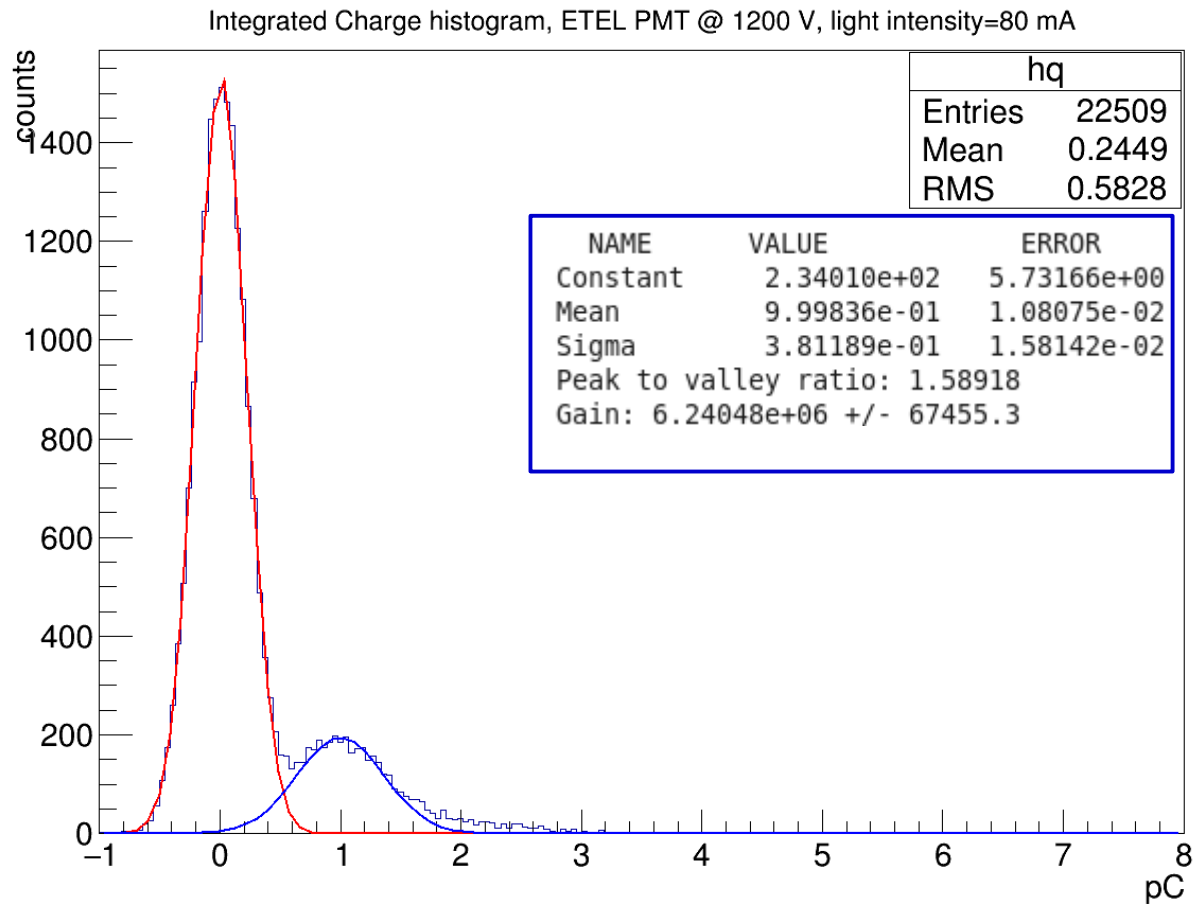


Figure 29

Integrated Charge histogram, ETEL PMT @ 1250 V, light intensity=80 mA

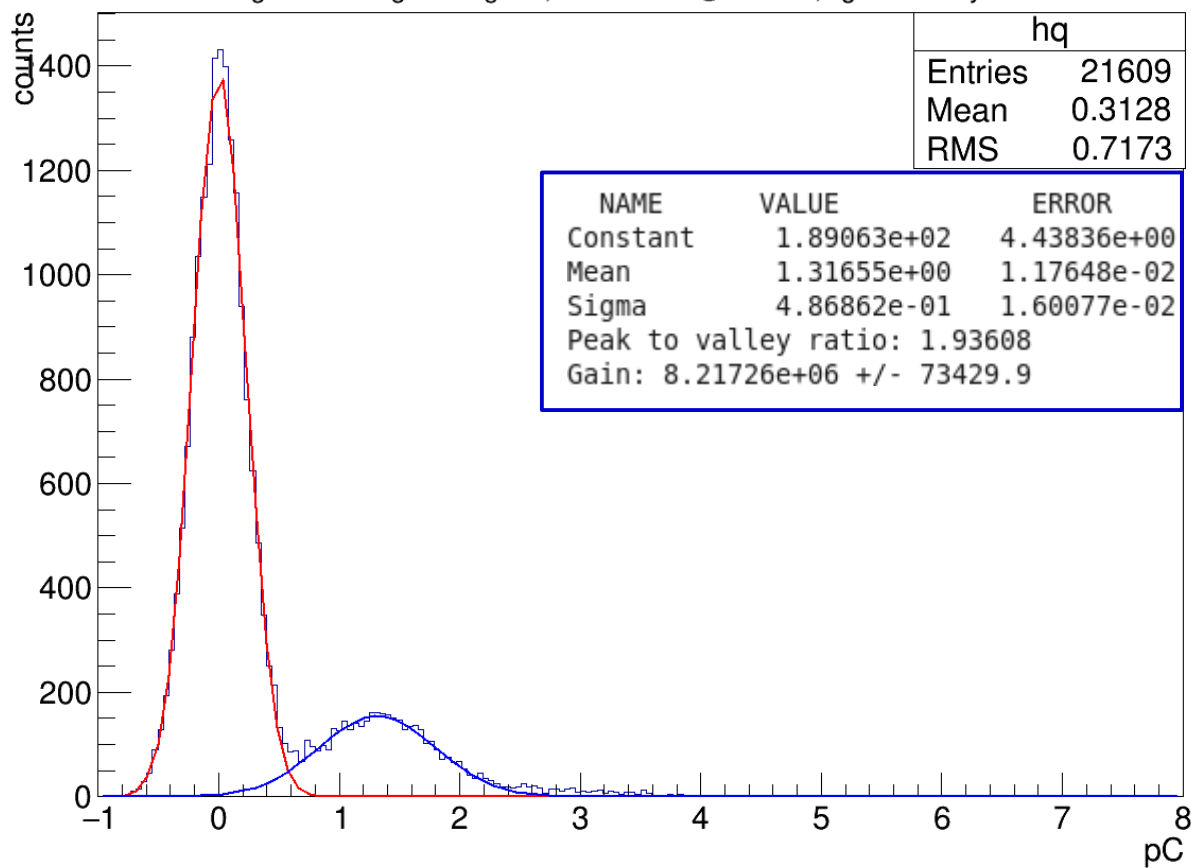


Figure 30

Integrated Charge histogram, ETEL PMT @ 1300 V, light intensity=80 mA

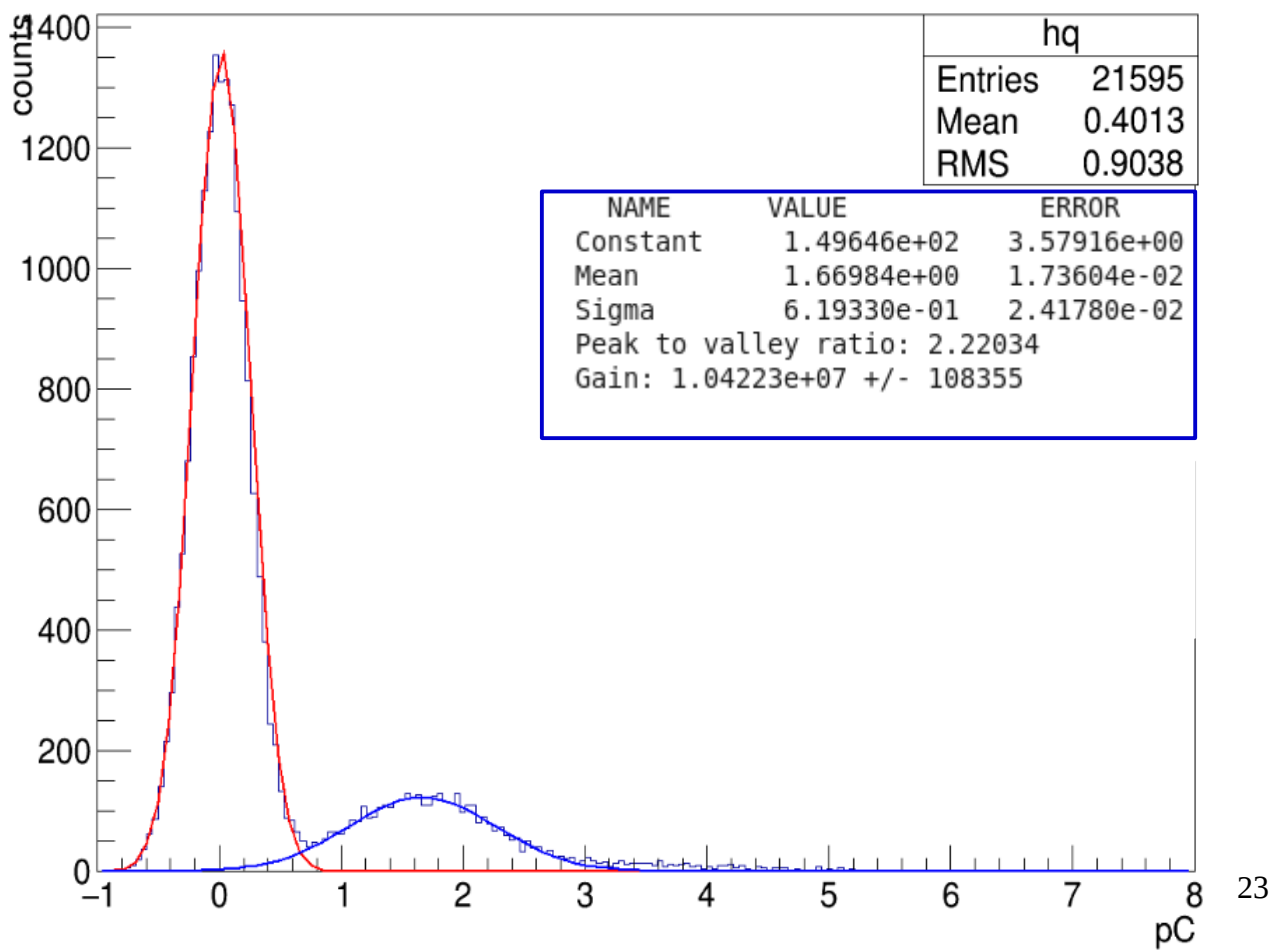


Figure 31

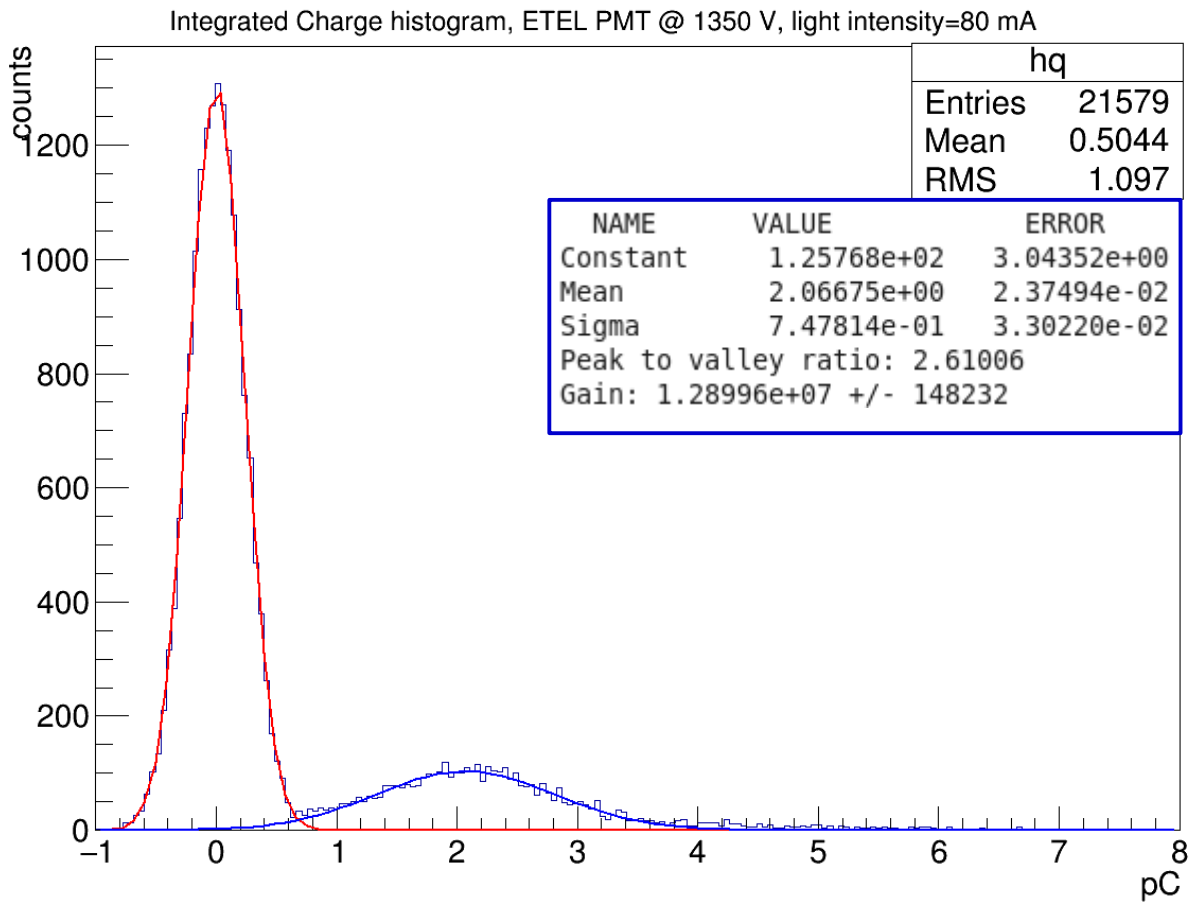


Figure 32

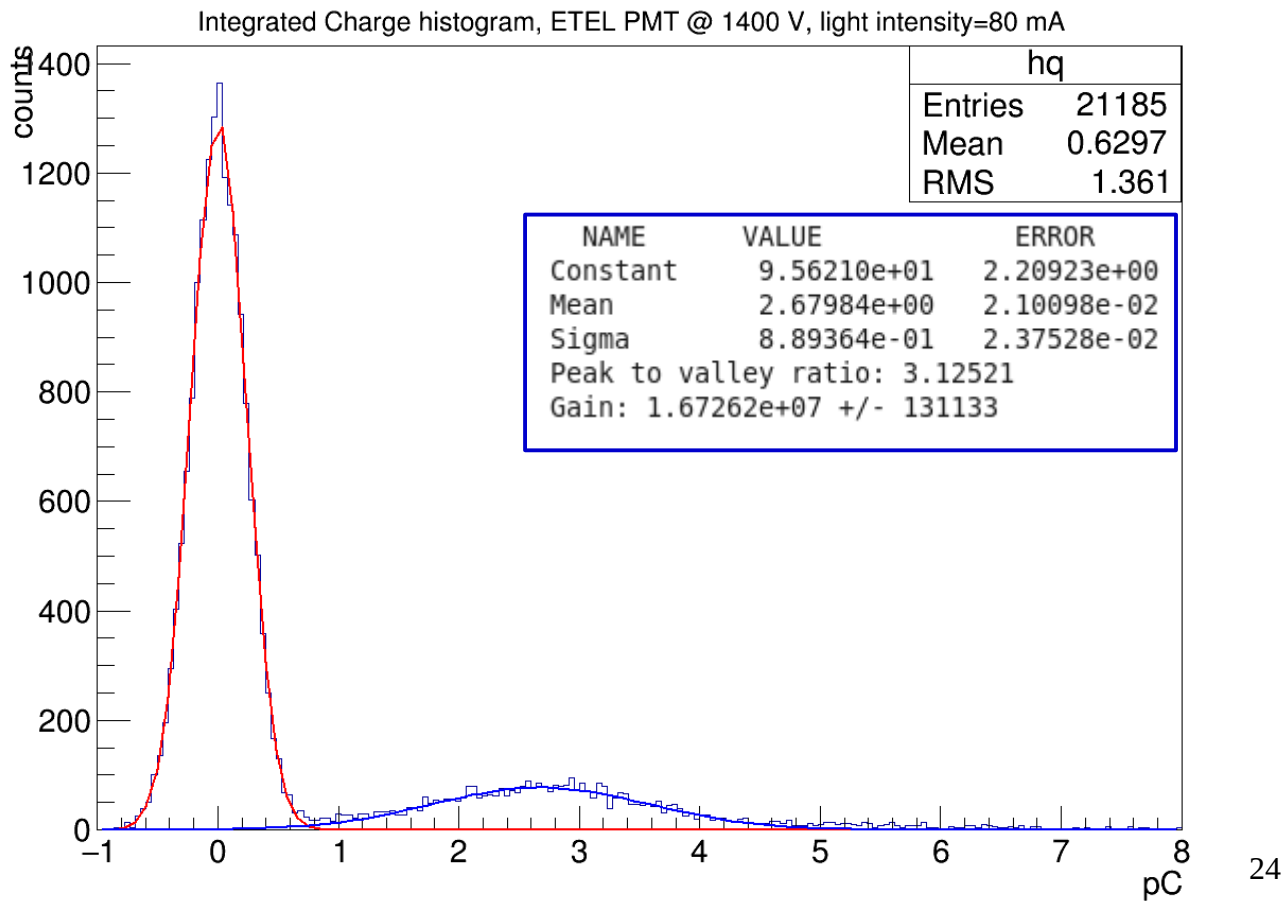


Figure 33

Below is the plot of the natural logarithm of gain vs high voltage:

Gain vs HV for ETEL PMT, 80.0 mA light intensity

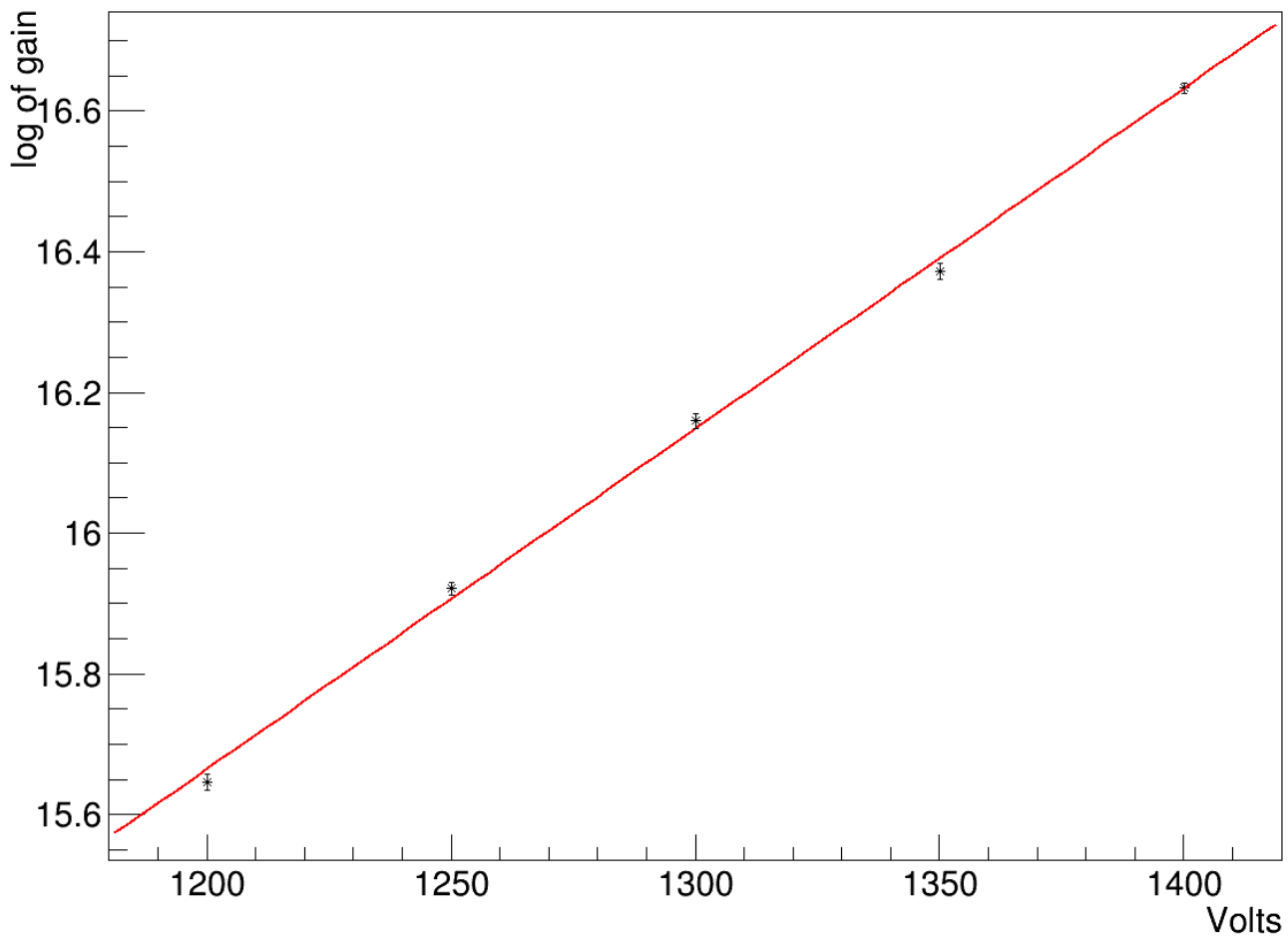


Figure 34: Natural logarithm of gain (from integrated charge plots in figures 29-33) plotted vs high voltage.

We made the (somewhat arbitrary) choice of doing our measurements at a gain of 10^7 , which corresponds to a high voltage of 1293.7 V for the 3-inch ETEL PMT and 1325.8 V for the 3-inch Hamamatsu PMT.

Chapter 4

Dark Count Versus Gain

Dark count is when current is produced in the absence of shining light at the PMT. At room temperature and operating voltages, thermionic emission of electrons is the dominant source of dark counts. We wish to know dark count as a function of voltage in order to find an operating voltage that minimizes the dark count. Our dark count threshold is 40% the voltage of a 1 p.e. pulse (figure 35). Dark count is the number of these dark count pulses divided by the total number of waveforms (figure 36).

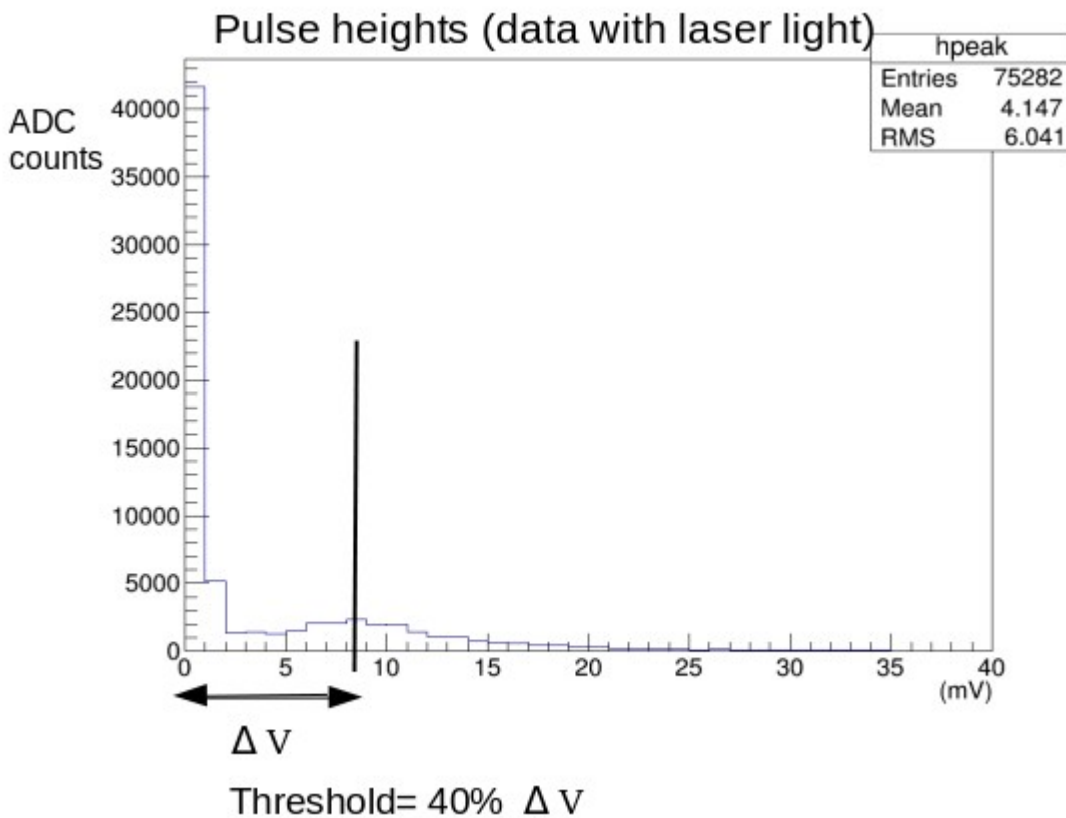


Figure 35: We produce a histogram of the pulse height of all the waveforms when we shine laser light at the PMT, find the voltage of maximum of the 1 p.e. peak (ΔV). We then look at data where the PMT's are in darkness, and declare a dark count pulse if we find a pulse whose height is greater than 40% ΔV .

Pulse heights (data without laser light)

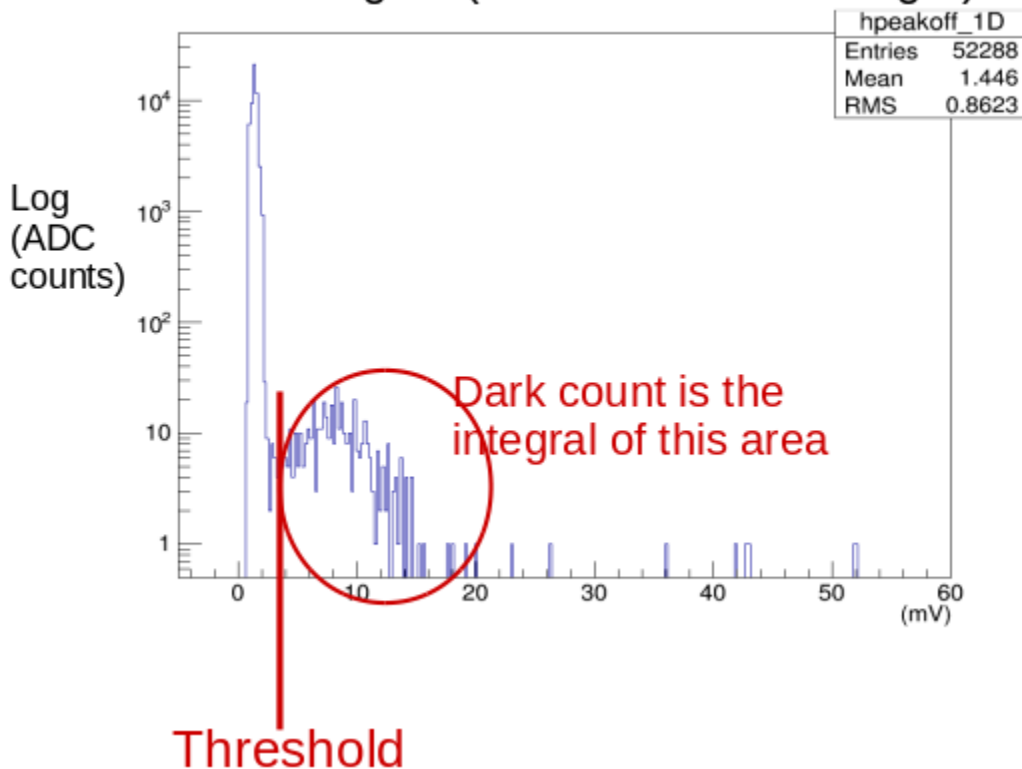
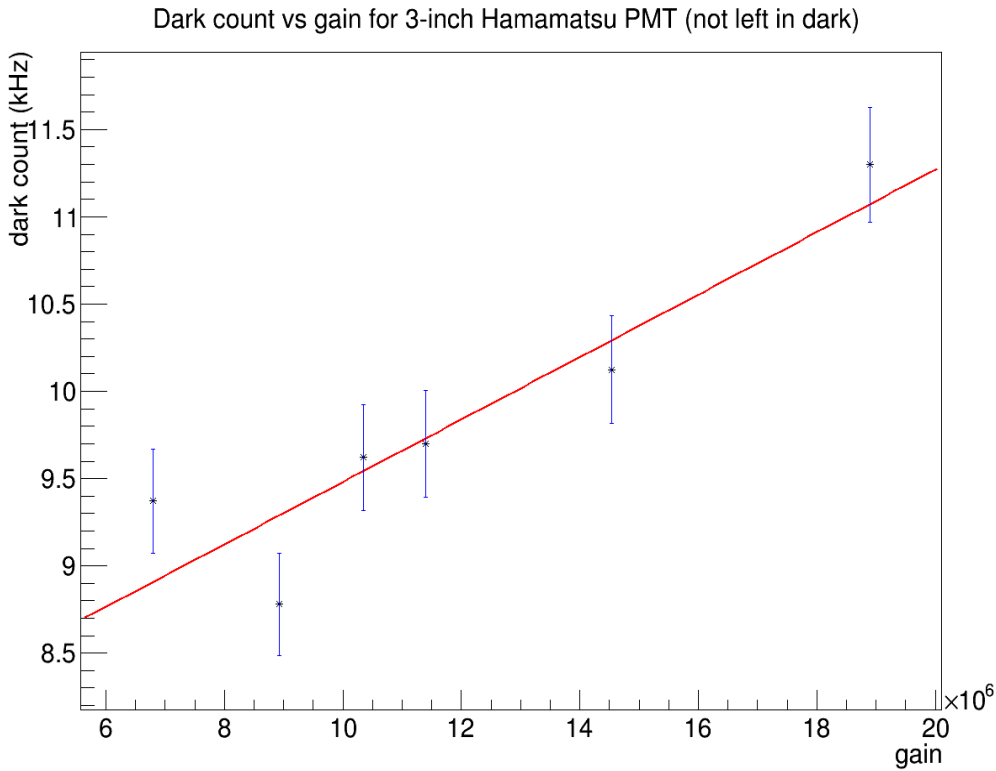


Figure 36: Dark count is the integral of the area to the right of the threshold.

The following is the dark count vs gain plot for the 3-inch Hamamatsu PMT' (made by /home/pmt_pc_2/software/code/fast_hama_darkrate.C):



$$\begin{aligned} p_0 &= 7.69248 \quad +/- \quad 0.397165 \\ p_1 &= 1.7886e-07 \quad +/- \quad 3.2678e-08 \end{aligned}$$

Figure 37: Where p_0 is the y-intercept and p_1 is the slope of the line

The dark count increases as a function of gain, which is expected. The following is the same plot for the 3-inch ETEL PMT (made by `fast_etel_darkrate.C`):

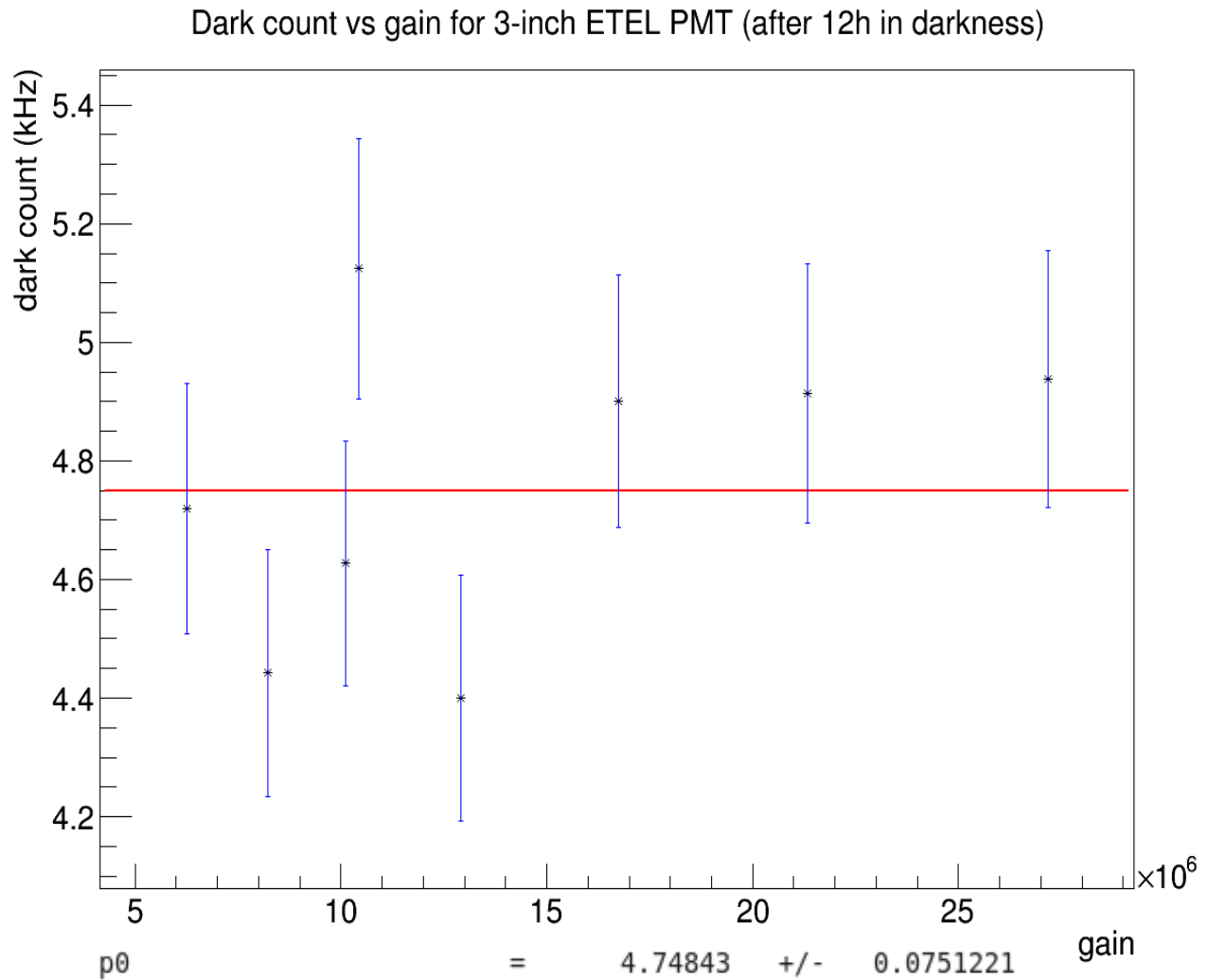


Figure 38: Where $p0$ is the value of the constant.

In this case, the dark count is constant since light leakage (as opposed to operating voltage) is the dominant source of dark counts. We later fixed the light leakage and will redo this measurements.

Chapter 5

Dark count over time

The purpose is to measure dark count as a function of time that the PMT is left in darkness in order to find its minimum dark rate. We also measured the temperature for each data point, and observed that temperature varies a maximum of around 5 degrees Celsius, which is too small to cause variation in dark count. We run “/home/pmt_pc_2/software/code/test_hist_g.C” on the .root file to create pulse height histograms. We then run “/home/pmt_pc_2/software/code/test_darkrate.C” on the pulse height histograms to find the dark count, and plot all the dark counts using “/home/pmt_pc_2/software/code/dcount_time_all.C”. The following is a dark count vs time plot for the 3-inch HZC XP72B20 PMT:

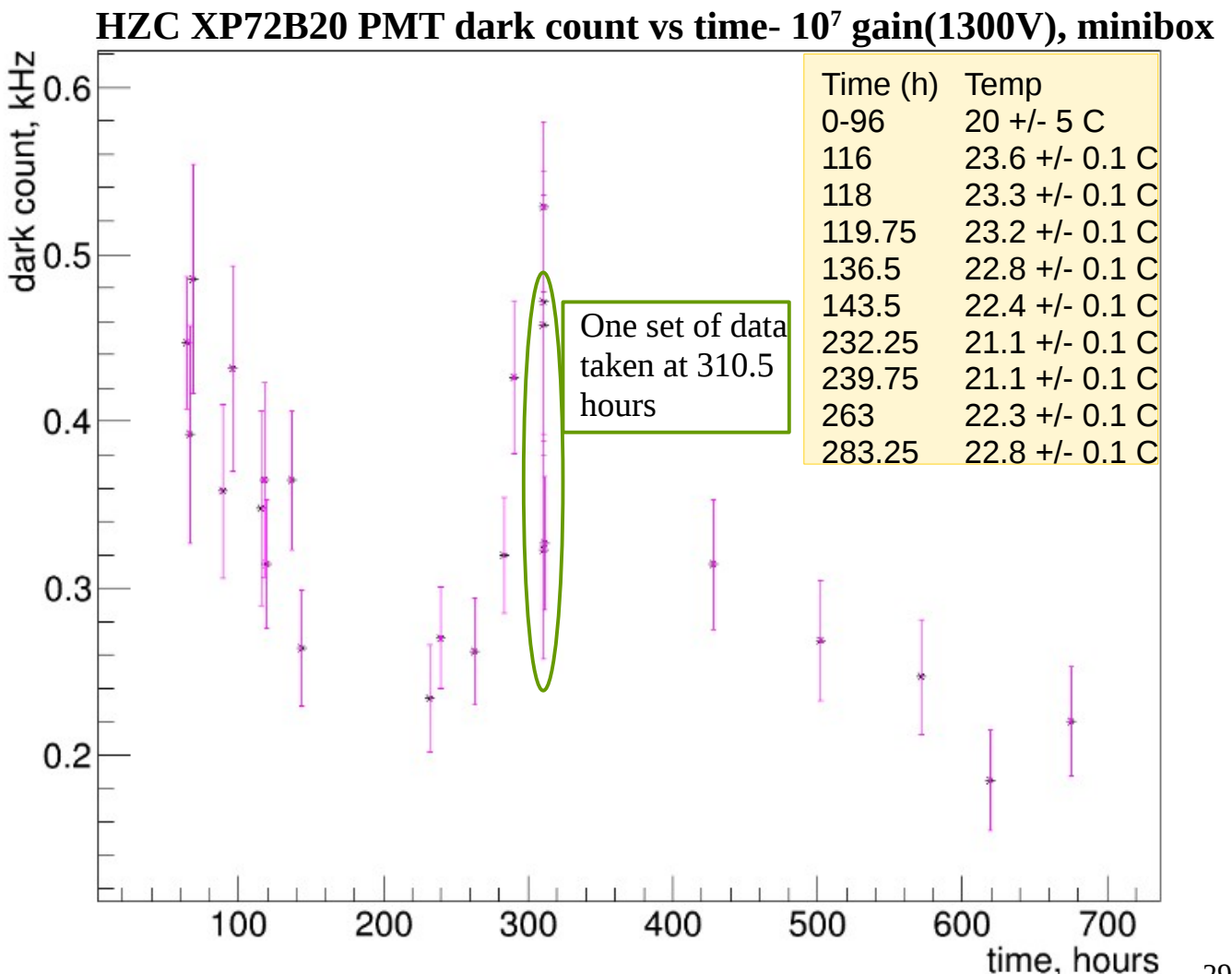


Figure 39: Dark count vs time plot for HZC 72B20 PMT. Notice that I've split one set of data taken at 310.5 hours into three different sets to observe the variation in dark count in three identical sets of data.

The unstable dark count around 200-300 hours is due to the fact that the HZC and Hamamatsu PMT were placed really close to each other until 400 hours. A more representative dark count vs time plot follows:

HZC XP72B20 PMT darkcount vs time- 10^7 gain (1300V) (minibox)

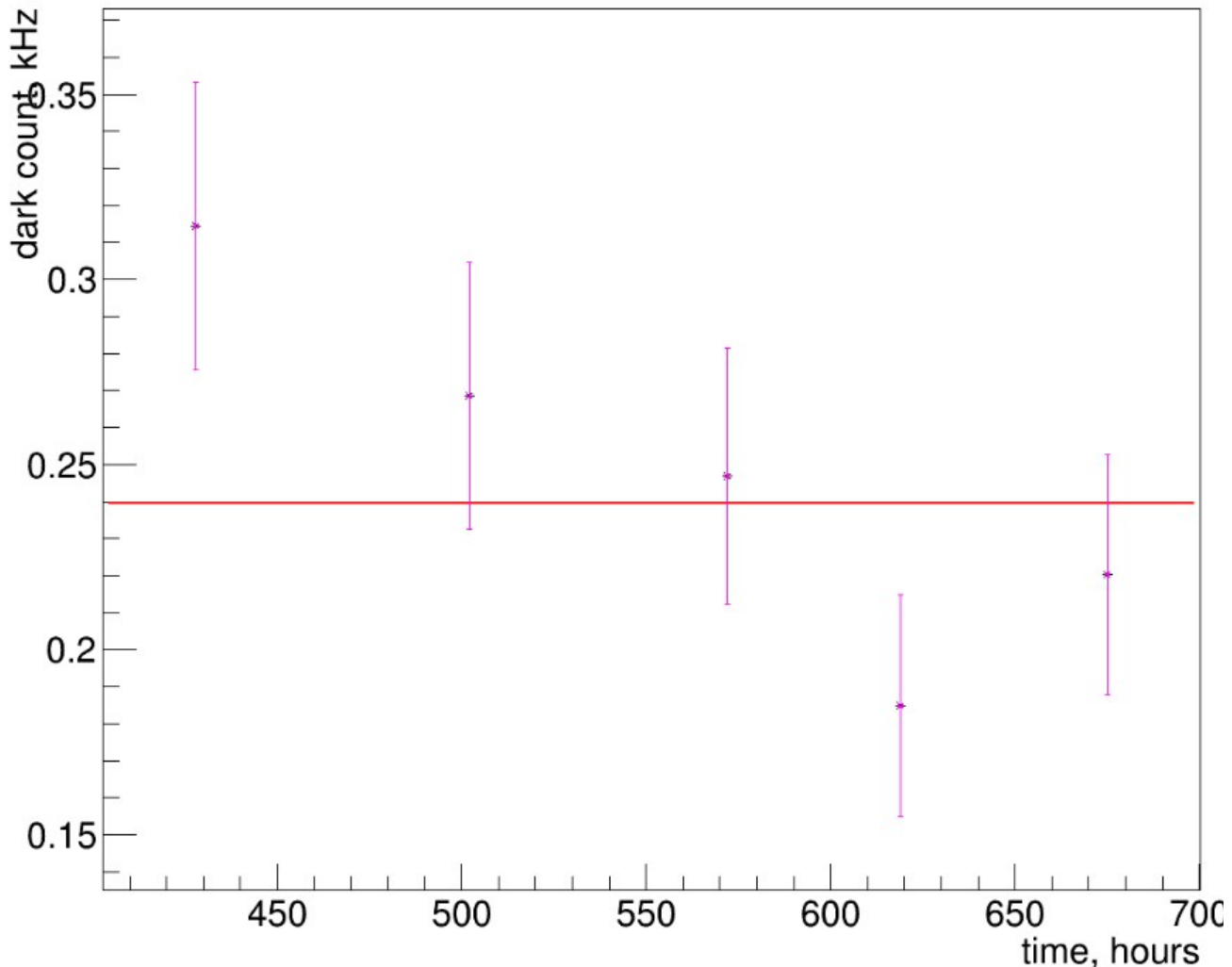


Figure 40: Dark count vs time plot for the HZC PMT after 312 hours, created by Christian Wittemeier, another summer student working on PMT analysis.

Notice that figure 40 is essentially figure 39 without the data from 0 to 312 hours, since we fixed the position of the PMT's in the dark box after 312 hours to ensure the three PMT's are far enough to not affect each other. We conclude that the dark count of the HZC XP72B20 PMT is 0.239 KHz.

The following is the dark count vs time plot for the 3-inch Hamamatsu PMT:

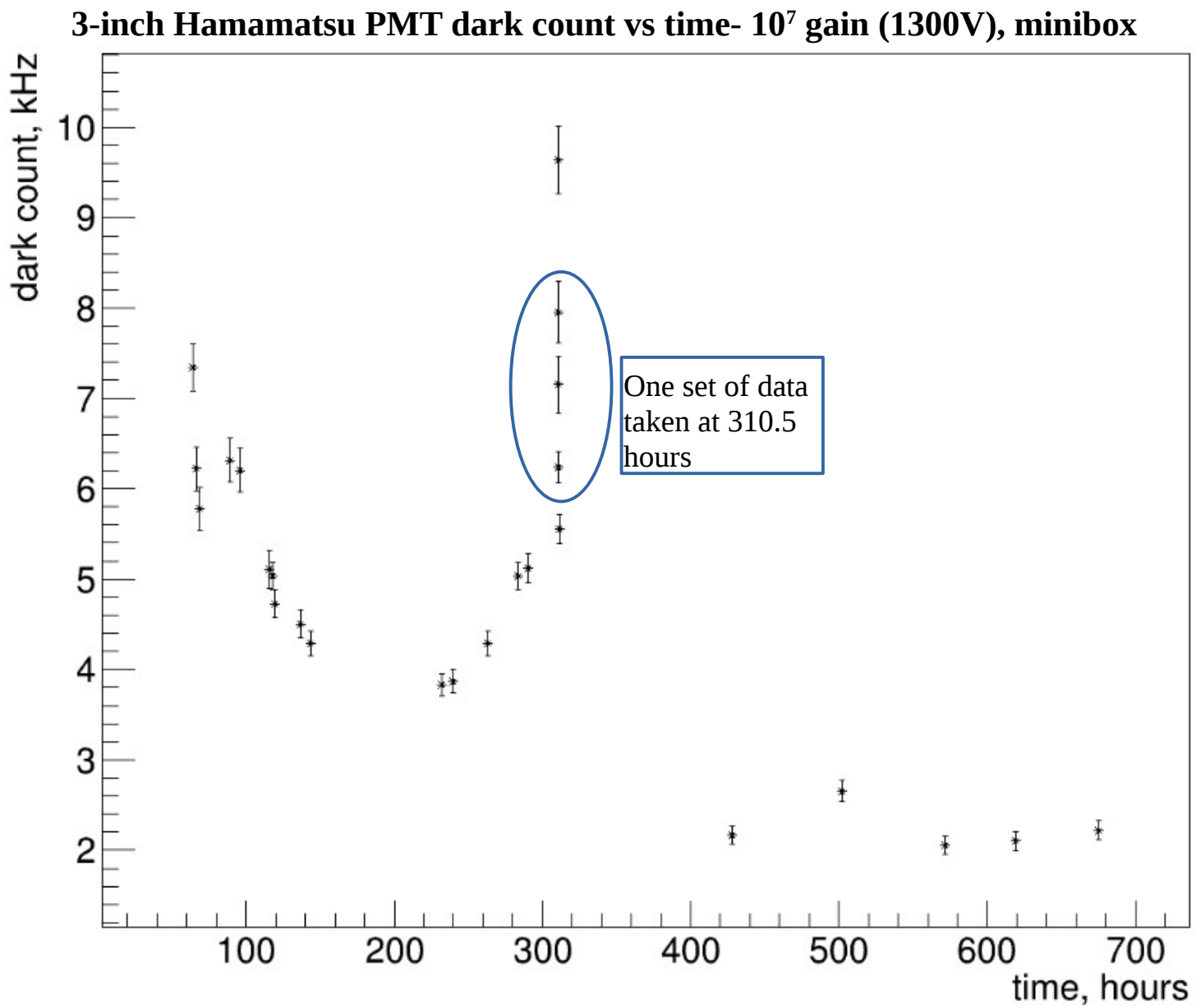


Figure 41

The same issue is observed with the Hamamatsu PMT. A more representative plot of dark count vs time follows:

Hamamatsu PMT darkcount vs time- 10^7 gain (1325V) (minibox)

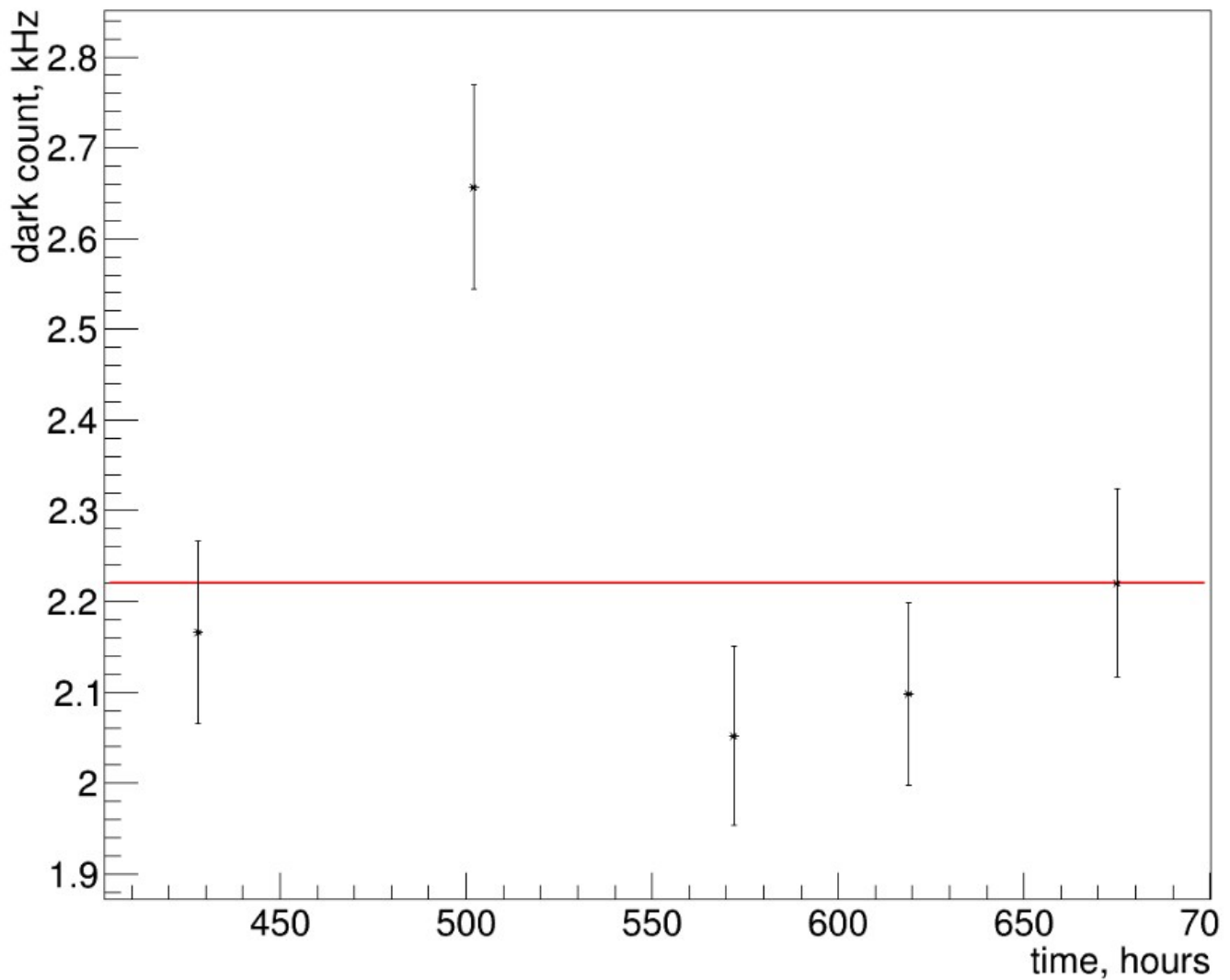


Figure 42: Dark count vs time for the 3-inch Hamamatsu PMT.

We conclude that the dark count of the Hamamatsu PMT is 2.22 kHz.

The following is the dark count vs time plot for the 3-inch ETEL PMT at 10^7 gain:

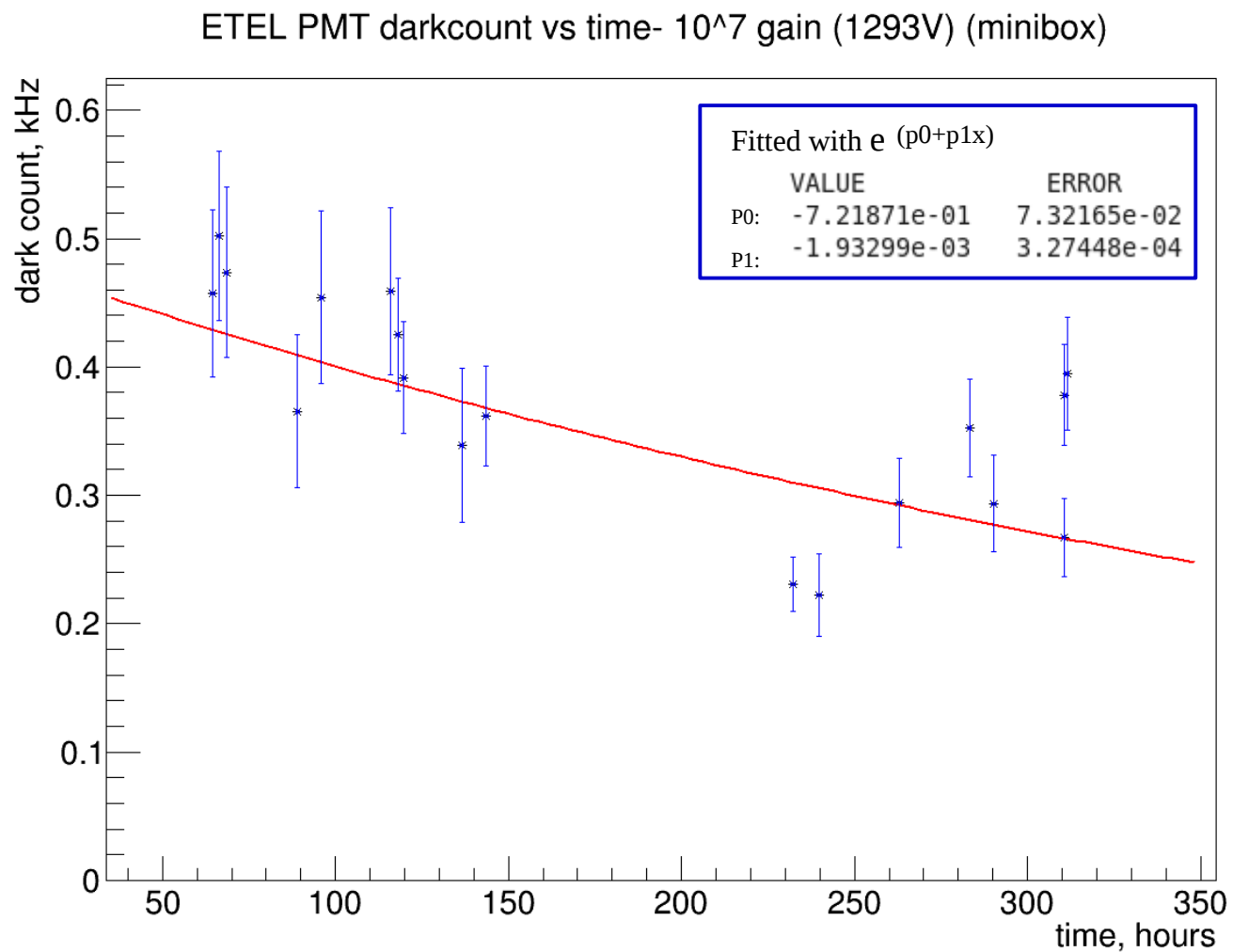


Figure 43:

We conclude that the dark count is 0.070 ± 0.023 kHz (fit evaluated at 1000 hours).

Chapter 6

Timing Resolution Measurements

Our purpose is to shine 405 nm laser light at the 3-inch Hamamatsu and ETEL PMT's to measure their timing resolution. We used the CAEN DT5720 digitizer, which inputs the signal from the PMT's and creates waveforms like the one in figure 44. Since this digitizer has a timing resolution of 4 ns, the data points in the waveform are at least 4 ns apart. Since the pulses are ~ 15 ns, there are only only ~ 4 data points in the pulse. This makes it difficult to fit the pulse and measure the true peak time.

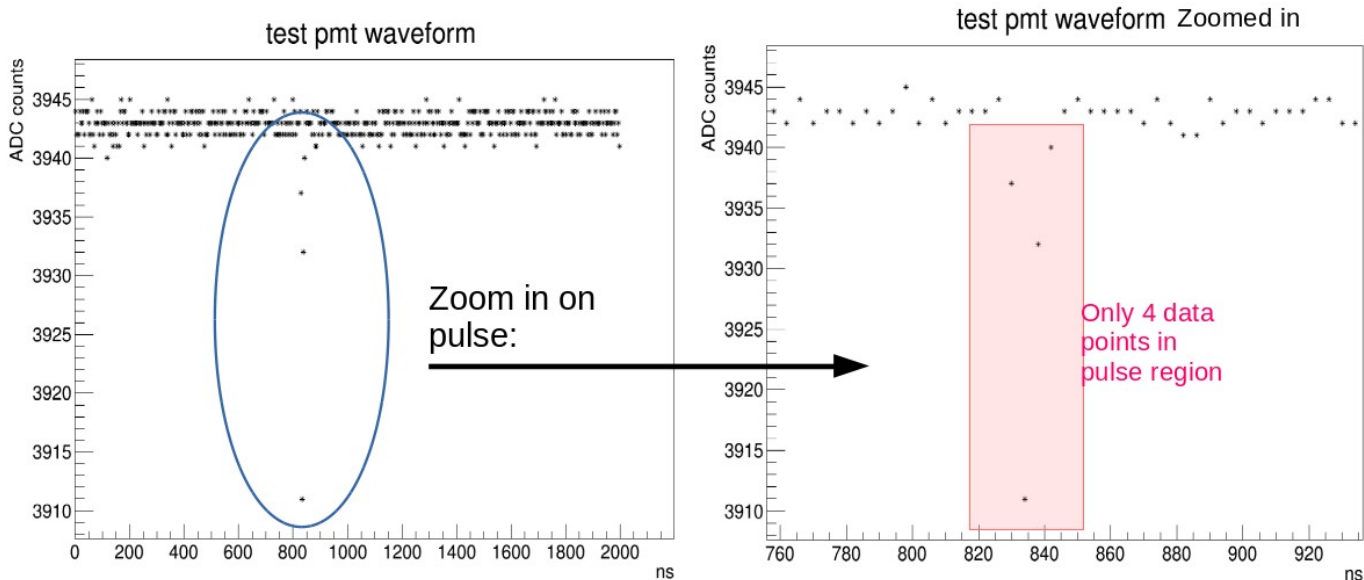


Figure 44: A waveform created by the CAEN DT5720 digitizer. Notice there are only a few data points in the pulse.

We fit the pulses in the test and monitor PMT using a modified version of an Exponentially Modified Gaussian (EMG):

$$f(x; \mu, \sigma, c) = b + a \exp \frac{\mu + \frac{\sigma^2}{2c} - x}{c} \operatorname{Erf} \left(\frac{\mu + \frac{\sigma^2}{c} - x}{\sqrt{2}\sigma} \right)$$

Where

- a = amplitude
- b = baseline of pulse
- c = decay constant
- mu = mean of pulse

We found that fitting with an EMG resulted in some failed fits, so we modified the EMG by changing the parameters for amplitude, which gave us better fits. Figure 45 shows sample monitor and test PMT pulses with the modified EMG fit (created by /home/pmt_pc_2/software/code/master_timing_res.cpp by setting the Boolean single_waveform=true)

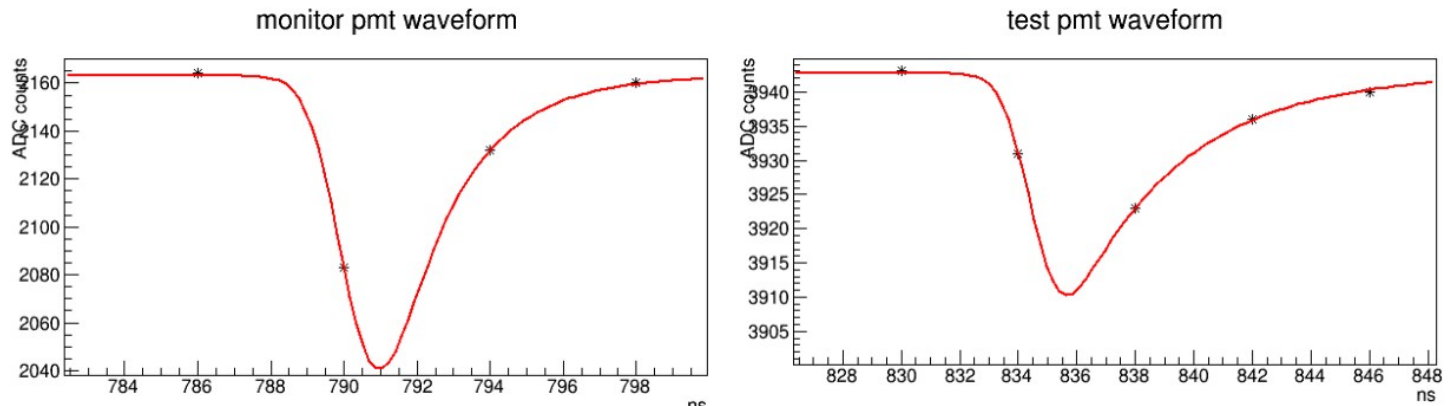


Figure 45: Monitor and test PMT waveforms with the modified EMG fit.

Figures 46 and 47 show the pulse height distributions (calculated from the fit) of the monitor and test PMT (created using master_timing_res.cpp, by setting single_waveform=false). Notice that we only consider events where the the test PMT registers a pulse, which corresponds to events where height of the test PMT's pulse is greater than 6 ADC counts (figure 47).

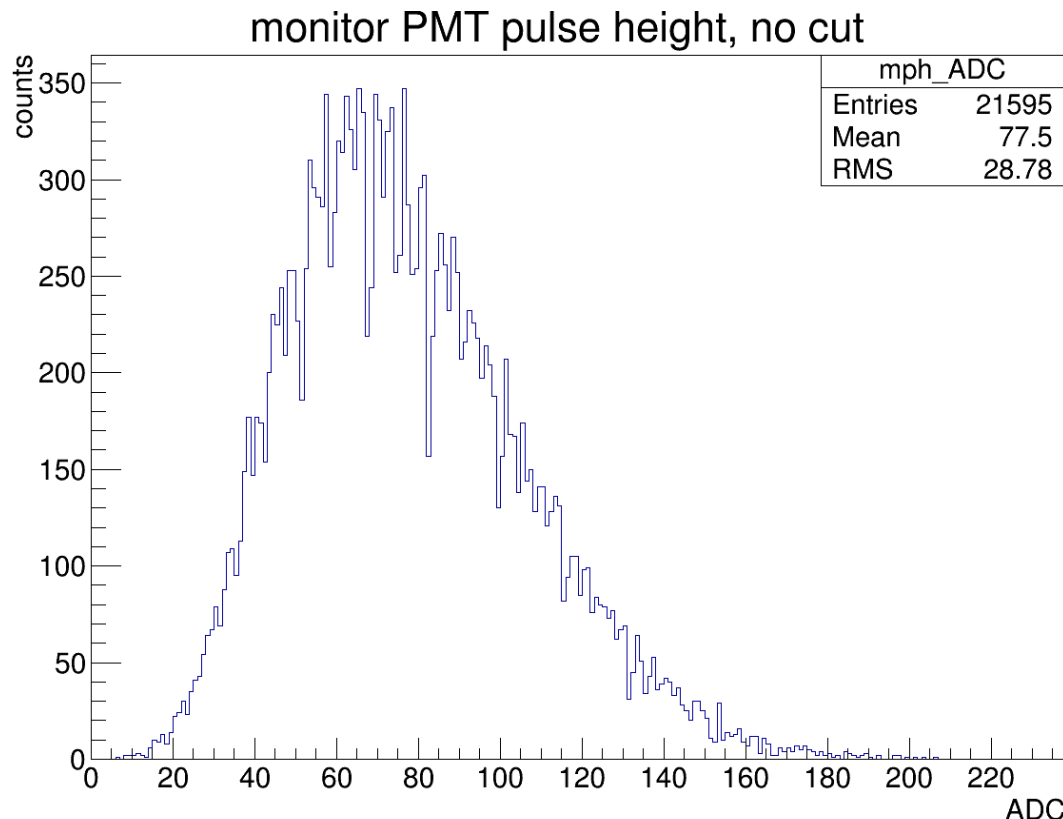


Figure 46

test PMT pulse height, before cuts, ETEL PMT @ 1300 V, light intensity=80mA, digitizer data, file 157

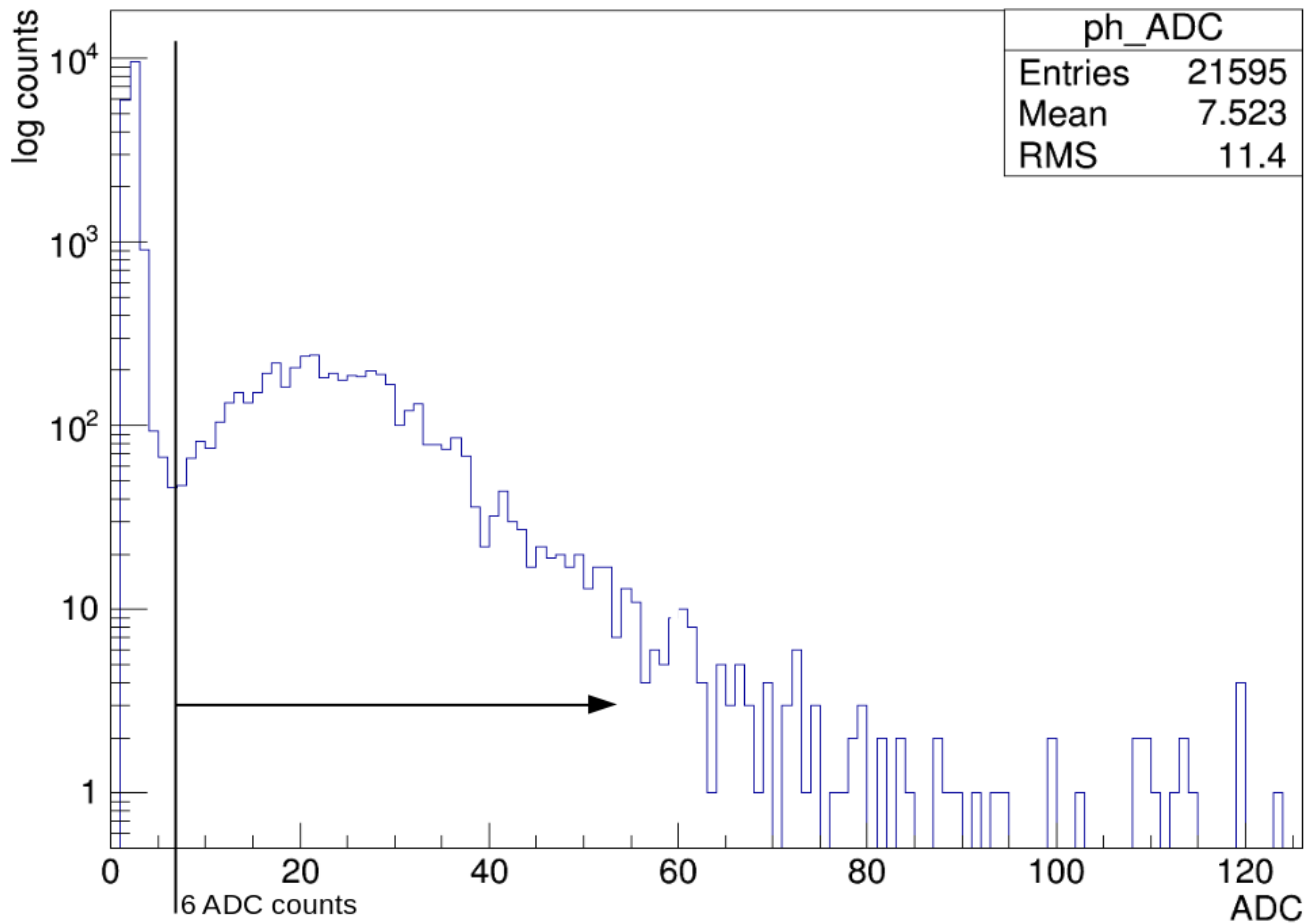


Figure 47: Histogram of the test PMT pulse heights (from the fit). We only consider events where the test PMT pulse height > 6 ADC counts. Note that the file number in the title tells us the name of the root file that generated this plot (in this case, output00000157.root)

Figure 48 shows histograms of the monitor and test PMT peak times. In addition to the restriction of test PMT pulse height, we only consider events where the pulse happens between 700-1100 ns because events outside this region are dark noise pulses, which are not the subject of this measurement. Notice there are several peaks that are each 4 ns apart. This is because there are only a few data points in the pulse, so the value of the peak from the fit is dragged toward one of the data points. Since the data points are 4 ns apart (resolution of the digitizer), the peak values from the fit are also 4 ns apart.

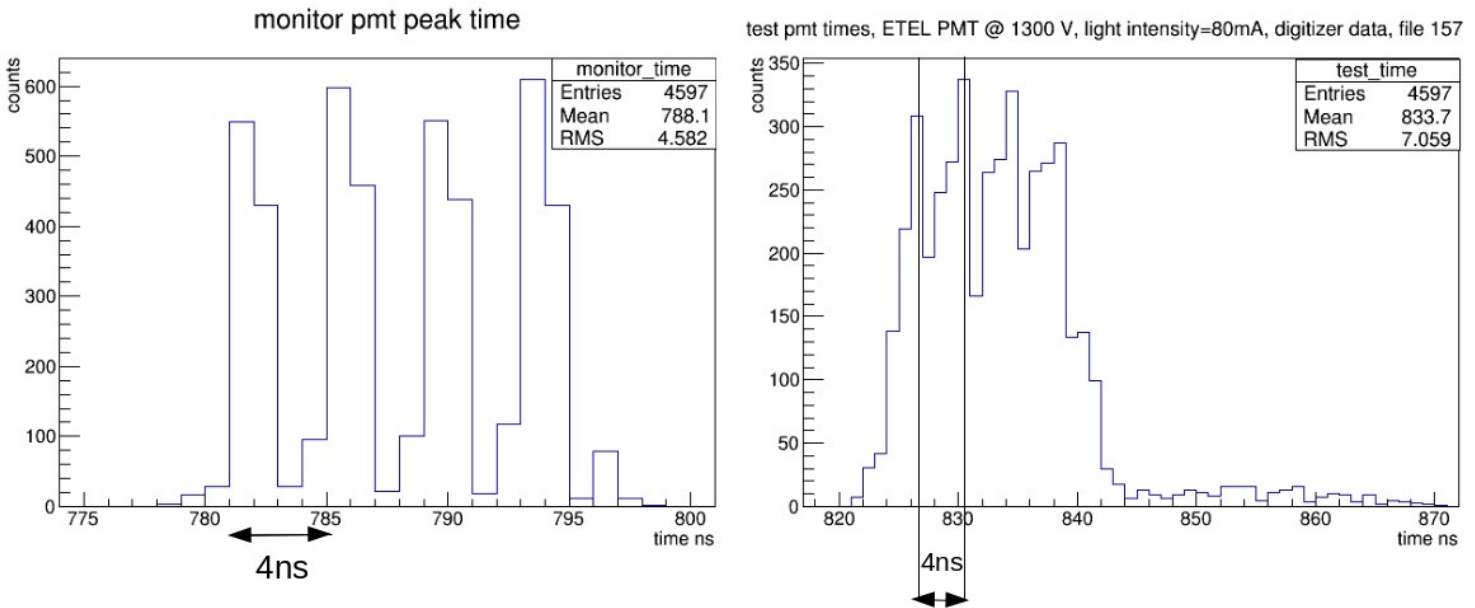


Figure 48

We define timing difference as the peak time of the test PMT minus the peak time of the monitor PMT (figure 49). Figure 50 shows the timing difference histogram. The full width half maximum of the histogram (FWHM) is 4.00 ± 0.05 ns.

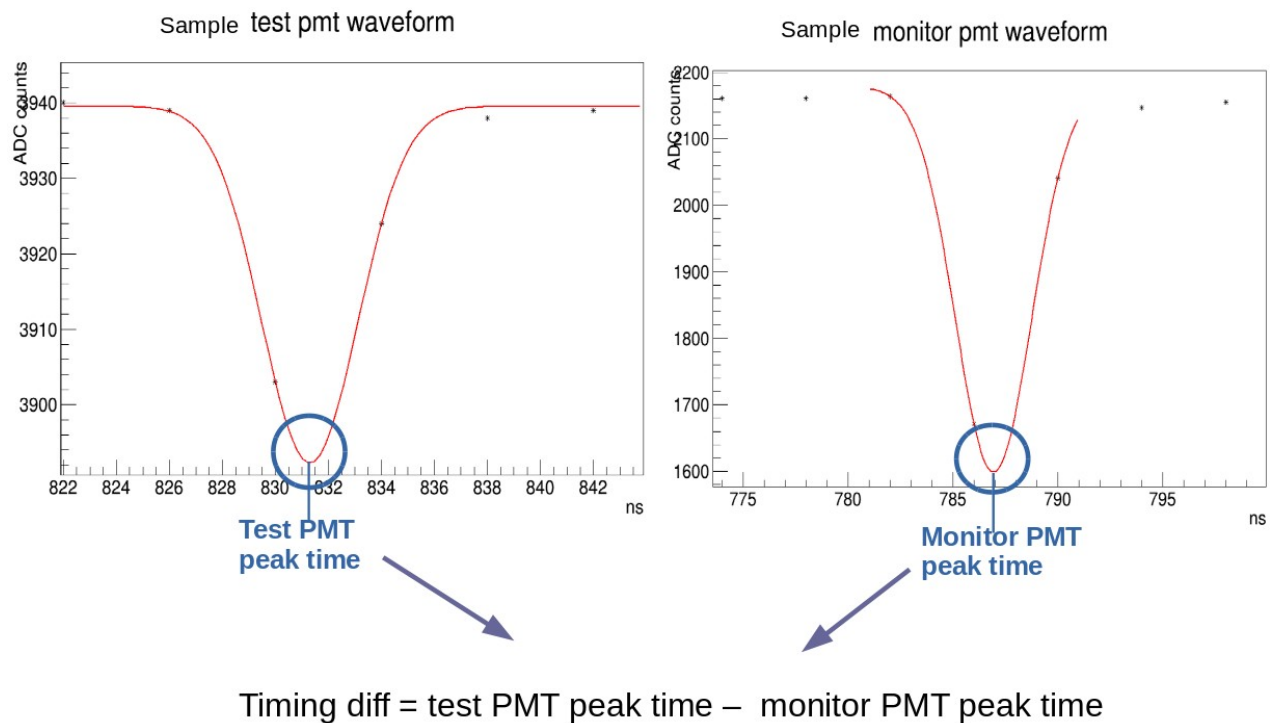


Figure 49

Timing difference histogram: ETEL PMT @ 1300 V, light intensity=80mA, digitizer data, file 157

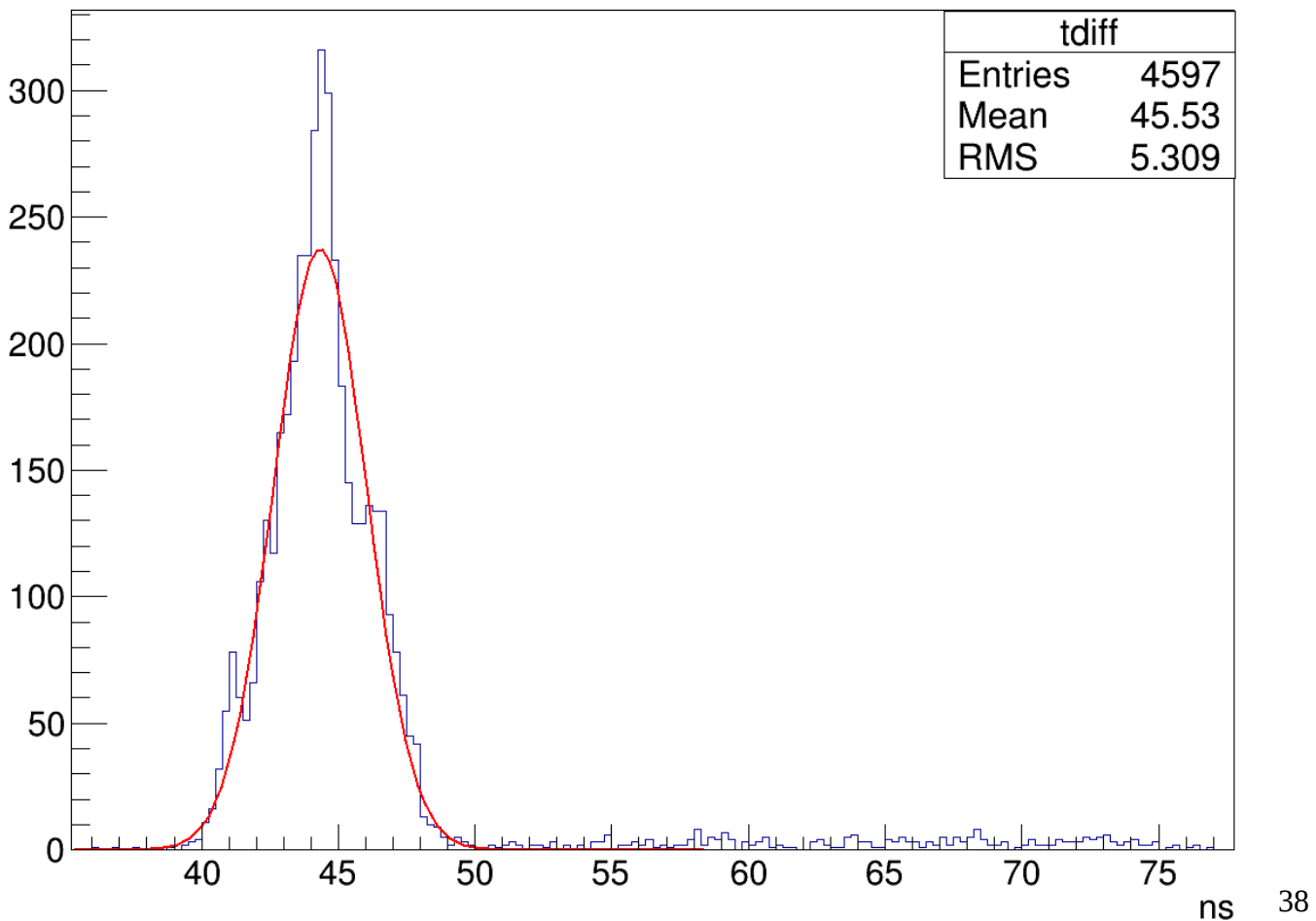


Figure 50: FWHM is 4.00 ± 0.05 ns, where the error is from the fit.

Double Pulses

We noticed that some waveforms had two pulses (figure 51). In figure 52, we plot the difference in the time of the two pulses. Waveforms enter this histogram if there is second a pulse outside ± 10 ns of the biggest pulse, and if the height of the second pulse is greater than 5 ADC counts.

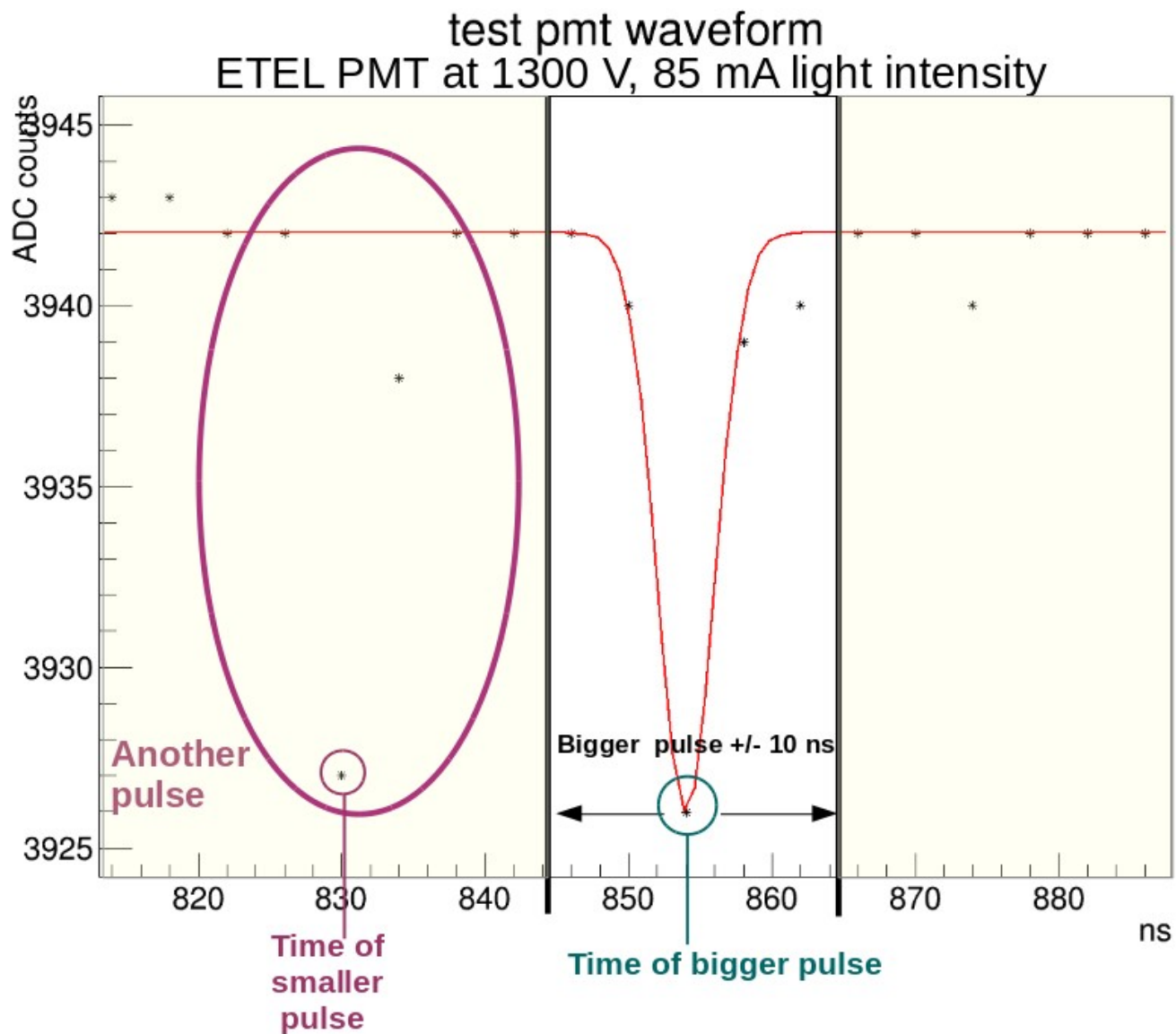


Figure 51: This waveform has two pulses

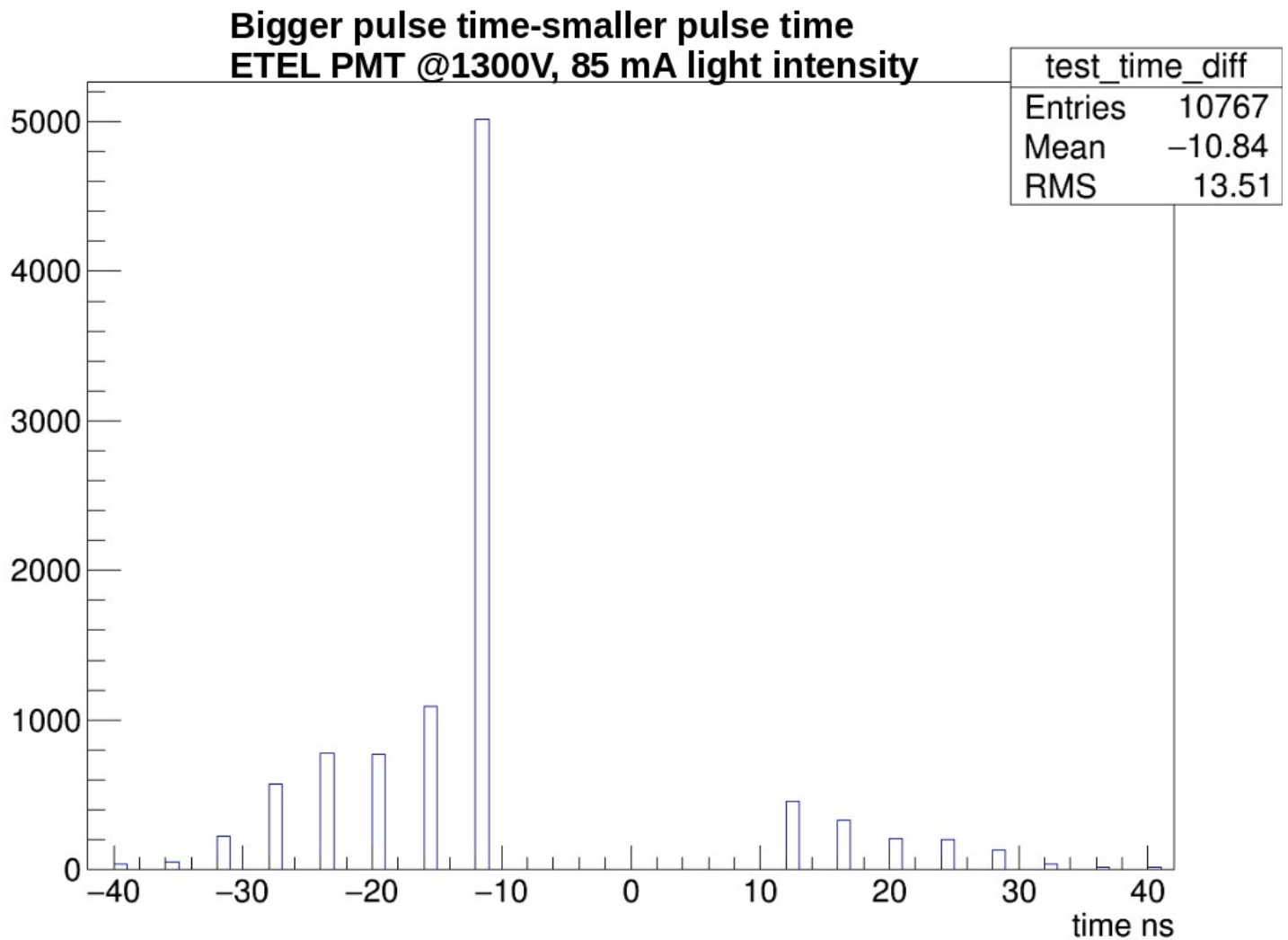


Figure 52: Histogram shows the difference between the time of the bigger pulse and the smaller pulse.

We find that about 20% of our waveforms have a second pulse outside the ± 10 ns region of the first pulse. These second pulses are caused by the elastic scattering of electrons off the first dynode. We observe the same phenomenon with the Hamamatsu R12199 PMT.

Next, we investigate the effect of the 4ns timing resolution of the digitizer on the timing resolution. I plot the timing difference histogram without fitting the waveforms (bottom plot in figure 54). Notice there are two large peaks that are 4 ns apart. This comes from the 4ns discreteness of the data points created by the digitizer. The interesting plot, however, is figure 53. Here, I take all the data points in the first peak of the no fit histogram, fit them, and plot them (the red histogram). Similarly, I take all the data points that fall in the second peak of the no fit histogram, fit them, and plot them (the blue histogram). So, in the right histogram of figure 53, the timing difference histogram with *all* the entries (black line) is approximately¹ the addition of the histograms created by fitting the two peaks from the no-fit histogram(black histogram \approx blue histogram + red histogram). Since the components of the total timing difference histogram are two separate histograms whose means' difference arises from the 4ns timing resolution of the digitizer, the FWHM (of the total timing difference histogram) is artificially increased and this is not a reliable result.

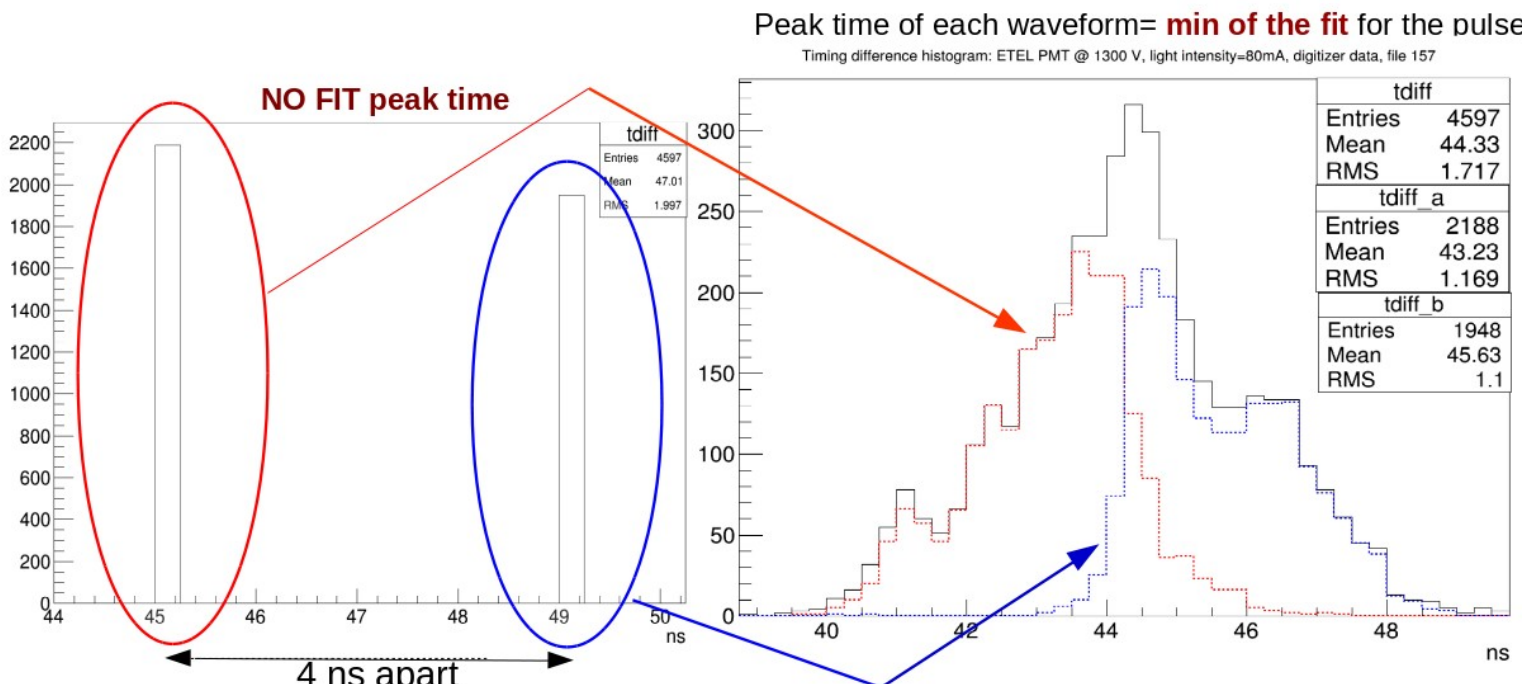


Figure 53: The timing difference histogram (black line) is the addition of two separate histograms that arise from the 4 ns timing resolution of the digitizer. As a result, the FWHM of the timing resolution histogram (4.00 ± 0.05 ns) is artificially increased.

1- The timing difference histogram with all the entries (black line) is the addition of the two histograms (blue and red) whose entries' timing difference without fitting the waveforms falls in one of the two peaks **plus** the few entries where the timing difference doesn't fall into one of the two peaks in the no-fit histogram.

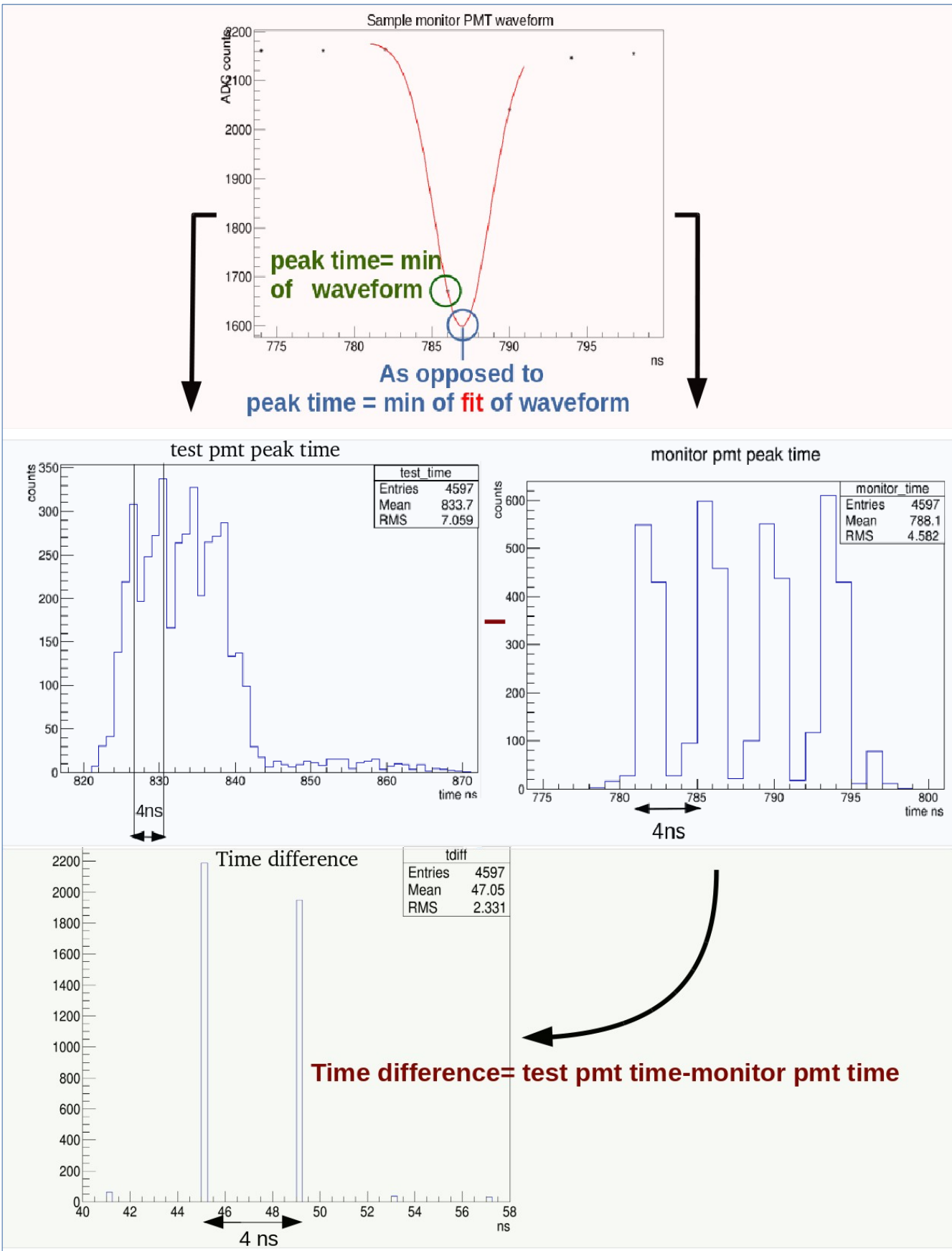


Figure 54

We also look at the time of half the falling height (figure 55) from the fit of the pulse. We wanted to see if these times are less affected by the 4ns discreteness of the data points. However, the red and blue histograms that make up the total timing difference histogram in figure 55 are even more separated than before, meaning that the half times are more affected by the discreteness of the data points. As a result, the FWHM is artificially increased (4.17 ± 0.05 ns). The same situation happens for the time of 10% the falling height (figure 56).

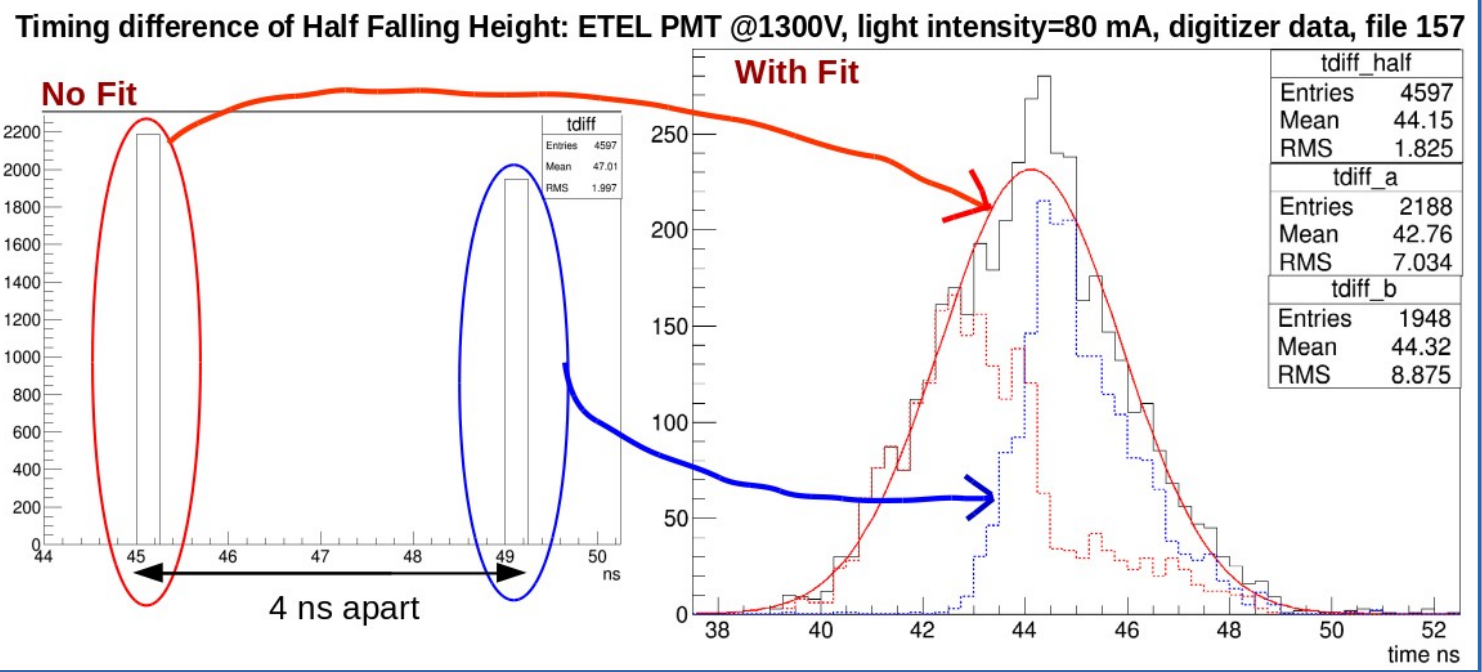
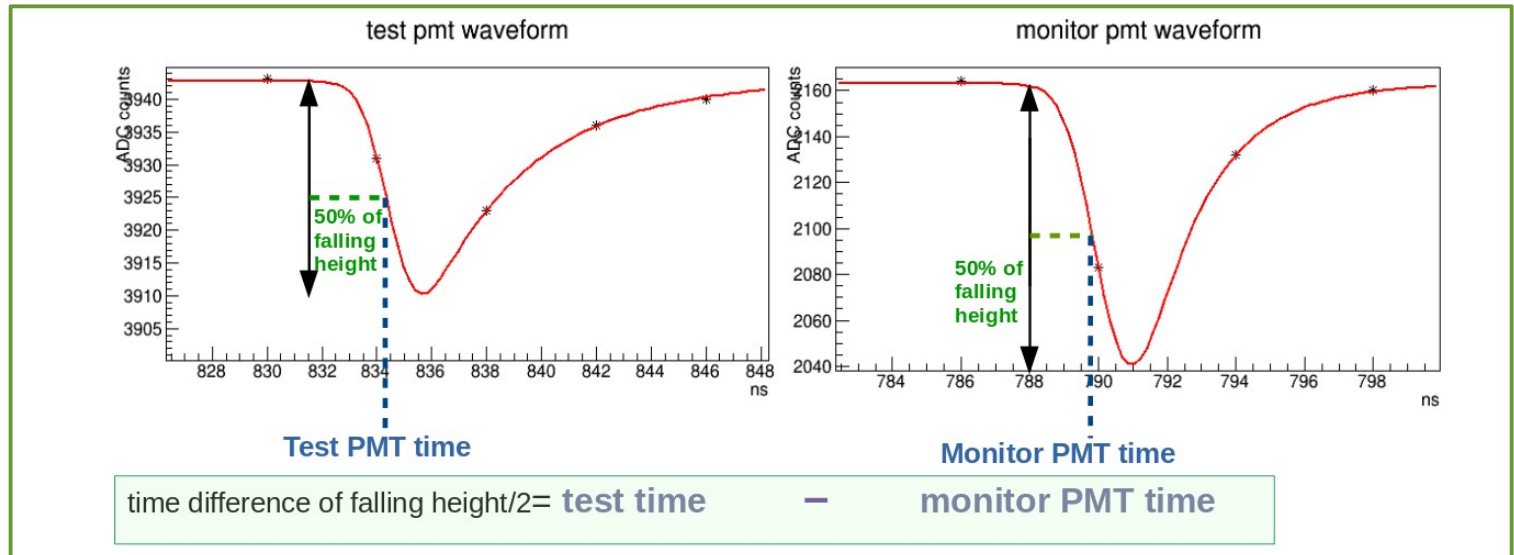
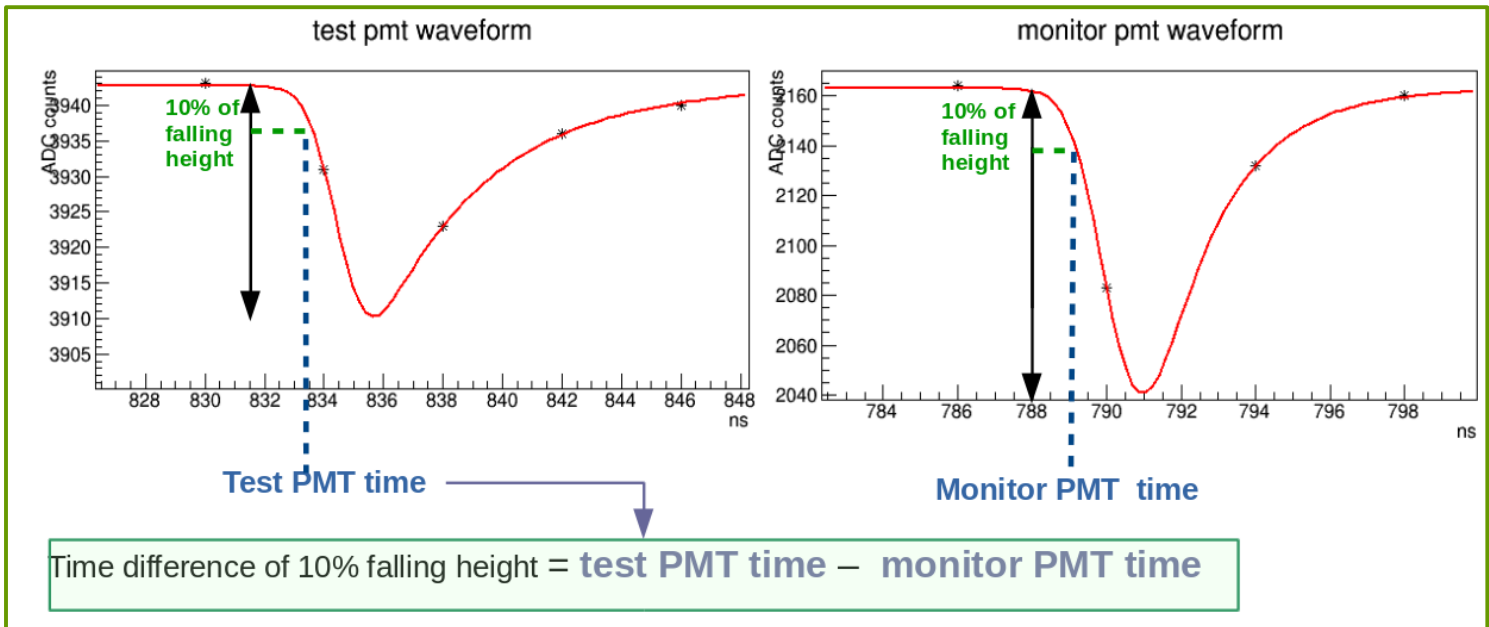


Figure 55: The red (blue) histogram is the timing difference of half the falling height for entries where the timing difference from the minimum of the pulse (without the fit) is ~45 ns (49 ns). The timing difference of all the entries (black line) is approximately the sum of the red and blue histograms. Notice that the red and blue histograms have different means that arise from the 4ns timing resolution of the digitizer. As a result, the FWHM (4.17 ± 0.05 ns) of the black histogram is artificially increased.



Timing difference of 10% Falling Height: ETEL PMT @1300V, light intensity=80 mA, digitizer data, file 157

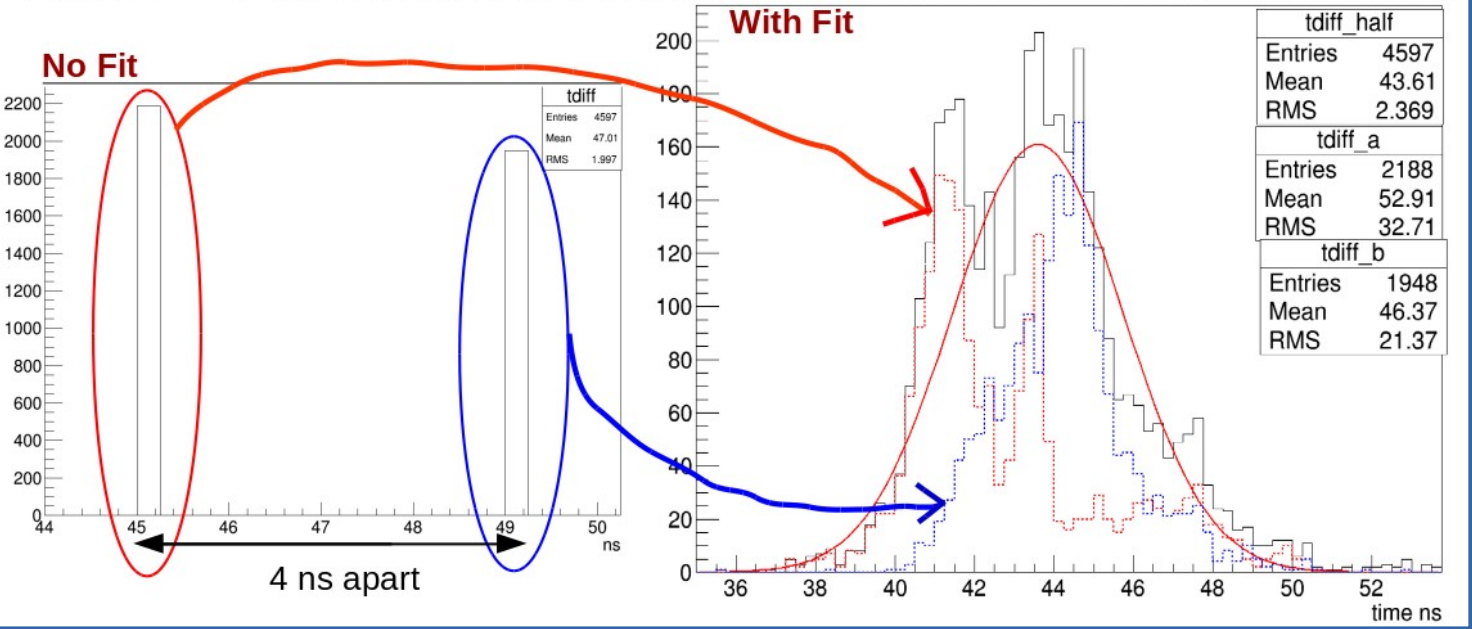


Figure 56: In the bottom plot, the red histogram is the 10% falling height timing difference of entries where the peak time difference without the fit is ~45 ns. Similarly, the blue histogram is the 10% falling height timing difference of entries where the peak time difference without the fit is ~49 ns. The timing difference of all the entries (black line) is approximately the sum of the red and blue histograms. Notice that the red and blue histograms have different means that arise from the 4ns timing resolution of the digitizer. As a result, the FWHM (5.05 ± 0.07 ns) of the black histogram is artificially increased.

Although the oscilloscope takes a much longer time to take data, it has a much better timing resolution (0.4 ns), so we decided to measure timing resolution with the oscilloscope. Figure 57 shows that waveforms created by the oscilloscope have many points in the pulse region, which allows us to get the true peak time of the pulse.

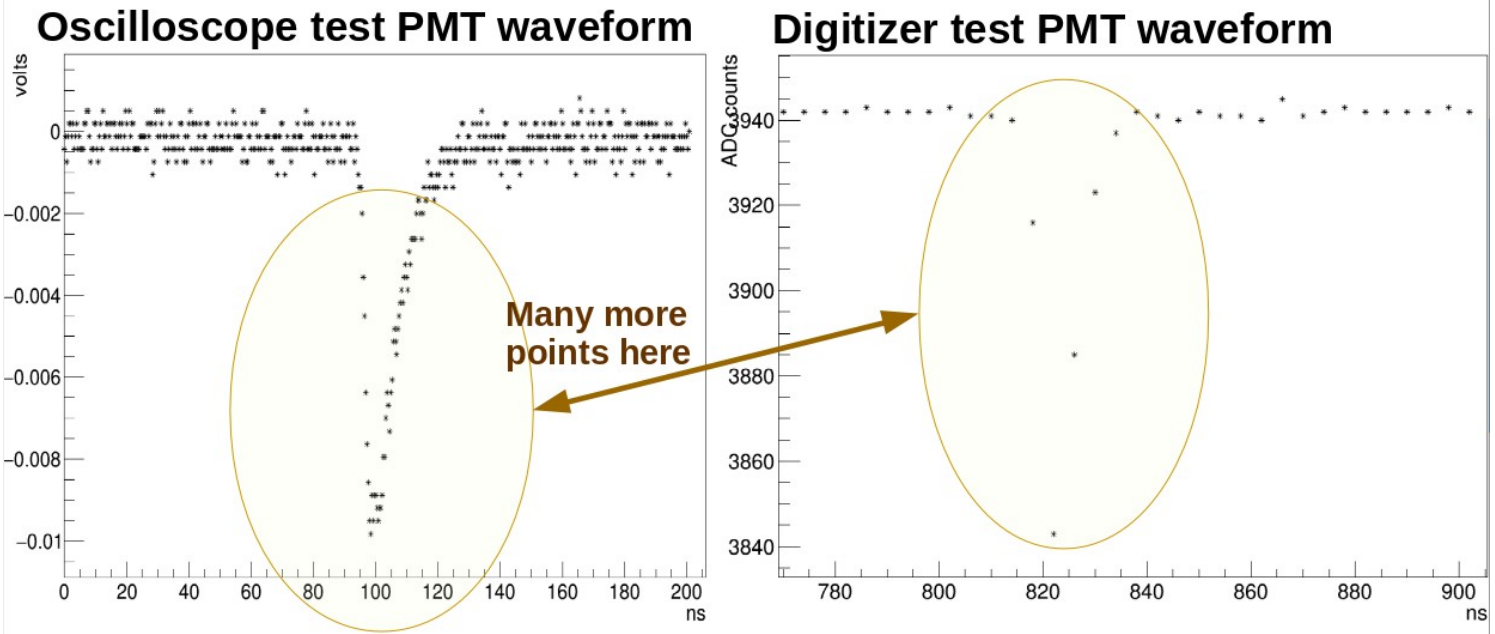


Figure 57: Waveforms created by the oscilloscope have many more points in the pulse region compared to waveforms created by the digitizer.

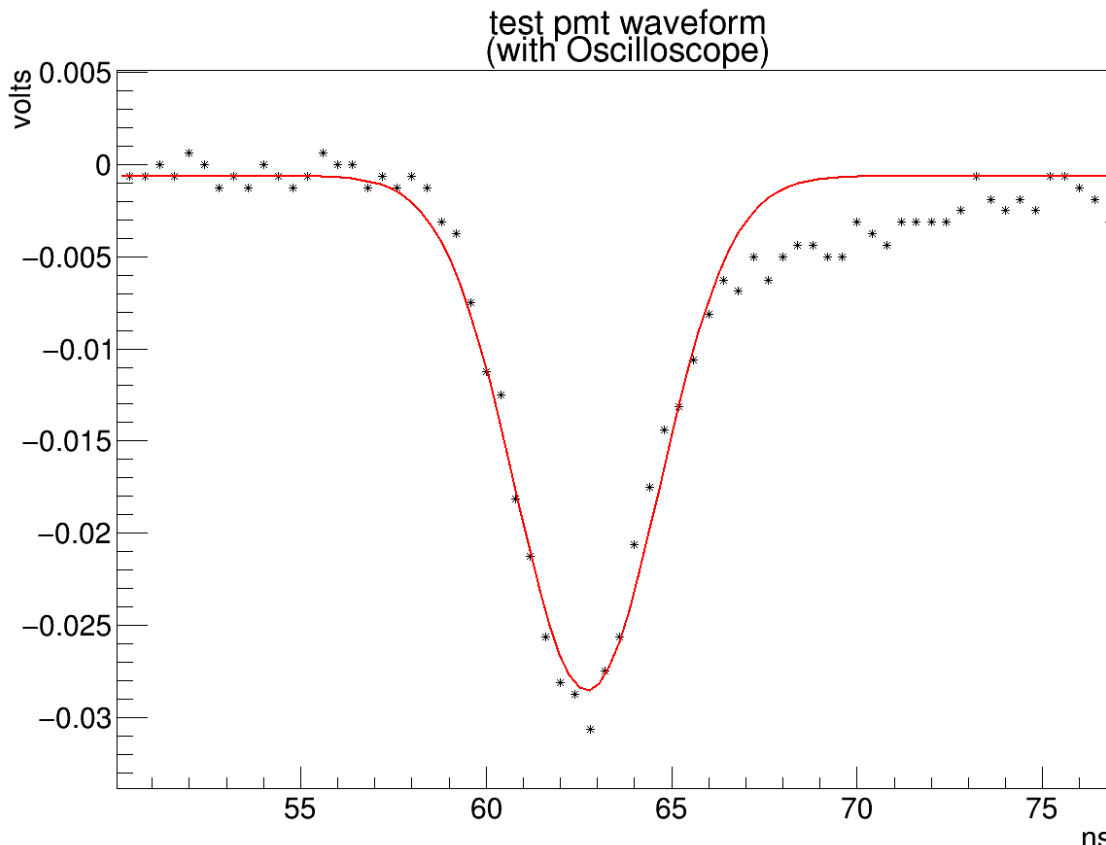


Figure 58: A test PMT waveform from oscilloscope data (fitted with the modified EMG).

monitor PMT pulse height, no cut

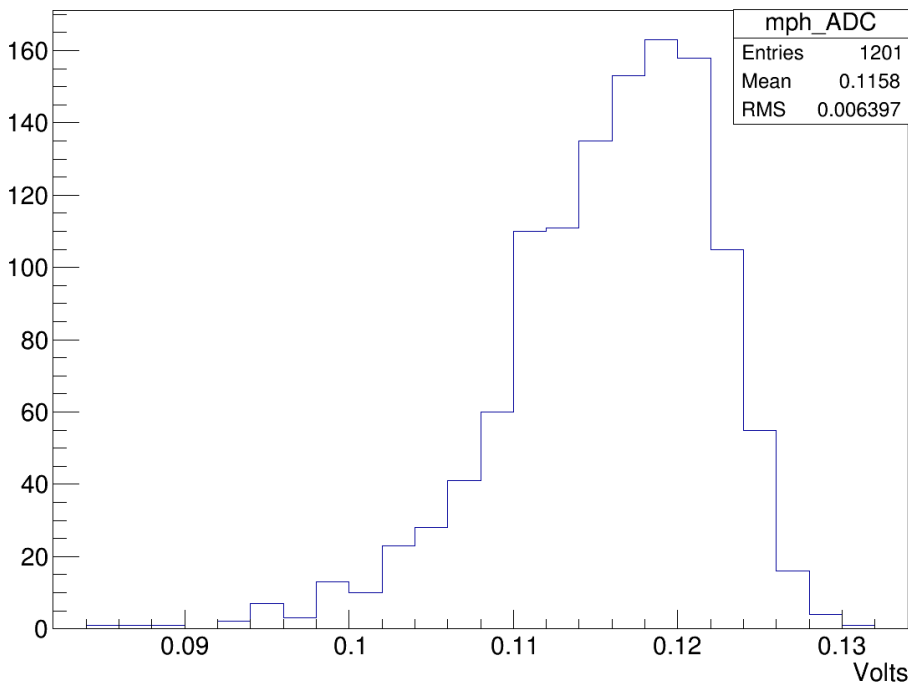


Figure 58: Histogram of monitor PMT pulse heights

Figures 58 and 59 show the histograms of the monitor and test PMT pulse heights (respectively). We accept entries where the test PMT has a pulse, which corresponds to entries where the test PMT pulse height is greater than 0.002 V. These histograms were created using the code `master_timing_res.cpp`, by setting the boolean `osci` equal to true.

test PMT pulse height, before cuts, ETEL PMT @1293 V, light intensity=85mA, oscilloscope data('waveforms03.root')

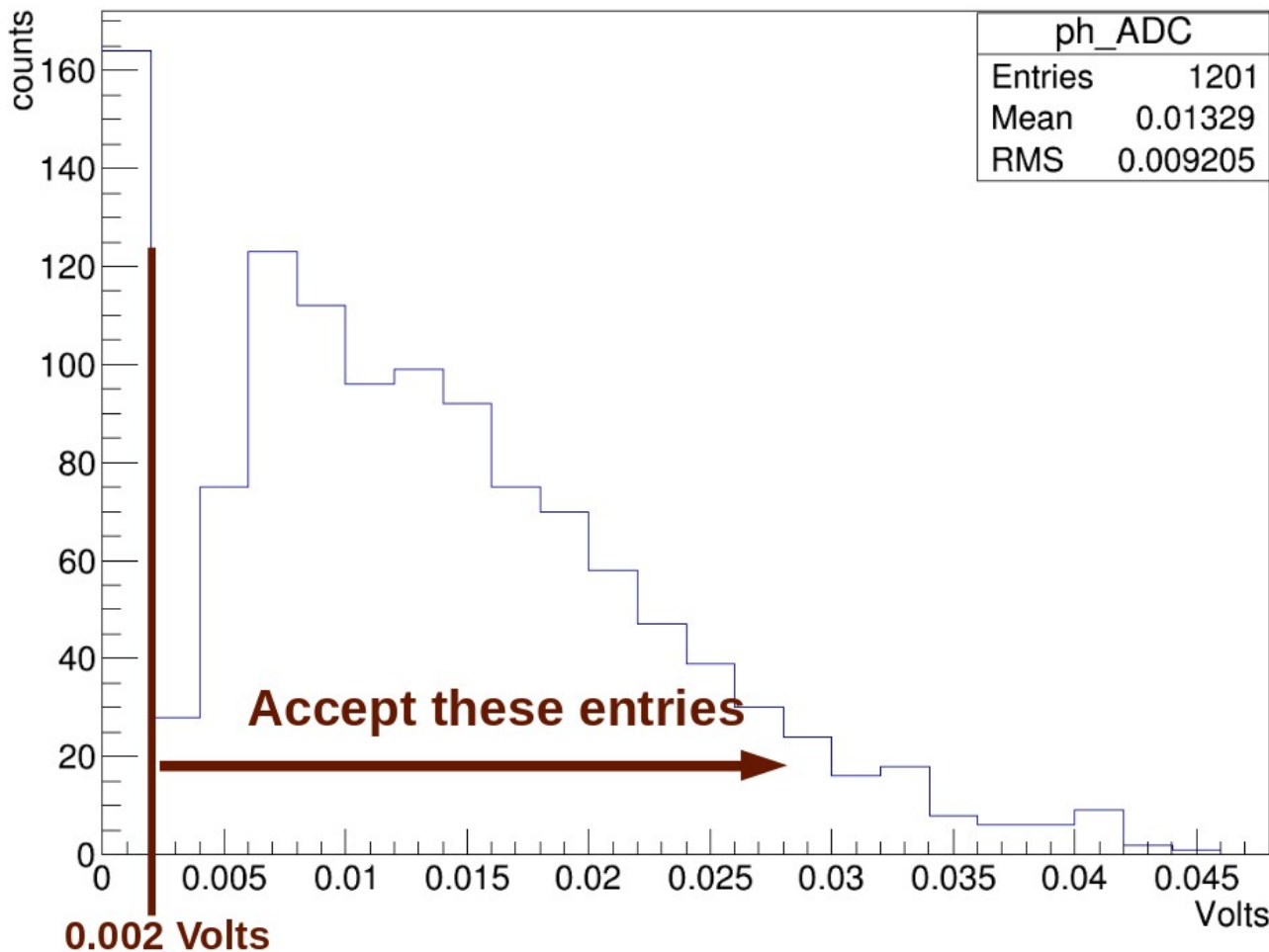
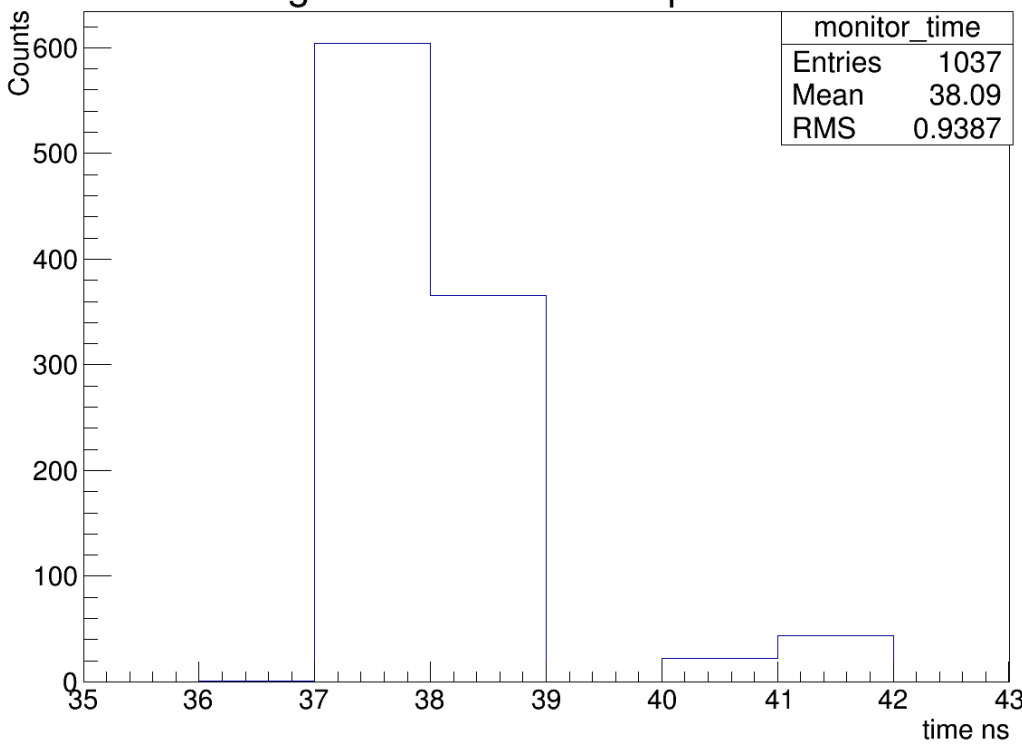


Figure 59: Histogram of test PMT pulse heights for all the entries. We only accept waveforms where the test PMT pulse height is greater than 0.002 V.

Histogram of monitor PMt peak times



Figures 60 and 61 show the histogram of the monitor and test PMT peak times, respectively. Notice that these distributions are not discretized like the peak time distributions for digitizer data (figure 48). Figure 62 shows the timing difference histogram. The FWHM is 2.80 ± 0.07 ns, which is much smaller than the FWHM from the histogram with digitizer data

Figure 60

Histogram of test PMT peak times: ETEL PMT @ 1293 V, 85 mA light intensity, oscilloscope data (waveforms3.root)

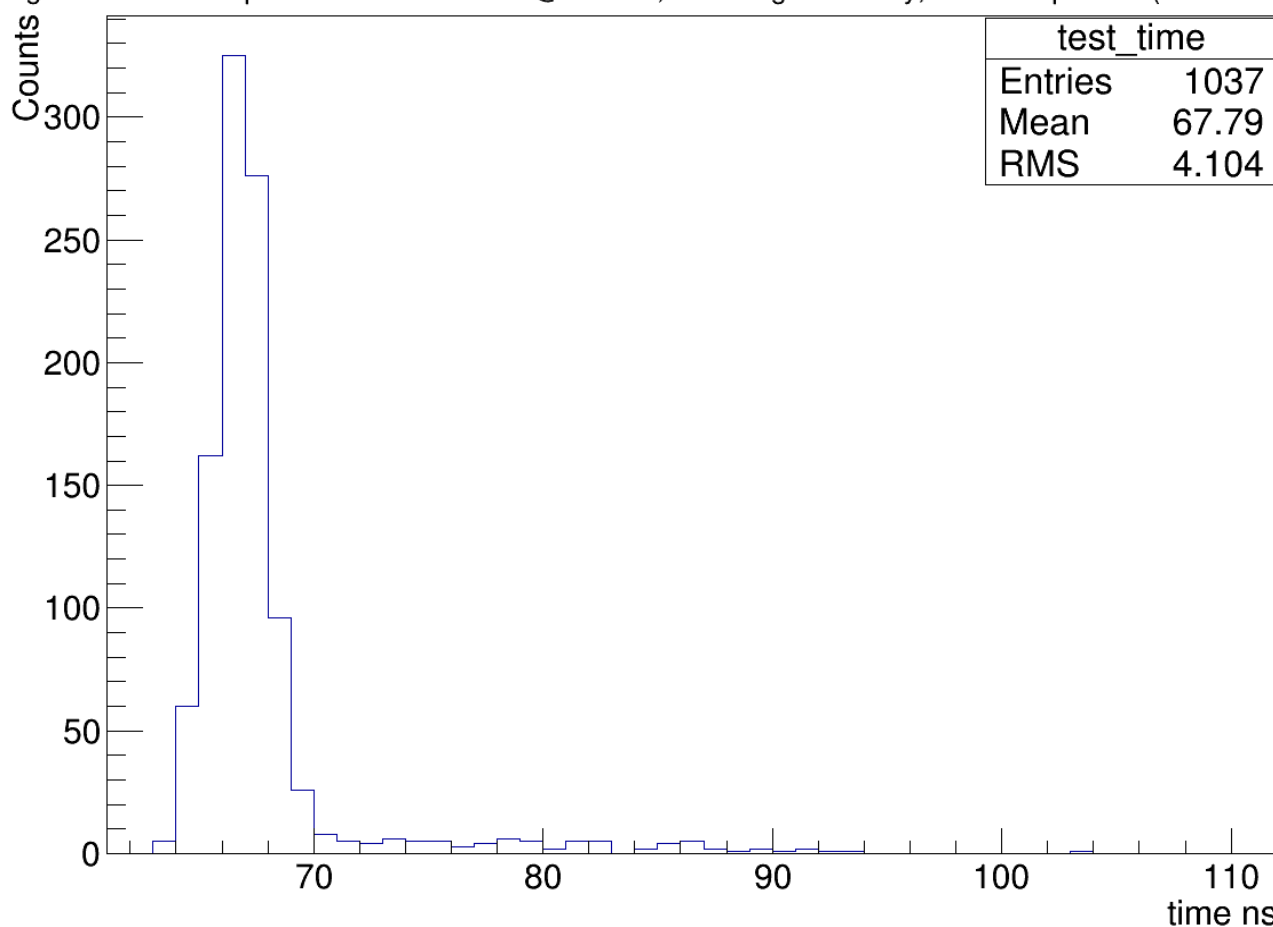


Figure 61

Timing difference histogram: ETEL PMT @ 1293 V, light intensity=85 mA, oscilloscope data, ('waveforms3.root')

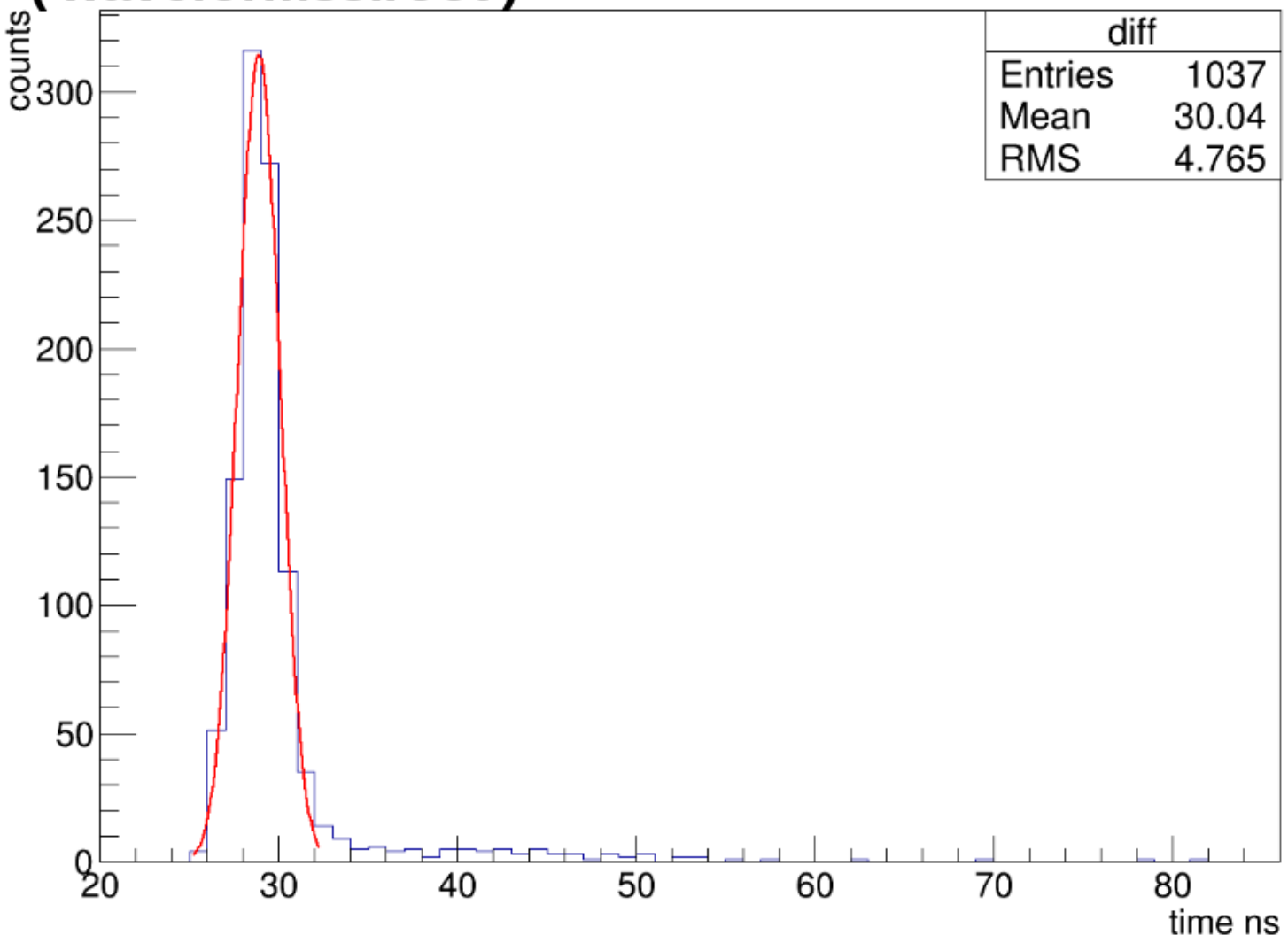


Figure 62: FWHM is 2.80 ± 0.07 ns (error reported is from the fit only). The tail on the right of the Gaussian arises from test PMT pulses with double peaks and late pulses. (Created using the code `master_timing_res.cpp` by setting the Boolean `osci=true`).

Figures 63 and 64 on the next page show the monitor and test PMT pulse height distributions. We only consider waveforms that have a pulse, which correspond to waveforms where the test PMT pulse height > 0.002 V. Figures 65 and 66 show the monitor and test PMT peak time distributions. Notice that these distributions are not discretized like the peak time distributions for digitizer data (figure 48). Figure 67 shows the timing difference histogram. The FWHM is 2.57 ± 0.09 ns.

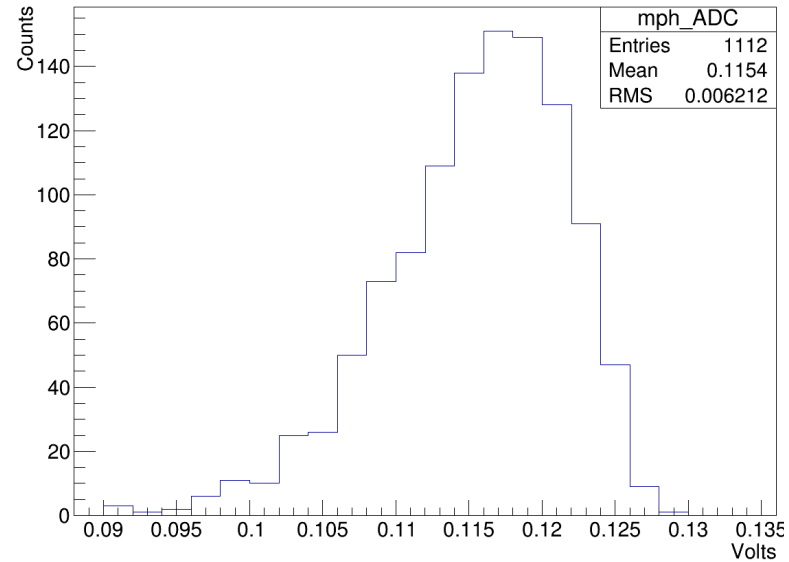


Figure 63

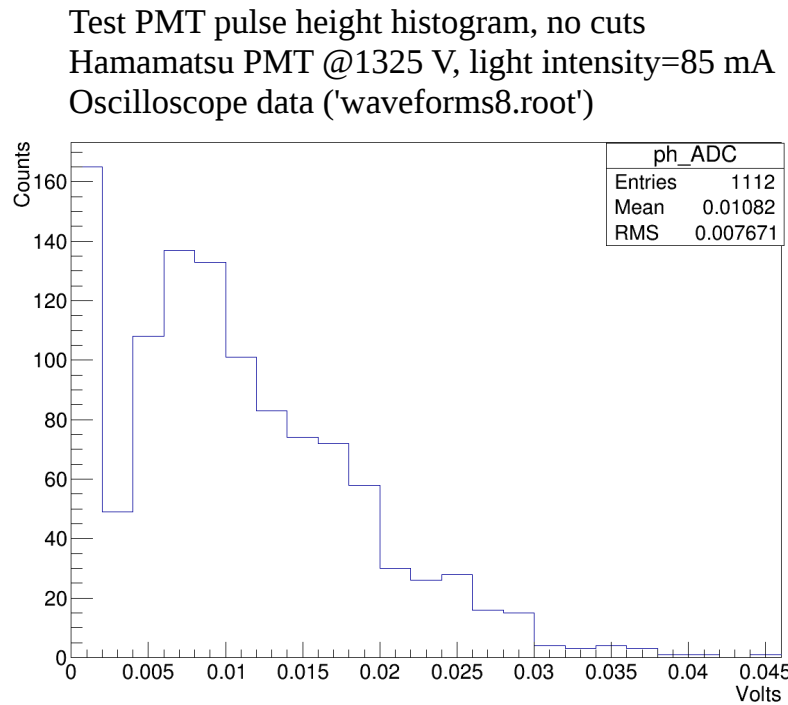


Figure 64: we only accept entries where the test PMT pulse height > 0.002 V

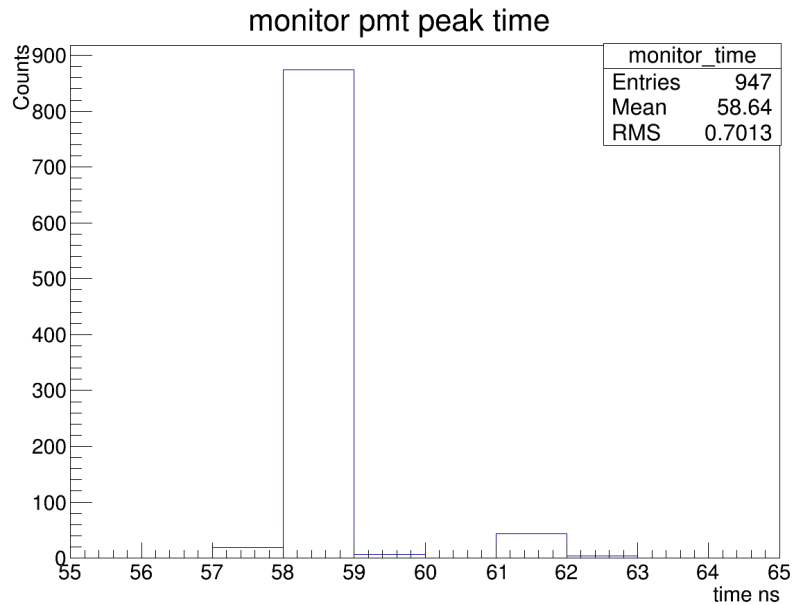


Figure 65

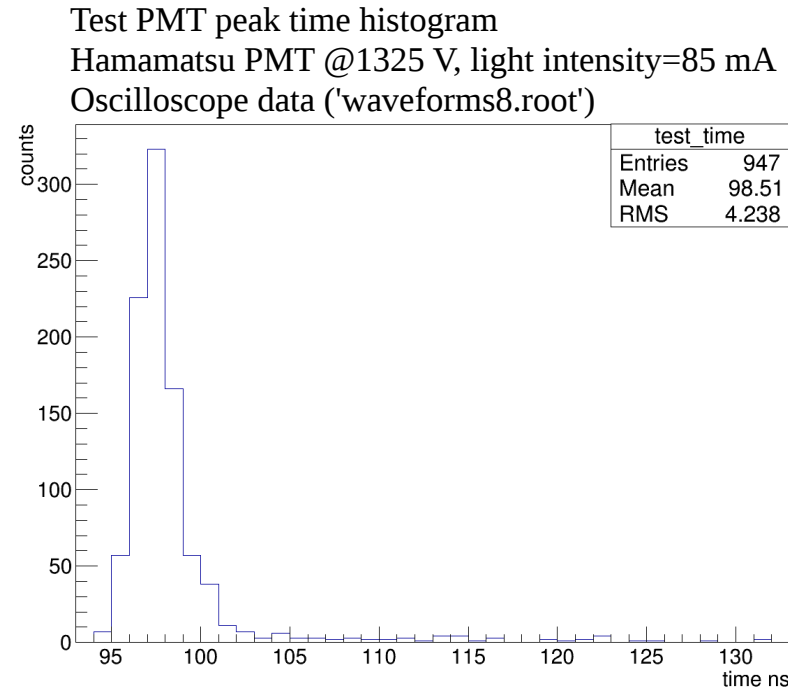


Figure 66

**Timing difference histogram, Hamamatsu PMT
@ 1325 V, light intensity=85 mA, oscilloscope
data ('waveforms8.root')**

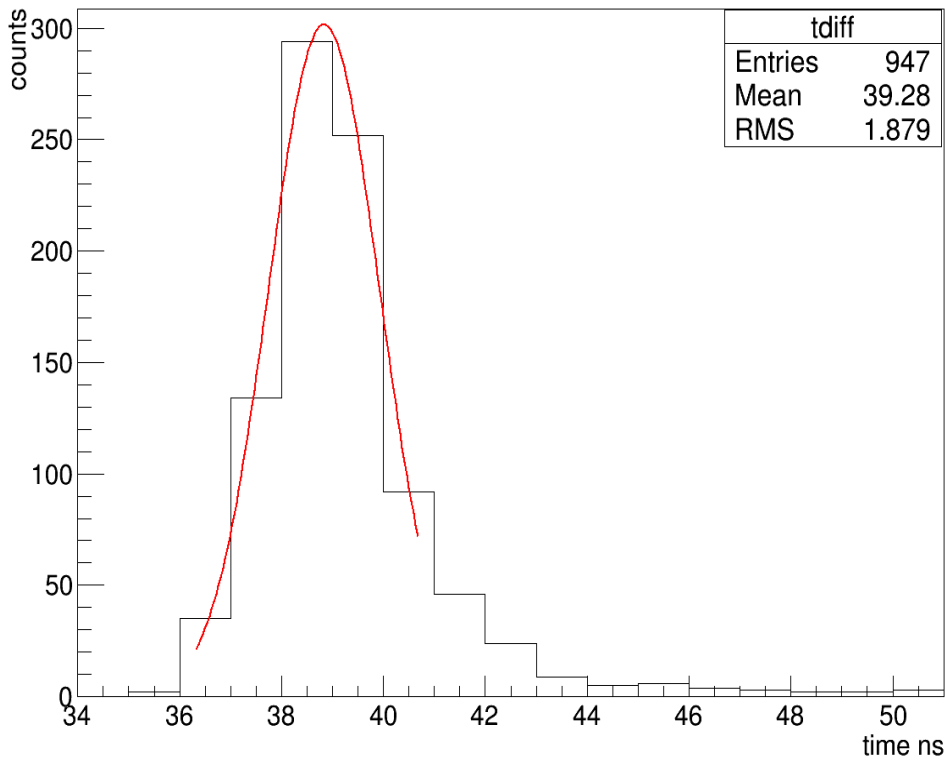


Figure 67: FWHM is 2.57 ± 0.09 ns.

Some of the waveforms that enter the timing difference histogram have two pulses, which is caused by the elastic scattering of electrons off the first dynode (figure 68):

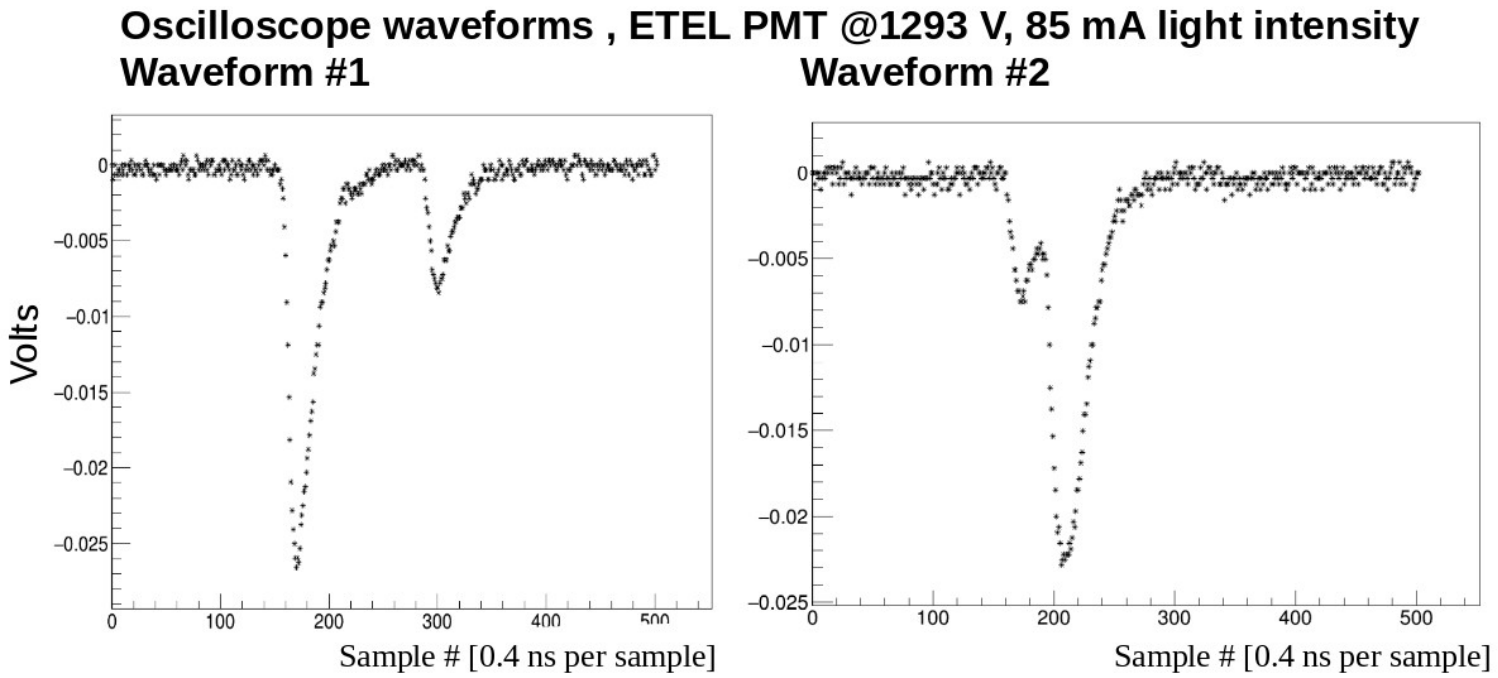


Figure 68

We want to measure timing resolution vs position of the PMT. We use the oscilloscope to measure timing resolution at each position of the PMT (figure 69), rotate the PMT 90° and repeat (figure 70). At this point, the task of measuring timing resolution and other PMT analysis work was passed on to Christian Wittemeier, the other summer student working at York. His preliminary results of timing resolution vs position for the 3-inch ETEL, Hamamatsu, and HZC PMT are shown in figure 71. Note that in this plot, the error bars only include the error from the fit of the timing resolution histogram, which is one of the smaller sources of error in our measurements.

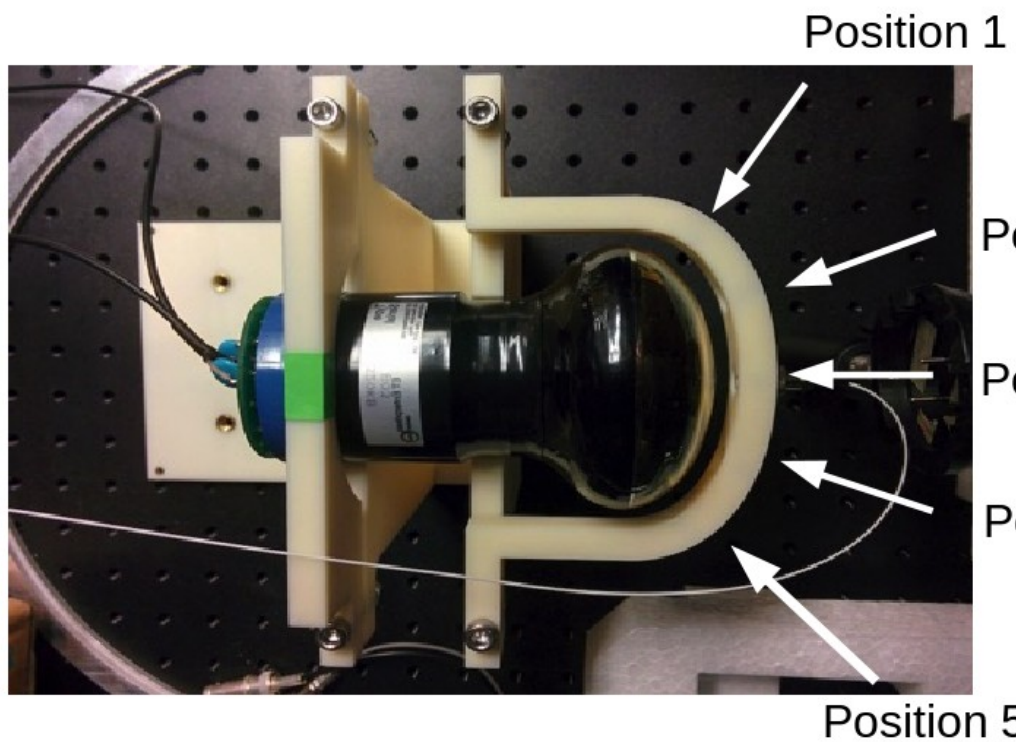


Figure 69

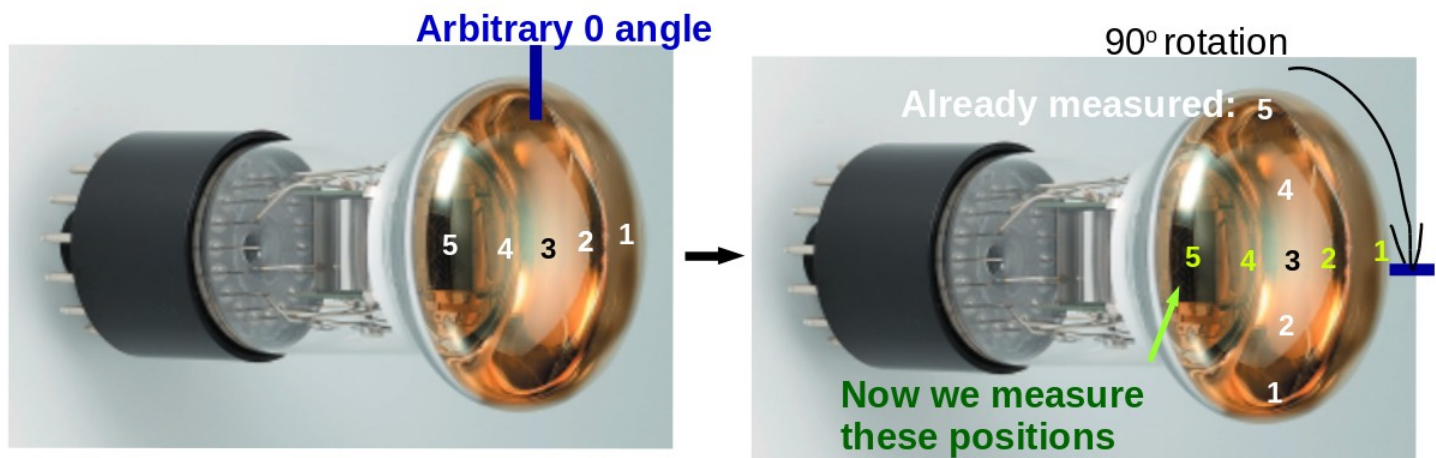


Figure 70

Timing resolution with position slot

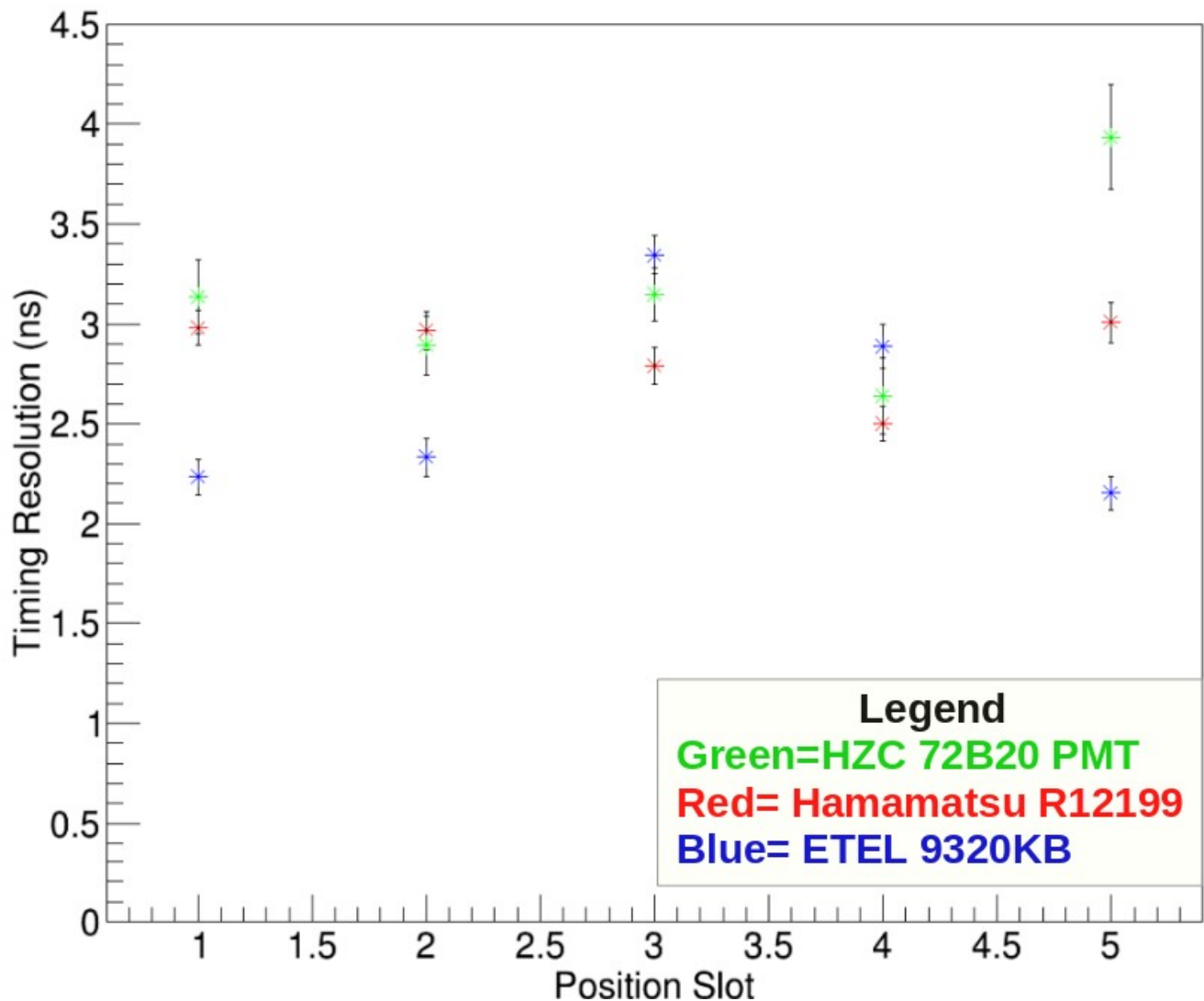


Figure 71

Part 2: Simulations with Neutrino Oscillation Formulae

Chapter 7: Simulations with electron neutrino appearance probability as a function of length and energy

The purpose of this section is to write a fast and simple code (/home/pmt_pc_2/software/code/original_code_neutrino_osci.C) that inputs neutrino oscillation parameters and produces plots of neutrino oscillation probability vs length or energy.

Electron Neutrino Appearance Probability vs Energy

To ensure that my code functions, I reproduce figure 26 of “A Long Baseline Neutrino Oscillation Experiment Using J-PARC Neutrino Beam and Hyper-Kamiokande”. I use the following electron neutrino appearance probability equation (equation 4 of the paper):

$$P(\nu_\mu \rightarrow \nu_e) = 4c_{13}^2 s_{13}^2 s_{23}^2 \cdot \sin^2 \Delta_{31} \quad \text{Leading term}$$

CP even	$+8c_{13}^2 s_{12} s_{13} s_{23} (c_{12} c_{23} \cos \delta_{CP} - s_{12} s_{13} s_{23}) \cdot \cos \Delta_{32} \cdot \sin \Delta_{31} \cdot \sin \Delta_{21}$
CP odd	$-8c_{13}^2 c_{12} c_{23} s_{12} s_{13} s_{23} \sin \delta_{CP} \cdot \sin \Delta_{32} \cdot \sin \Delta_{31} \cdot \sin \Delta_{21}$
Solar term	$+4s_{12}^2 c_{13}^2 (c_{12}^2 c_{23}^2 + s_{12}^2 s_{23}^2 s_{13}^2 - 2c_{12} c_{23} s_{12} s_{23} s_{13} \cos \delta_{CP}) \cdot \sin^2 \Delta_{21}$
Matter effect	$-8c_{13}^2 s_{13}^2 s_{23}^2 \cdot \frac{aL}{4E_\nu} (1 - 2s_{13}^2) \cdot \cos \Delta_{32} \cdot \sin \Delta_{31}$ $+8c_{13}^2 s_{13}^2 s_{23}^2 \frac{a}{\Delta m_{31}^2} (1 - 2s_{13}^2) \cdot \sin^2 \Delta_{31},$

where Δ_{ij} is $\Delta m_{ij}^2 L / 4E_\nu$, and $a[\text{eV}^2] = 7.56 \times 10^{-5} \times \rho[\text{g/cm}^3] \times E_\nu[\text{GeV}]$.

where I replace Δ_{ij} by $1.27 \times 4 \times \Delta_{ij}$ in order to express energy in GeV, length in km, and mass differences in eV². I use the following parameters found in the paper² to plot electron neutrino appearance probability vs energy at a fixed length of 295 km (T2K's baseline):

2- A Long Baseline Neutrino Oscillation Experiment Using J-PARC Neutrino Beam and Hyper-Kamiokande

Parameters:

$$\begin{aligned}\theta_{23} &= 0.785 \text{ (rad)} \\ \theta_{13} &= 0.161 \text{ (rad)} \\ \theta_{12} &= 0.601 \text{ (rad)} \\ \Delta m_{32}^2 &= 0.00242 \text{ (eV}^2\text{)} \\ \Delta m_{31}^2 &= 0.00242 \text{ (eV}^2\text{)} \\ \Delta m_{21}^2 &= 7.6 \times 10^{-5} \text{ (eV}^2\text{)} \\ \delta_{cp} &= 1.57 \text{ (rad)} \\ L &= 295 \text{ (km)} \\ \rho &= 2.2 \text{ (g/cm}^3\text{)}\end{aligned}$$

Note : values in code aren't rounded

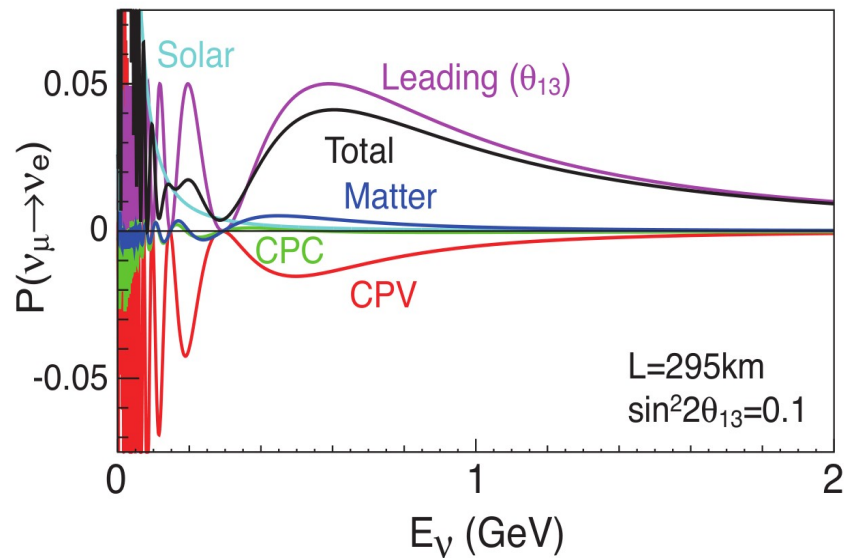


Figure 72: Electron neutrino appearance probability vs neutrino energy from the Hyper-K² paper

Electron neutrino appearance probability vs Energy (fixed at 295 km), with Matter Effect and Normal Hierarchy, $\delta_{CP}=\pi/2$, $\theta_{23}=45^\circ$

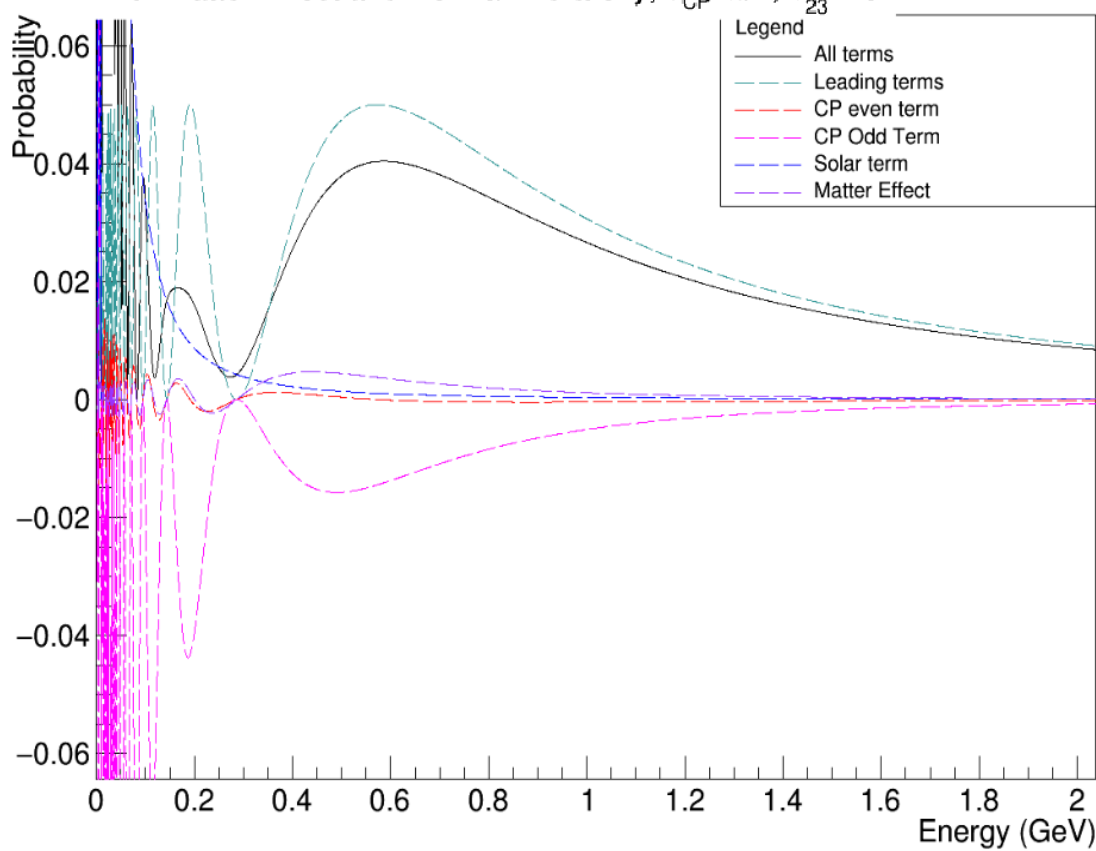


Figure 74: Plot created by original_code_neutrino_osci.C

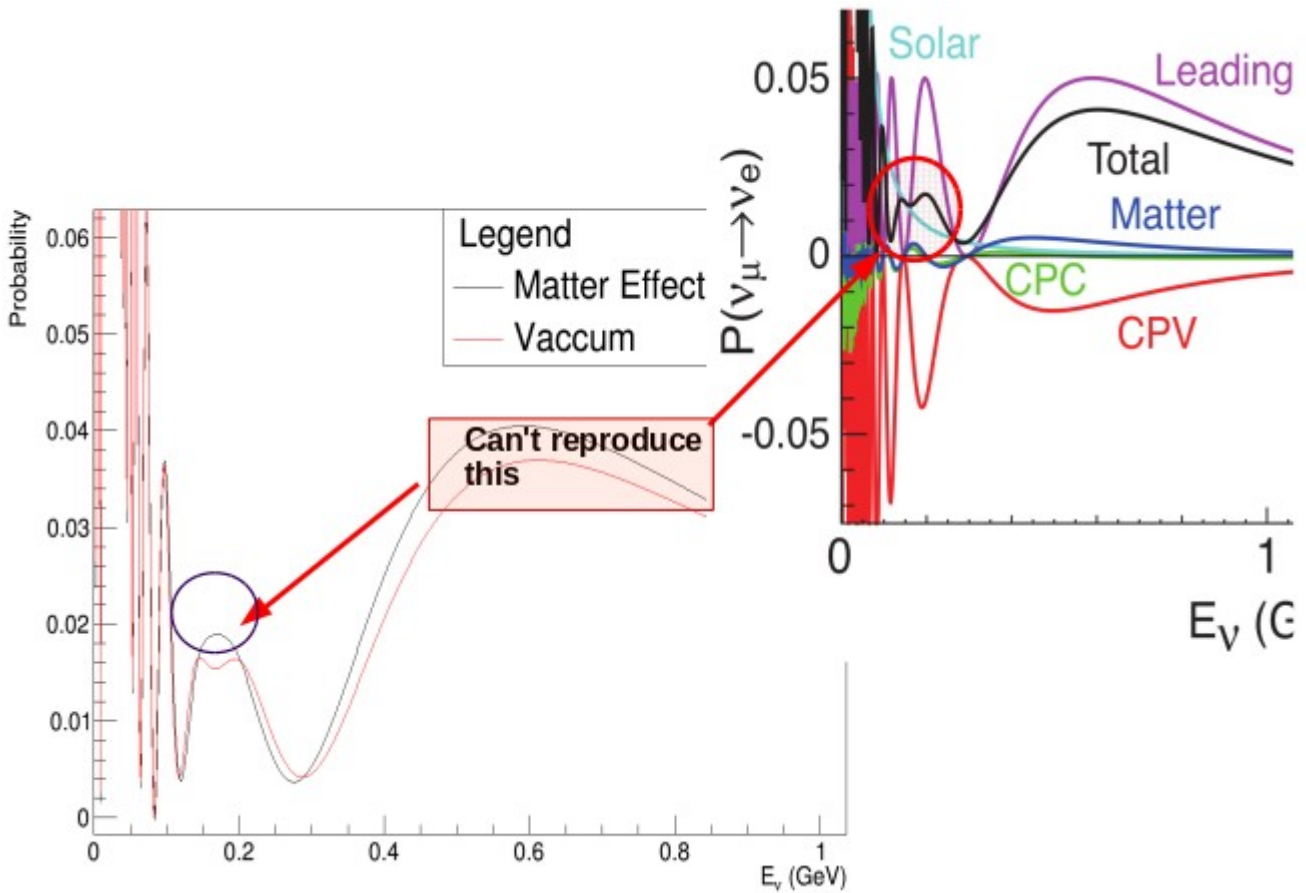


Figure 75: Comparing the paper plot (top right) to my plot (bottom left)

Notice that my plot looks slightly different than the paper's plot at 0.2 GeV (figure 75) because the formula that I'm using is an approximation.

We can see that the appearance probability has a maximum at 0.6 GeV (figure 74), which is the energy used in the T2K experiment. One can produce plots like this for any parameters.

Figure 76 shows electron neutrino appearance probability vs length plotted for five different values of θ_{23} (with energy fixed at 0.6 GeV, normal hierarchy, and $\delta_{CP}=\pi/2$). This plot confirms that appearance probability has a maximum at ~ 300 km, which is T2K's baseline. Notice that it is easiest to distinguish between the values θ_{23} of for the first maximum compared to the second maximum and third maximum because the appearance probability for the different θ_{23} 's is more separated in the first maximum. Thus, one would want a detector placed at the first maximum (we already have Super-K). If we make this plot with the energy used for the proposed detector in Korea that is ~ 1100 km from J-PARC, one would observe the second max at ~ 1100 km.

Electron neutrino appearance probability vs length (fixed at 0.6 GeV) with normal hierarchy, delta cp=pi/2

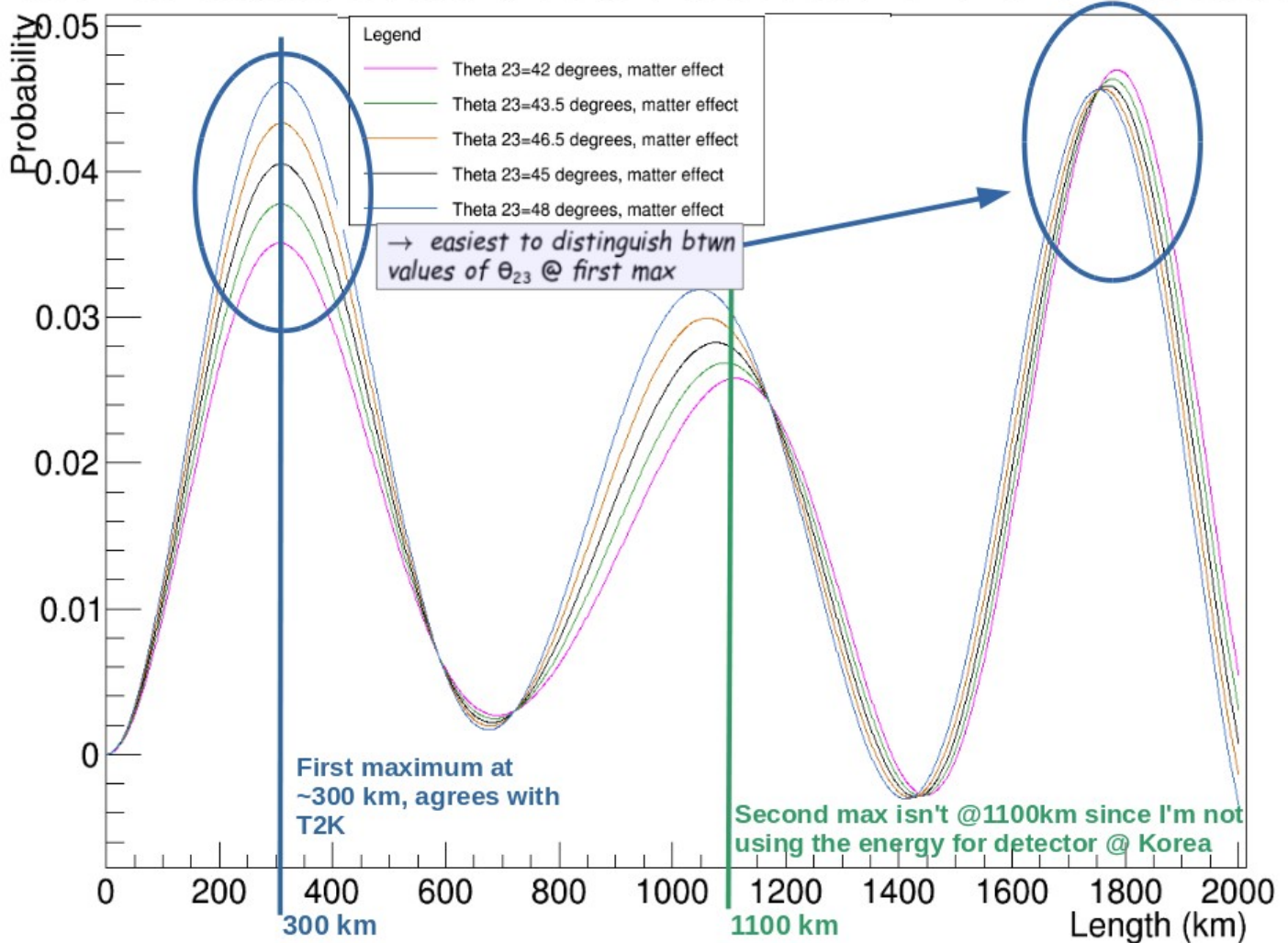


Figure 76

Figures 77 and 78 are the same plot for $\delta_{CP}=0$ and $\delta_{CP}=-\pi/2$ (respectively). Again, we see that the first max occurs around 300 km and that the effect of θ_{23} is more easily seen at the first maximum compared to the second and third maxima.

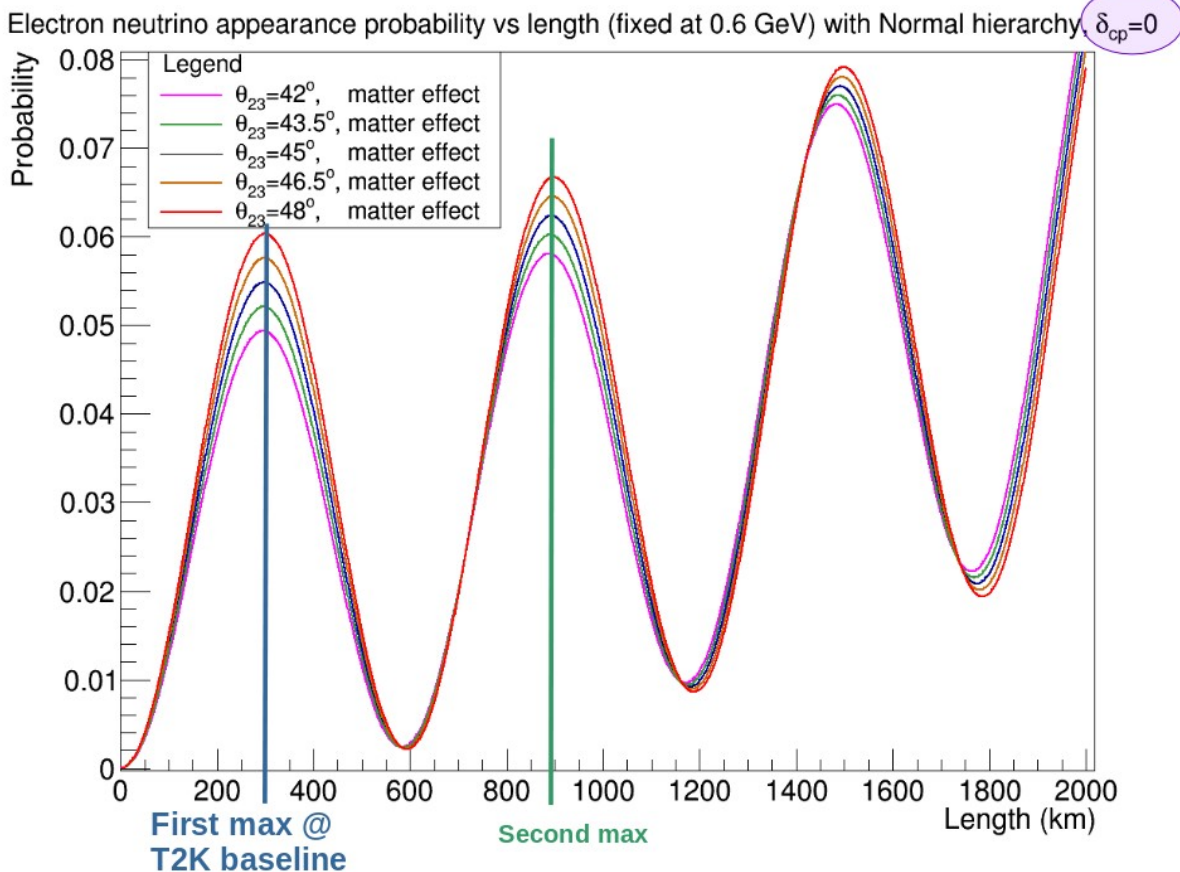


Figure 77

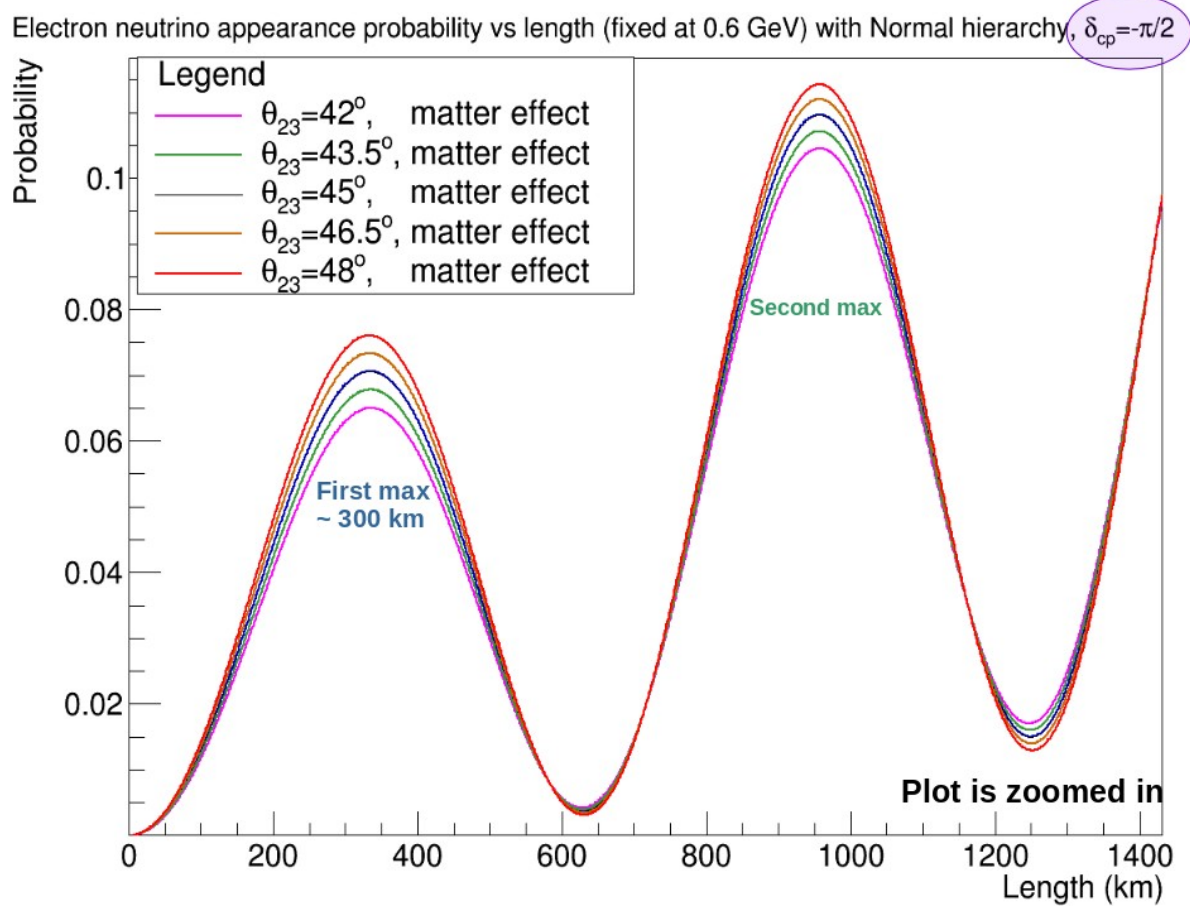


Figure 78

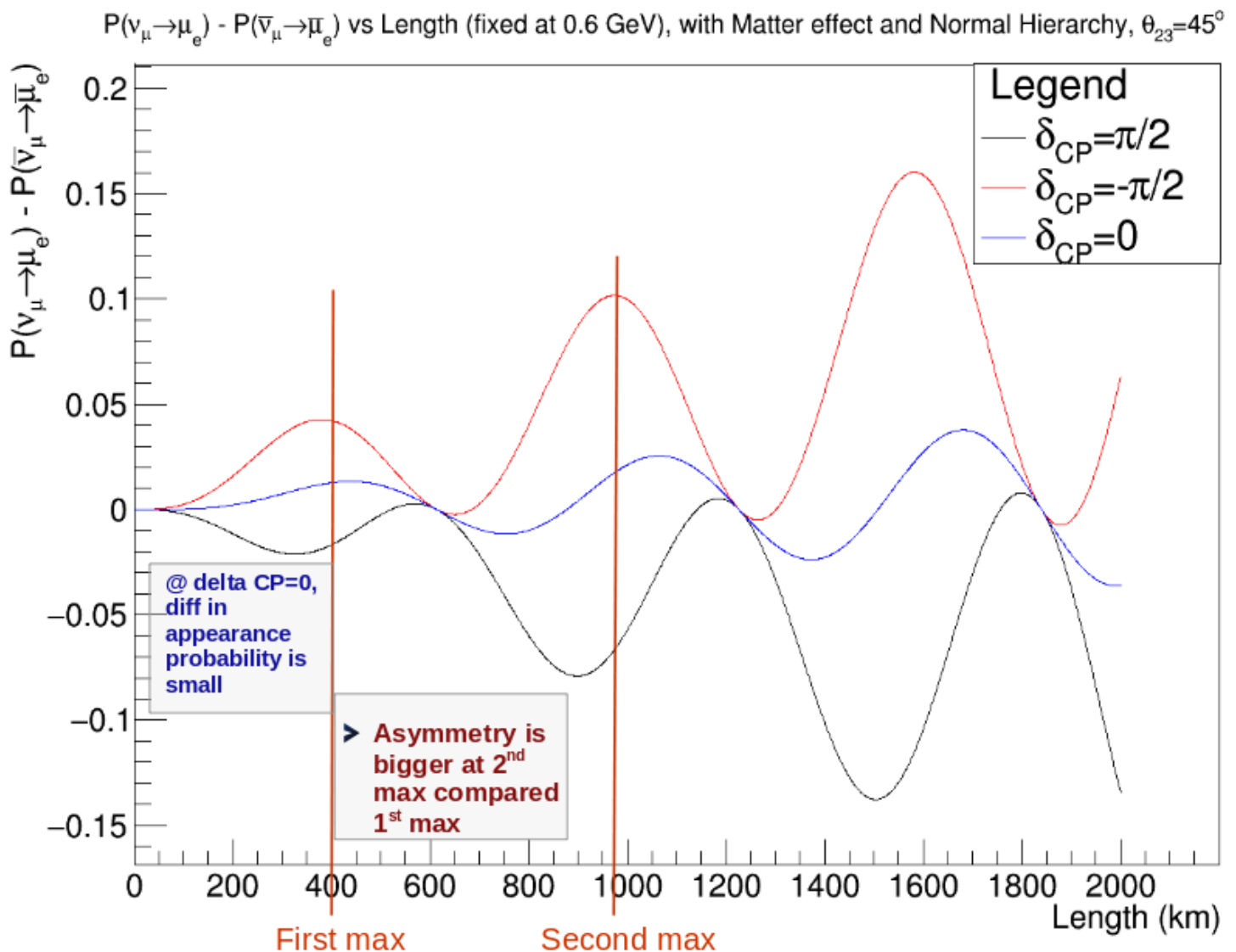


Figure 79

Figure 79 plots the difference between electron neutrino appearance probability for matter versus antimatter for different values of δ_{CP} . Notice that for $\delta_{CP}=0$, the difference in probability is very small. Also notice that the second and third maxima of asymmetry are larger than the first maximum of asymmetry. Thus, it is easier to observe asymmetry with a detector placed at the second or third maxima. Figure 80 shows the same plot for inverted hierarchy, which looks similar to figure 79.

$P(\nu_\mu \rightarrow \mu_e) - P(\bar{\nu}_\mu \rightarrow \bar{\mu}_e)$ vs Length (fixed at 0.6 GeV), with Matter effect and Inverted Hierarchy, $\theta_{23}=45^\circ$

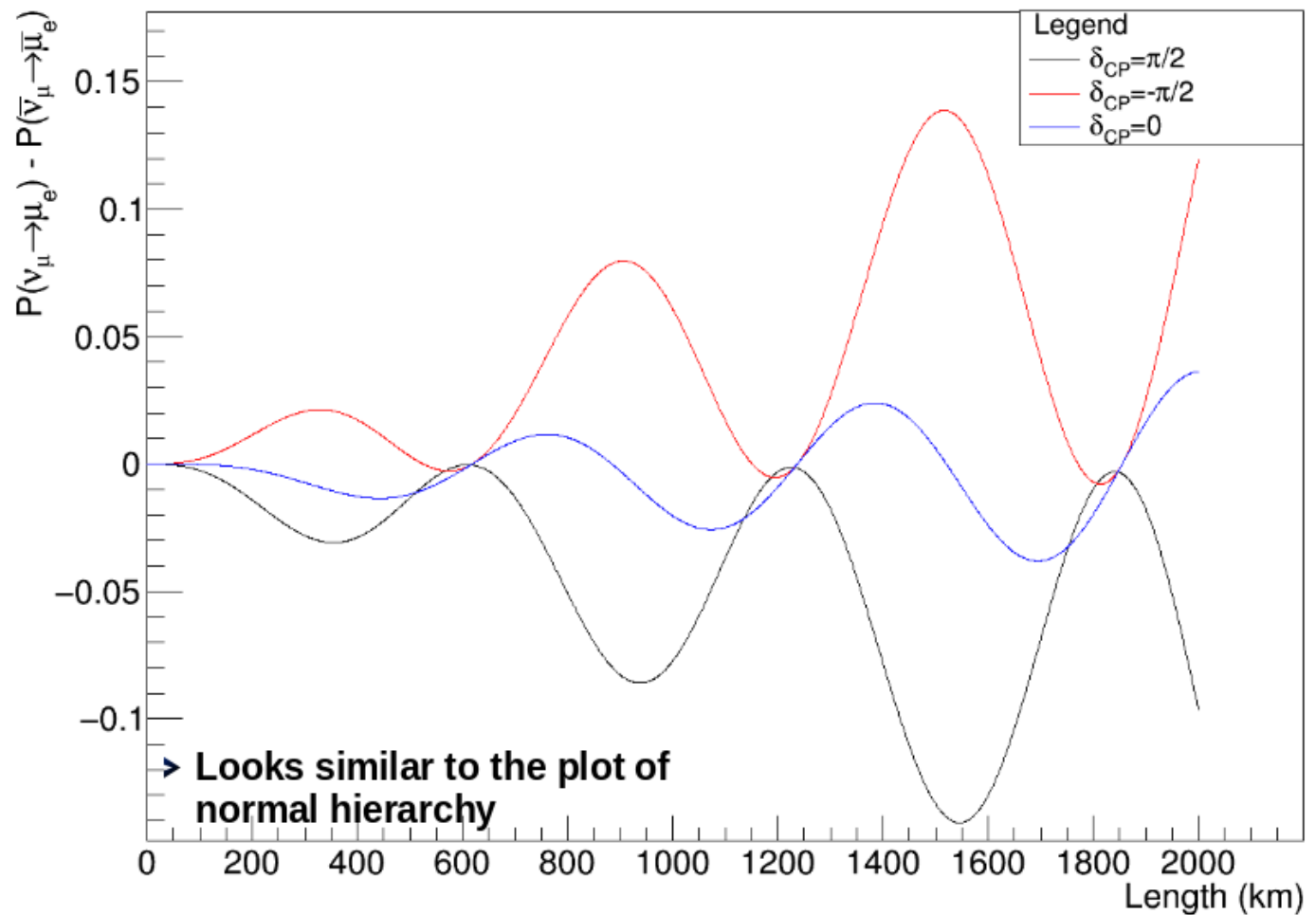


Figure 80: Looks similar to the plot of normal hierarchy, except the curvature is inverted.

Electron neutrino appearance probability vs length (fixed at 0.6 GeV) with normal hierarchy & matter effect, $\theta_{23}=45^\circ$

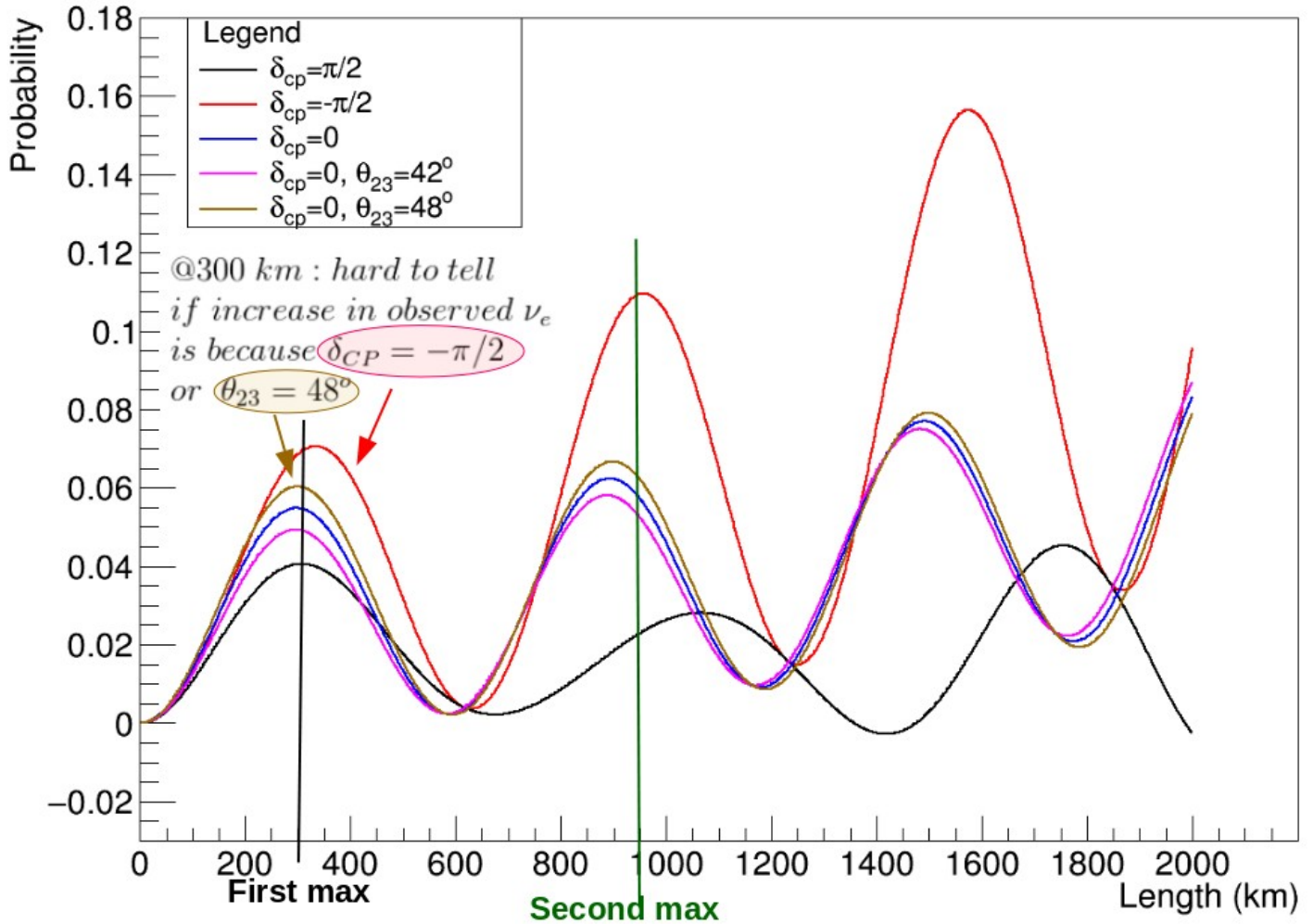


Figure 81

Figure 81 shows the electron neutrino appearance probability vs length for $\theta_{23}=45^\circ$ and different δ_{CP} 's, and $\delta_{CP}=0$ and different values of θ_{23} . At the first maximum, the probability for $\theta_{23}=45^\circ$ and $\delta_{CP}=-\pi/2$ is very close to the probability for $\delta_{CP}=0$ and $\theta_{23}=48^\circ$. Also notice that the effect of δ_{CP} on the probability is more distinguished for the second and third maxima compared to the first maximum (red, blue and black lines are more separated in second and third maxima). Since we want to distinguish between $\delta_{CP}=0$ (which does not imply matter anti-matter asymmetry) and $\delta_{CP}=-\pi/2$ (which *does* imply matter anti-matter asymmetry), we would want a detector at a later maximum. However, the effect of θ_{23} on the probability is most obvious at the first and second maxima, so the ideal position for a new detector is the second maximum, which is ~ 1100 km for T2KK's energy.

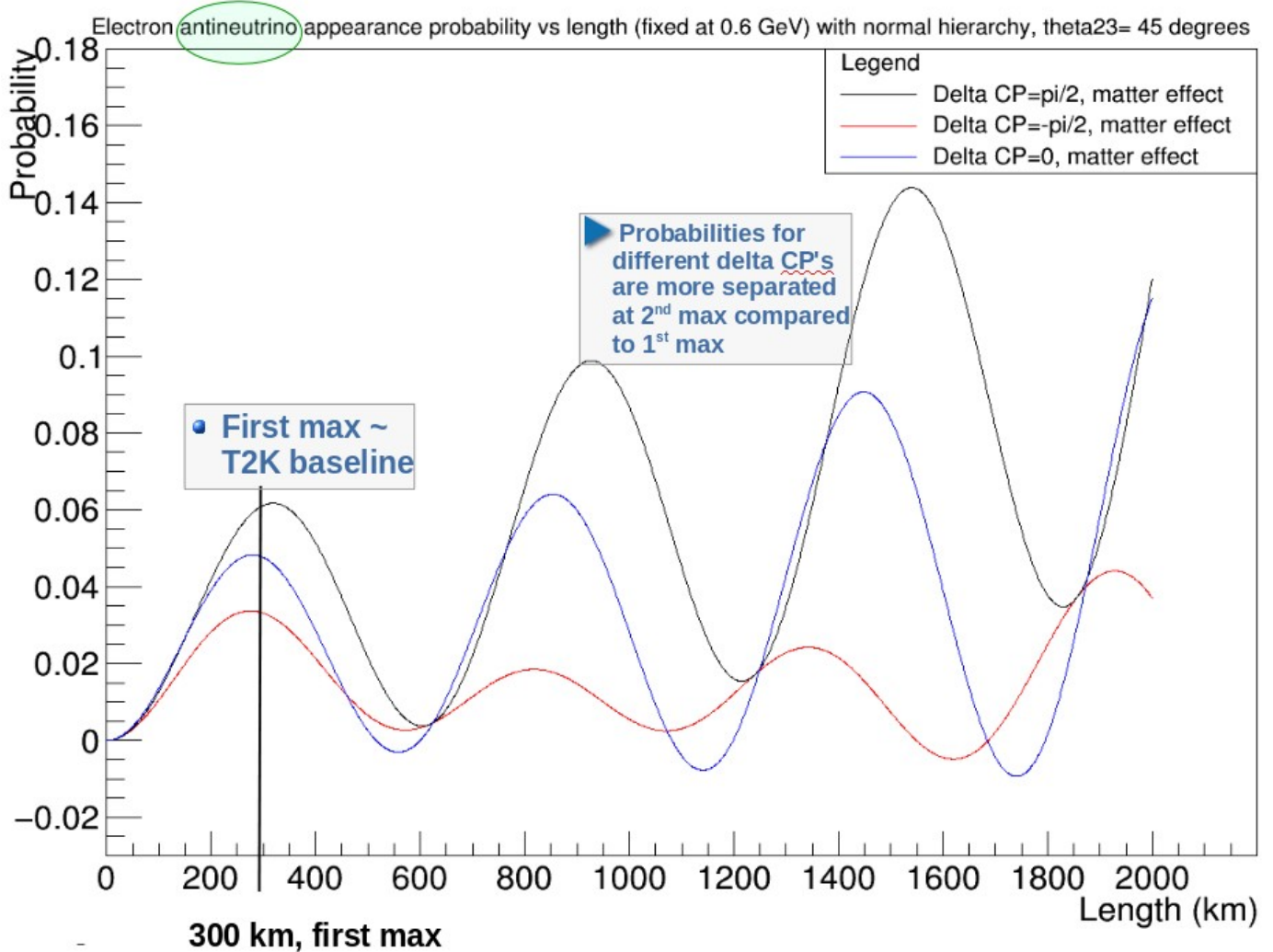


Figure 82

Figure 82 is the same plot as before, but for antineutrinos. Notice that the effect of δ_{CP} on the probability is flipped for antineutrinos. For instance, at the first maximum, $\delta_{CP}=\pi/2$ gives the lowest probability (out of the three δ_{CP} 's) for neutrinos and the highest probability for antineutrinos. Figure 83 is the same ν_e appearance probability plot for neutrinos and inverted hierarchy, which looks similar to the plot for neutrinos and normal hierarchy. Figure 84 is the plot for antineutrinos and inverted hierarchy, which looks similar to the plot for antineutrinos and normal hierarchy. Again, notice that δ_{CP} has the opposite effect of antimatter as it does on matter.

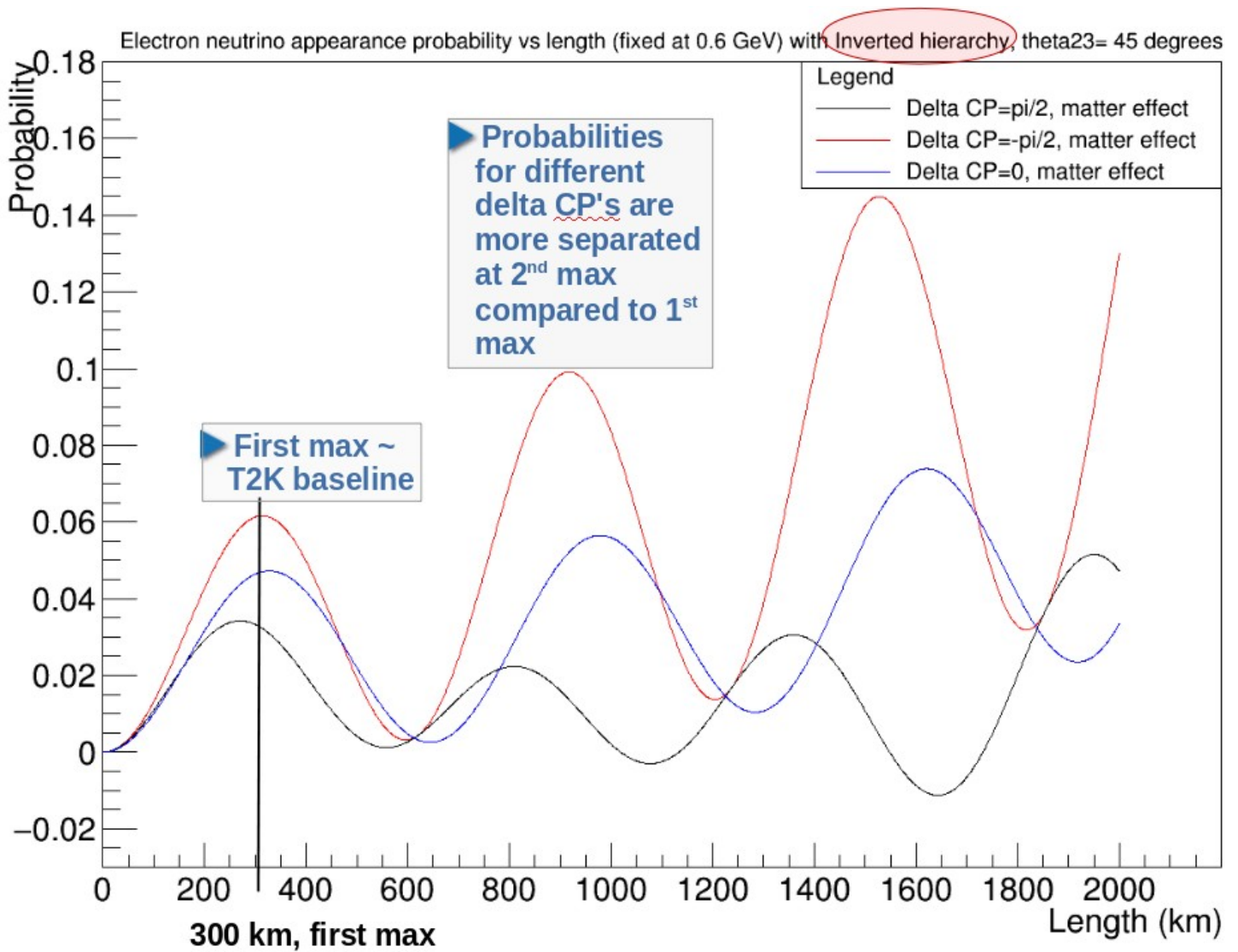


Figure 83

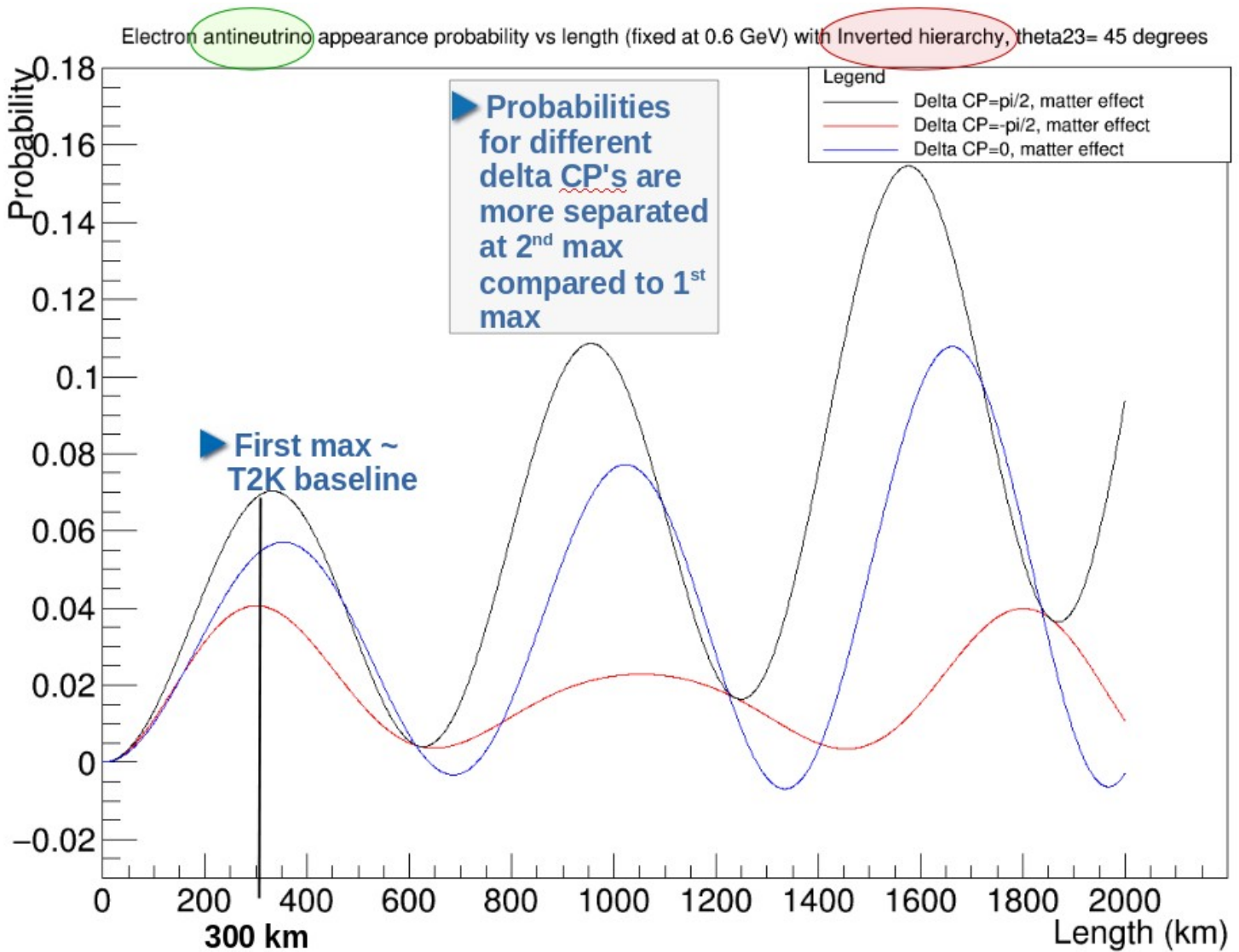


Figure 84

Conclusion

Since the effect of δ_{CP} on the probability is more distinguished for the later maxima but the effect of θ_{23} is most obvious at the earlier maxima, we conclude that the second maximum, which is ~ 1100 km for T2KK's energy, is an ideal position for a new detector.

Chapter 8

Simulations of muon neutrino survival probability vs electron muon neutrino appearance probability

The purpose of this chapter is to plot muon neutrino survival probability vs electron neutrino appearance probability for $\delta_{CP} \in [-\pi, \pi]$ and different values of $\sin^2(\theta_{23})$ because this plot shows a lot of information about neutrino oscillations. Essentially, we wish to reproduce figure 25 of “Measurements of neutrino oscillation in appearance and disappearance channels by the T2K experiment with 6.6×10^{20} protons on target”, shown below:

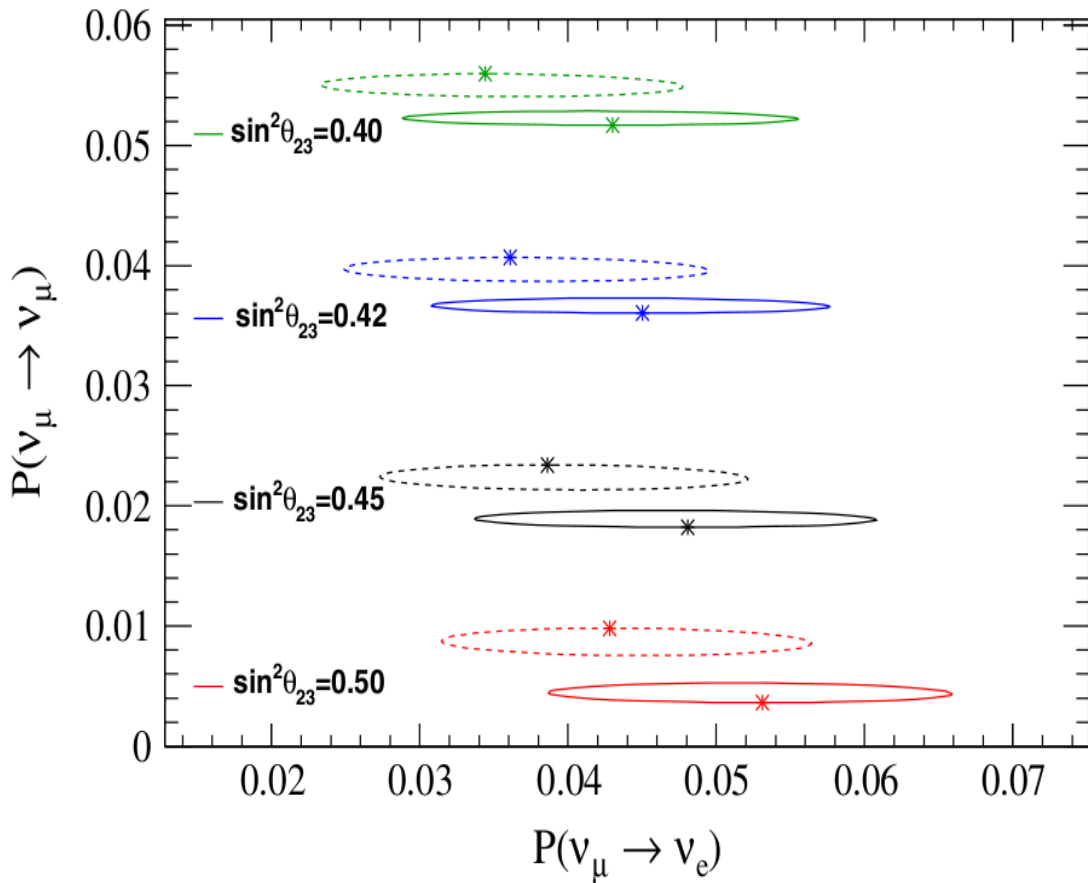


Figure 85: Figure 25 of the paper. The solid line represents normal hierarchy, the dash line represents inverted hierarchy

We use equation 18 of the T2K³ paper for electron neutrino appearance probability, and a more complete version of the muon neutrino survival probability equation than the equation in the T2K paper³ (we use equation 33 of “Series expansion for three-flavor neutrino oscillation probabilities in matter”):

$$\begin{aligned}
 P_{\mu\mu} = & 1 - \sin^2 2\theta_{23} \sin^2 \Delta + \alpha c_{12}^2 \sin^2 2\theta_{23} \Delta \sin 2\Delta \\
 & - \alpha^2 \sin^2 2\theta_{12} c_{23}^2 \frac{\sin^2 A\Delta}{A^2} - \alpha^2 c_{12}^4 \sin^2 2\theta_{23} \Delta^2 \cos 2\Delta \\
 & + \frac{1}{2A} \alpha^2 \sin^2 2\theta_{12} \sin^2 2\theta_{23} \left(\sin \Delta \frac{\sin A\Delta}{A} \cos(A-1)\Delta - \frac{\Delta}{2} \sin 2\Delta \right) \\
 & - 4 s_{13}^2 s_{23}^2 \frac{\sin^2(A-1)\Delta}{(A-1)^2} \\
 & - \frac{2}{A-1} s_{13}^2 \sin^2 2\theta_{23} \left(\sin \Delta \cos A\Delta \frac{\sin(A-1)\Delta}{A-1} - \frac{A}{2} \Delta \sin 2\Delta \right) \\
 & - 2 \alpha s_{13} \sin 2\theta_{12} \sin 2\theta_{23} \cos \delta_{CP} \cos \Delta \frac{\sin A\Delta}{A} \frac{\sin(A-1)\Delta}{A-1} \\
 & + \frac{2}{A-1} \alpha s_{13} \sin 2\theta_{12} \sin 2\theta_{23} \cos 2\theta_{23} \cos \delta_{CP} \sin \Delta \left(A \sin \Delta - \frac{\sin A\Delta}{A} \cos(A-1)\Delta \right), \\
 V(x) \simeq & 7.56 \times 10^{-14} \left(\frac{\rho(x)}{\text{g/cm}^3} \right) Y_e(x) \text{ eV}
 \end{aligned} \tag{33}$$

From “Series expansions for three-flavor neutrino oscillation probabilities in matter”

$\Delta \equiv \frac{\Delta m_{31}^2 L}{4E}$,
$A \equiv \frac{2EV}{\Delta m_{31}^2} = \frac{VL}{2\Delta}$
$\alpha \equiv \frac{\Delta m_{21}^2}{\Delta m_{31}^2}$

$$\begin{aligned}
 P(\nu_\mu \rightarrow \nu_e) = & 4c_{13}^2 s_{13}^2 s_{23}^2 \sin^2 \phi_{31} \left(1 + \frac{2a}{\Delta m_{31}^2} (1 - 2s_{13}^2) \right) + 8c_{13}^2 s_{12} s_{13} s_{23} (c_{12} c_{23} \cos \delta - s_{12} s_{13} s_{23}) \cos \phi_{23} \sin \phi_{31} \sin \phi_{21} \\
 & - 8c_{13}^2 c_{12} c_{23} s_{12} s_{13} s_{23} \sin \delta \sin \phi_{32} \sin \phi_{31} \sin \phi_{21} \\
 & + 4s_{12}^2 c_{13}^2 (c_{12}^2 c_{23}^2 + s_{12}^2 s_{23}^2 s_{13}^2 - 2c_{12} c_{23} s_{12} s_{23} s_{13} \cos \delta) \sin^2 \phi_{21} \\
 & - 8c_{13}^2 s_{13}^2 s_{23}^2 (1 - 2s_{13}^2) \frac{aL}{4E_\nu} \cos \phi_{32} \sin \phi_{31}.
 \end{aligned} \tag{18}$$

Illustration 3: Equations used (where $Y_e(x)=0.5$).

³ T2K paper: Measurements of neutrino oscillation in appearance and disappearance channels by the T2K experiment with 6.6×10^{20} protons on target.

Figure 86 below shows the preliminary plot of $P(\nu_\mu \rightarrow \nu_\mu) vs P(\nu_\mu \rightarrow \nu_e)$ for $\delta_{CP} \in [-\pi, \pi]$ created by original_code_neutrino_osc.i.C :

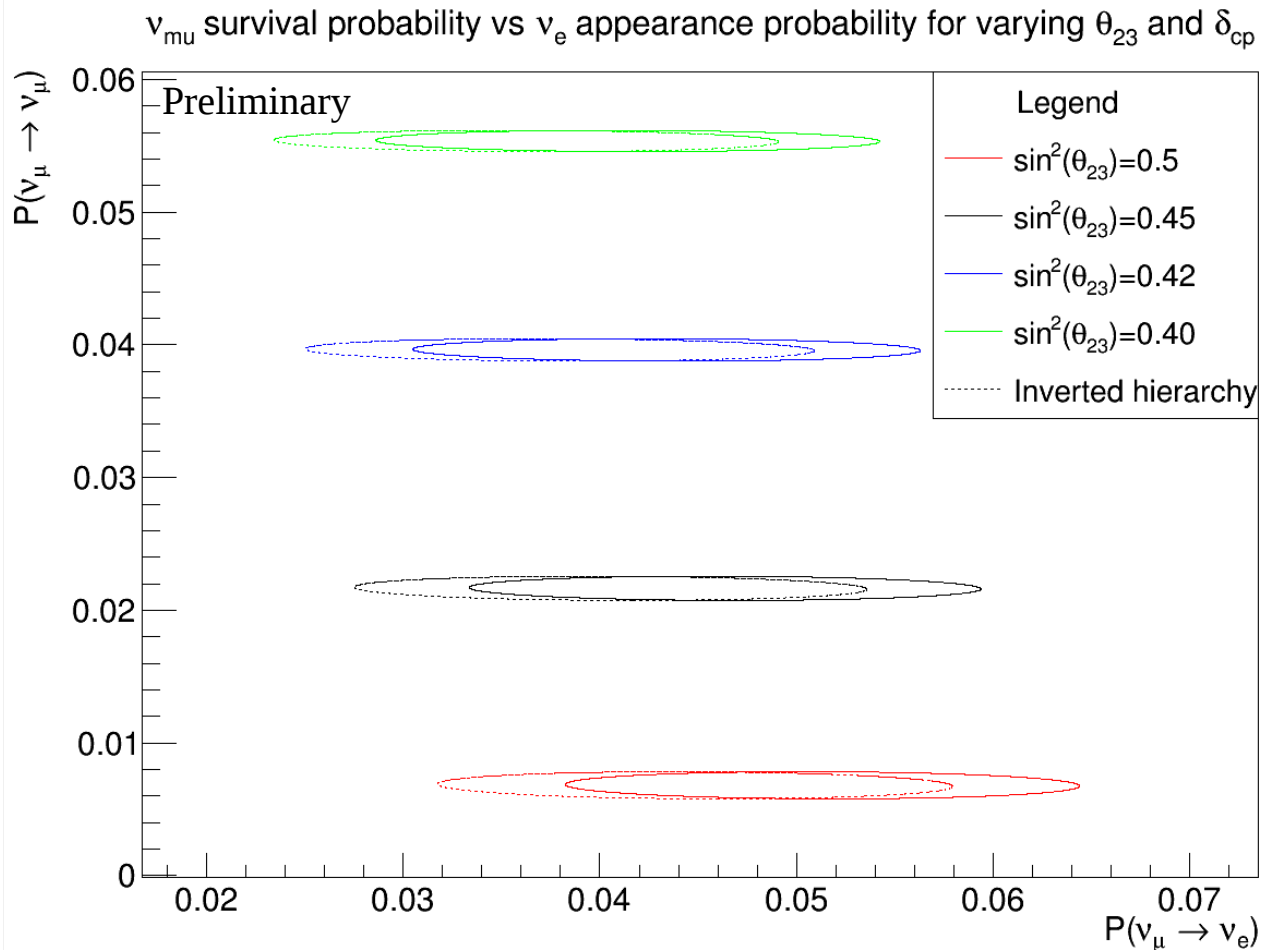


Figure 86

Notice that the inverted hierarchy plots do not agree with figure 25 of the T2K paper³ that we saw in figure 85. One possible cause is that my code uses approximations for the survival and appearance probabilities (illustration 3). The next step is to use the root package that calculates neutrino oscillation probabilities and the class BargerPropagators, which use exact formulae, to recreate figure 86.

³ T2K paper: Measurements of neutrino oscillation in appearance and disappearance channels by the T2K experiment with 6.6×10^{20} protons on target.

Chapter 9

Neutrino Oscillation Applet:

The code `/home/pmt_pc_2/software/code/neutrino_oscillation_applet.C` uses the interface from Shu Wang's (past summer student at York) neutrino oscillation applet in combination with my code (`original_code_neutrino_osci.C`) to allow users to input values for mixing angles, mass differences and delta CP to create the plots shown in chapter 7 and 8 (figure 87).

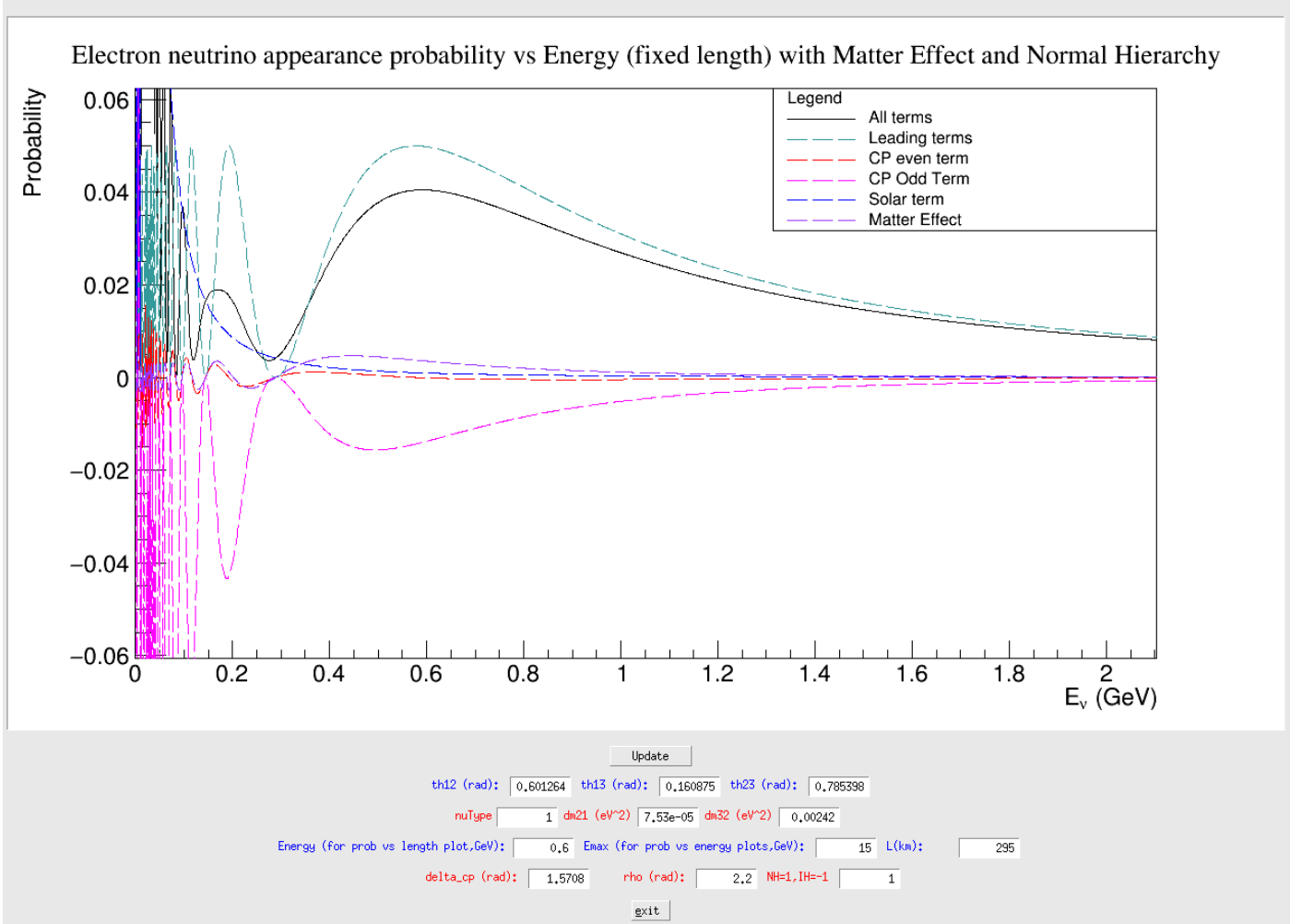


**Figure 87: A screen shot of my neutrino oscillation applet
(`/home/pmt_pc_2/software/code/neutrino_oscillation_applet.C`)**

The applet also produces all the other plots shown in chapter 7 and 8.

Images

Illustration 1:

<http://virtualreality.duke.edu/project/super-kave/>

Illustration 2:

<http://www.slideshare.net/YoshitaroTakaesu/t2kk-t2ko-cp>

Figure 2:

<http://www.ammrf.org.au/myscope/confocal/confocal/lasers.php?popup=true&iframe=true&width=800&height=600>

Figure 5:

<http://hzcpotonics.com/products/XP5312.pdf>